NASA Technical Memorandum 110304

Wind Tunnel Results of the Aerodynamic Performance of a 1/8-Scale Model of a Twin-Engine Transport With Multi-Element Wing

Brenda E. Gile Laflin, Zachary T. Applin, and Kenneth M. Jones
Langley Research Center, Hampton, Virginia

March 1997

National Aeronautics and
Space Administration
Langley Research Center
Hampton, Virginia 23681-0001

Summary

A wind tunnel investigation was performed in the Langley Research Center 14- by 22-Foot Subsonic Tunnel on a pressure instrumented 1/8-scale twin-engine subsonic transport to better understand the flow physics on a multi-element wing section. The wing consisted of a part-span, triple-slotted trailing-edge flap, inboard leading-edge Krueger flap and an outboard leading-edge slat. The model was instrumented with flush pressure ports at the fuselage centerline and seven spanwise wing locations.

The model was tested in cruise, take-off and landing configurations at dynamic pressures and Mach numbers from 10 lbf/ft^2 to 50 lbf/ft^2 and 0.08 to 0.17, respectively. This resulted in corresponding Reynolds numbers of 0.8×10^5 to 1.8×10^6. Pressure data were collected using electronically scanned pressure devices and force and moment data were collected with a six-component strain gauge balance.

Results are presented for various control surface deflections over an angle-of-attack range from -4° to 16° and sideslip angle range from -10° to 10°. Longitudinal and lateral directional aerodynamic data are presented as well as chordwise pressure distributions at the seven spanwise wing locations and the fuselage centerline.

Introduction

As part of the subsonic transport high-lift program at Langley Research Center, wind tunnel tests were conducted on a 1/8-scale wind tunnel model. A major objective was to obtain detailed flow characteristics to aid in understanding the flow physics on a multi-element, high-lift wing. An understanding of this flow is important in attempting to find a simpler flap system with equivalent or improved performance levels. Work was conducted on this model in the late 1970's (ref. 1) but major revisions have been made to the model slat and flap geometry since that time to

better match the airplane geometry.

The model was instrumented with flush pressure ports on the fuselage centerline and at seven spanwise wing locations. The model was tested in cruise, take-off and landing configurations with various deflections of elevator, stabilizer, rudder and ailerons. The longitudinal and lateral-directional aerodynamic characteristics, in addition to wing and fuselage surface pressure distributions, are presented for the four basic test configurations. The data are presented without analysis.

Symbols

All measurements and calculations were made in U.S. Customary Units. The model moment reference center was 25 percent of the mean aerodynamic chord. Names in parentheses are used in electronic data tables.

b		wing span, ft
$\bar{c}$		wing mean aerodynamic chord, ft
c_{af}	(caf)	local aft flap chord, in.
c_{ff}	(cff)	local foreflap chord, in.
c_{mf}	(cmf)	local midflap chord, in.
c_s	(cs)	local slat chord, in.
c_w	(cw)	local wing chord, in.
C_D	(CD)	drag coefficient, $\frac{Drag}{q_\infty S}$
C_L	(CL)	lift coefficient, $\frac{Lift}{q_\infty S}$
C_P	(Cp)	pressure coefficient, $\frac{P_n - P_\infty}{q_\infty}$

C_l		rolling-moment coefficient, $\frac{\text{Rolling moment}}{q_\infty S b}$
C_m		pitching-moment coefficient, $\frac{\text{Pitching moment}}{q_\infty S \bar{c}}$
C_n		yawing-moment coefficient, $\frac{\text{Yawing moment}}{q_\infty S b}$
C_Y		side-force coefficient, $\frac{\text{Side force}}{q_\infty S}$
i_t	(Isubt)	stabilizer angle, deg
l		fuselage length, ft
M_∞	(M)	freestream Mach number
P_∞		freestream static pressure, lb/ft^2
P_n		pressure at a specific model port n=1,2,...
q_∞	(q)	freestream dynamic pressure, lb/ft^2
R		Reynolds number based on wing mean aerodynamic chord
S		wing area, ft^2
x	(x)	chordwise distance aft of leading-edge, in.
y	(y)	spanwise distance from model centerline, in.
α	(Alpha)	angle of attack, deg
β	(Beta)	sideslip angle, deg
δ_{fl}		flap deflection angle, deg
δ_{Kr}		Krueger flap deflection angle, deg
δ_{sl}		slat deflection angle, deg

Model Description

The model was a 1/8-scale twin-engine subsonic transport with multi-element wing shown

in figure 1. The empennage consisted of a vertical tail with rudder and a motorized horizontal stabilizer with elevator. The engines were represented by two flow-through nacelles. Specific model geometric characteristics are given in table 1.

The model was tested in cruise, take-off and landing configurations with control surfaces varied as shown in table 2. For convenience, the model control surfaces are defined and numbered in figure 2. The four basic test configurations are shown in the table below.

Configuration	Leading Edge	Flap Deflection
Cruise	$\delta_{Kr}=0°$, $\delta_{sl}=0°$	$\delta_{fl}=0°$
Take-off	$\delta_{Kr}=112°$, $\delta_{sl}=20°$	$\delta_{fl}=15°$
Landing 1	$\delta_{Kr}=112°$, $\delta_{sl\ 3,4}=20°$, $\delta_{sl\ 1,2,5,6}=30°$	$\delta_{fl}=30°$
Landing 2	$\delta_{Kr}=112°$, $\delta_{sl\ 3,4}=20°$, $\delta_{sl\ 1,2,5,6}=30°$	$\delta_{fl}=40°$

The model was instrumented with approximately 700 flush pressure ports located on the centerline of the fuselage and at seven spanwise wing locations as shown in figure 3 and presented in tables 3-11.

Test Conditions and Corrections

The investigation was performed in the Langley 14- by 22-Foot Subsonic Tunnel (ref 2). The test was conducted at dynamic pressures, q_∞, from 10 lbf/ft^2 to 50 lbf/ft^2 corresponding to Reynolds numbers, based on $\bar{c}$, of 8.2 x 10^5 to 1.8 x 10^6 and Mach numbers of 0.08 to 0.17, respectively. Data were obtained over an angle-of-attack range from -4° through 16° with sideslip angles from -10° to 10°.

Aerodynamic forces and moments were obtained with a six-component strain-gauge balance and wing pressures were obtained with electronically scanned pressure devices from flush

mounted pressure ports. Angle of attack was measured with an electronic accelerometer installed inside the model and sideslip angle was measured with a digital encoder mounted to the model support system turntable drive. Transition of the boundary layer was fixed with transition grit and verified through the use of sublimating chemicals. Wing, body, and wake blockage corrections to freestream dynamic pressure were applied according to reference 3. Corrections were applied for tunnel wall interference using the technique of reference 4.

Presentation of Results

Data for the four basic test configurations are presented, without analysis, as shown below:

Test Parameter and Model Configuration	Figure
Effect of flap deflection on the longitudinal aerodynamic characteristics at q_∞=40 psf.	4
Wing pressure distributions for the Cruise configuration at q_∞=40 psf.	5
Effect of flap deflection of the wing pressure distributions at q_∞=40 psf.	6
$\alpha = 0°$.	(a)
$\alpha = 4°$.	(b)
$\alpha = 8°$.	(c)
$\alpha = 12°$.	(d)
Trimmed longitudinal aerodynamic characteristics at q_∞=40 psf.	7
Effect of tunnel speed on the longitudinal aerodynamic characteristics.	8
Cruise configuration.	(a)
Take-off configuration.	(b)
Landing 1 configuration.	(c)
Landing 2 configuration.	(d)
Effect of tunnel speed on the wing pressure distributions of the Cruise configuration.	9
$\alpha = 0°$.	(a)

References

1. Paulson, John P.: Wind-Tunnel Results of the Aerodynamic Characteristics of a 1/8-Scale Model of a Twin-Engine Short-Haul Transport. NASA TM X-74011, April 1977.

2. Gentry, Garl L., Jr; Quinto, P. Frank; Gatlin, Gregory M.; and Applin, Zachary T.: The Langley 14- by 22-Foot Subsonic Tunnel: Description, Flow Characteristics, and Guide for Users. NASA TP-3008, 1990.

3. Rae, W. H., Jr., and Pope, A.: Low-Speed Wind Tunnel Testing. John Wiley & Sons, Inc., 1984.

4. Heyson, Harry H.: Use of Superposition in Digital Computers to Obtain Wind-Tunnel Interference Factors for Arbitrary Configurations, With Particular Reference to V/STOL Models. NASA TR R-302, February 1969.

Table 1. Model Dimensions.

Overall length, ft	11.75
Fuselage length, ft	11.34
Wing	
Area, ft^2	15.31
Span, ft	11.63
Mean aerodynamic chord, ft	1.4
Sweep of quarter chord, deg	25
Aspect ratio	8.83
Taper ratio	0.34
Horizontal tail span, ft	4.5
Vertical tail height, ft	2.46

Table 2. Control Surface Deflections.

Control Surface	Range of Deflection
Inboard and outboard flap	0°,15°,30°,40°
Leading-edge slat	0°,20°,30°
Krueger flap	0°,112°
Ailerons	0°,±26°
Spoilers	0°,3°,40°
Stabilizer	2.6° to -15°
Elevator	0°,±10°
Rudder	0°,±26°

Table 3. Fuselage pressure port locations.

Upper surface	Lower surface
x/l	x/l
0.002	0.004
0.018	0.086
0.034	0.152
0.051	0.217
0.067	0.299
0.083	0.365
0.099	0.512
0.116	0.594
0.148	0.660
0.181	0.742
0.213	
0.262	
0.294	
0.327	
0.359	
0.441	
0.522	
0.587	
0.668	

Table 4. Cruise wing upper surface pressure port locations

Spanwise station y=						
16.08	28.20	37.44	40.56	49.56	58.92	63.00
x/c_w	x/c_w	x/c_w	x/c_w	x/c_w	x/c_w	x/c_w
0.000	0.000	0.000	0.000	0.0002	0.0003	0.0003
0.018	0.006	0.007	0.007	0.009	0.011	0.011
0.036	0.014	0.017	0.018	0.021	0.027	0.028
0.061	0.026	0.030	0.032	0.038	0.047	0.050
0.093	0.038	0.044	0.046	0.055	0.067	0.071
0.124	0.050	0.058	0.061	0.073	0.089	0.095
0.155	0.069	0.080	0.084	0.099	0.112	0.129
0.199	0.079	0.092	0.097	0.114	0.139	0.148
0.246	0.133	0.140	0.144	0.153	0.192	0.219
0.296	0.158	0.165	0.169	0.179	0.262	0.252
0.348	0.193	0.201	0.206	0.216	0.337	0.322
0.400	0.231	0.239	0.244	0.256	0.410	0.391
0.452	0.271	0.280	0.286	0.298	0.483	0.459
0.502	0.312	0.323	0.328	0.342	0.559	0.531
0.553	0.354	0.365	0.371	0.385	0.643	0.610
0.603	0.396	0.408	0.413	0.429	0.676	0.671
0.655	0.436	0.449	0.454	0.471	0.709	0.708
0.709	0.477	0.490	0.496	0.514	0.729	0.727
0.766	0.517	0.531	0.538	0.556	0.748	0.765
0.826	0.559	0.574	0.580	0.600	0.782	0.804
0.872	0.602	0.618	0.625	0.646	0.818	0.842
0.945	0.648	0.665	0.671	0.694	0.854	0.881
0.972	0.696	0.714	0.720	0.745	0.890	0.919
1.000	0.733	0.752	0.758	0.784	0.926	0.938
	0.770	0.789	0.795	0.822	0.962	
	0.792	0.812	0.818	0.845	0.980	
	0.814	0.834	0.841	0.868		
	0.837	0.857	0.864			

Table 5. Cruise wing lower surface pressure port locations.

Spanwise station y=						
16.08	28.20	37.44	40.56	49.56	58.92	63.00
x/c_w	x/c_w	x/c_w	x/c_w	x/c_w	x/c_w	x/c_w
0.018	0.003	0.070	0.0004	0.0004	0.0004	0.0003
0.124	0.014	0.091	0.003	0.004	0.004	0.0005
0.155	0.050	0.117	0.016	0.019	0.022	0.005
0.199	0.065	0.143	0.033	0.038	0.046	0.024
0.246	0.085	0.168	0.145	0.055	0.054	0.049
0.310	0.111	0.204	0.171	0.081	0.063	0.066
0.438	0.136	0.243	0.207	0.103	0.076	0.078
0.579	0.161	0.452	0.246	0.130	0.094	0.094
0.655	0.196	0.515	0.456	0.156	0.117	0.116
0.709	0.234	0.577	0.520	0.182	0.139	0.137
0.766	0.285	0.621	0.582	0.219	0.161	0.158
0.808	0.388	0.667	0.626	0.366	0.193	0.188
0.849	0.501	0.702	0.673	0.420	0.521	0.444
0.870	0.562	0.735	0.707	0.539	0.559	0.495
0.890	0.605	0.751	0.741	0.603	0.600	0.531
0.917	0.651	0.789	0.758	0.648	0.631	0.570
0.945	0.684	0.812	0.773	0.696	0.675	0.626
	0.717	0.834	0.796	0.732	0.709	0.653
	0.733	0.857	0.819	0.766	0.748	0.690
	0.749		0.841	0.784	0.782	0.727
	0.770			0.800	0.818	0.765
	0.793			0.822	0.854	0.804
	0.814			0.846	0.890	0.842
	0.837			0.864	0.926	0.881
					0.962	0.919
					0.980	0.938
					0.998	0.957

Table 6. Slat pressure port locations.

Spanwise station y=					
28.20	37.44	40.56	49.56	58.92	63.00
x/c_s	x/c_s	x/c_s	x/c_s	x/c_s	x/c_s
Upper surface					
0.000	0.000	0.000	0.000	0.000	0.000
0.011	0.011	0.011	0.011	0.011	0.011
0.088	0.088	0.088	0.088	0.088	0.088
0.186	0.186	0.186	0.186	0.186	0.186
0.306	0.306	0.306	0.306	0.306	0.306
0.421	0.421	0.421	0.421	0.421	0.421
0.543	0.543	0.543	0.543	0.543	0.543
0.718	0.718	0.718	0.718	0.718	0.718
0.814	0.814	0.814	0.814	0.814	0.814
1.000	1.000	1.000	1.000	1.000	1.000
Lower surface					
0.011	0.011	0.011	0.011	0.011	0.011
0.088	0.088	0.088	0.088	0.088	0.088
0.225	0.225	0.225	0.225	0.225	0.225
0.362	0.362	0.362	0.362	0.362	0.362
0.481	0.481	0.481	0.481	0.481	0.481
0.624	0.624	0.624	0.624	0.624	0.624
0.814	0.814	0.814	0.814	0.814	0.814
0.911	0.911	0.911	0.911	0.911	0.911

Table 7. High-lift wing upper surface pressure port locations.

Spanwise station y=						
16.08	28.20	37.44	40.56	49.56	58.92	63.00
x/c_w	x/c_w	x/c_w	x/c_w	x/c_w	x/c_w	x/c_w
0.000	0.000	0.000	0.000	0.000	0.000	0.000
0.018	0.017	0.018	0.018	0.019	0.014	0.013
0.036	0.036	0.036	0.036	0.037	0.046	0.044
0.061	0.061	0.061	0.061	0.063	0.094	0.067
0.093	0.093	0.093	0.093	0.096	0.151	0.089
0.124	0.124	0.124	0.124	0.128	0.224	0.111
0.155	0.155	0.155	0.155	0.159	0.303	0.143
0.199	0.199	0.199	0.199	0.205	0.380	0.176
0.246	0.296	0.246	0.246	0.253	0.457	0.212
0.296	0.348	0.296	0.296	0.304	0.537	0.287
0.348	0.400	0.348	0.348	0.358	0.626	0.360
0.400	0.452	0.400	0.400	0.411	0.661	0.432
0.452	0.502	0.452	0.452	0.465	0.695	0.508
0.502	0.553	0.502	0.502	0.516	0.716	0.592
0.553	0.603	0.553	0.553	0.569	0.737	0.657
0.603	0.655	0.603	0.603	0.620	0.773	0.696
0.655	0.709	0.655	0.655	0.674	0.811	0.755
0.709	0.766	0.709	0.709	0.729	0.849	0.796
0.766	0.826	0.766	0.766	0.788	0.886	0.837
0.826	0.872	0.826	0.826	0.850	0.924	0.878
0.872	0.917	0.872	0.872	0.897	0.962	0.918
0.945	0.945	0.917	0.917	0.943	0.981	0.959
0.972	0.972	0.945	0.945	0.972		0.980
1.000	1.000	0.972	0.972	1.000		
		1.000	1.000			

Table 8. High-lift wing lower surface pressure port locations.

Spanwise station y=						
16.08	28.20	37.44	40.56	49.56	58.92	63.00
x/c_w	x/c_w	x/c_w	x/c_w	x/c_w	x/c_w	x/c_w
0.018	0.018	0.036	0.124	0.005	0.004	0.013
0.124	0.036	0.061	0.155	0.037	0.014	0.026
0.155	0.061	0.093	0.199	0.063	0.027	0.044
0.199	0.093	0.124	0.246	0.096	0.046	0.067
0.246	0.124	0.155	0.502	0.128	0.071	0.089
0.310	0.155	0.199	0.579	0.159	0.094	0.111
0.438	0.199	0.246	0.655	0.205	0.117	0.143
0.579	0.246	0.502	0.709	0.385	0.151	0.415
0.655	0.310	0.579	0.766	0.451	0.496	0.469
0.709	0.438	0.655	0.808	0.596	0.537	0.508
0.766	0.579	0.709	0.849	0.674	0.580	0.549
0.808	0.655	0.766	0.870	0.729	0.612	0.608
0.849	0.709	0.808	0.890	0.788	0.659	0.638
0.870	0.766	0.849	0.917	0.831	0.695	0.677
0.890	0.808	0.870	0.945	0.873	0.737	0.716
0.917	0.849	0.917	0.972	0.895	0.773	0.755
0.945	0.870	0.945		0.916	0.811	0.796
	0.890	0.972		0.943	0.849	0.837
	0.917			0.972	0.886	0.878
	0.945				0.924	0.918
	0.972				0.962	0.959
					0.981	0.980

Table 9. Fore flap pressure port locations.

Spanwise station y=				
16.08	28.20	37.44	40.56	49.56
x/c_{ff}	x/c_{ff}	x/c_{ff}	x/c_{ff}	x/c_{ff}
Upper surface				
0.000	0.000	0.000	0.000	0.000
0.008	0.032	0.032	0.032	0.032
0.068	0.109	0.109	0.109	0.109
0.163	0.232	0.232	0.232	0.232
0.303	0.372	0.372	0.372	0.372
0.452	0.537	0.537	0.537	0.537
0.627	0.715	0.715	0.715	0.715
0.804	0.897	0.897	0.897	0.844
1.000	1.000	1.000	1.000	1.000
Lower surface				
0.017	0.017	0.017	0.017	0.017
0.037	0.068	0.068	0.068	0.068
0.109	0.168	0.168	0.168	0.168
0.232	0.303	0.303	0.303	0.303
0.372	0.452	0.452	0.452	0.452
0.537	0.627	0.627	0.627	0.627
0.715	0.804	0.804		0.804
0.897				

Table 10. Mid flap pressure port locations.

Spanwise station y=				
16.08	28.20	37.44	40.56	49.56
x/c_{mf}	x/c_{mf}	x/c_{mf}	x/c_{mf}	x/c_{mf}
Upper surface				
0.006	0.006	0.006	0.006	0.006
0.006	0.006	0.006	0.006	0.052
0.052	0.052	0.052	0.052	0.162
0.162	0.162	0.162	0.162	0.295
0.295	0.433	0.295	0.295	0.433
0.364	0.597	0.433	0.433	0.597
0.433	0.798	0.597	0.597	0.798
0.503	0.934	0.798	0.798	0.934
0.597	1.000	0.934	0.934	1.000
0.714		1.000	1.000	
0.798				
0.868				
0.934				
1.000				
Lower surface				
0.052	0.052	0.052	0.052	0.052
0.102	0.164	0.164	0.164	0.164
0.164	0.330	0.330	0.330	0.330
0.227	0.506	0.506	0.506	0.714
0.330	0.714	0.714	0.714	0.868
0.418	0.868	0.868	0.868	
0.506				
0.606				
0.714				
0.868				

Table 11. Aft flap pressure port locations.

Spanwise station y=				
16.08	28.20	37.44	40.56	49.56
x/c_{af}	x/c_{af}	x/c_{af}	x/c_{af}	x/c_{af}
Upper surface				
0.006	0.006	0.006	0.006	0.006
0.006	0.006	0.006	0.006	0.052
0.052	0.052	0.052	0.052	0.162
0.162	0.162	0.162	0.162	0.295
0.295	0.433	0.295	0.295	0.433
0.364	0.597	0.433	0.433	0.597
0.433	0.798	0.597	0.597	0.798
0.503	0.934	0.798	0.798	0.934
0.597	1.000	0.934	0.934	1.000
0.714		1.000	1.000	
0.798				
0.868				
0.934				
1.000				
Lower surface				
0.052	0.052	0.052	0.052	0.052
0.102	0.164	0.164	0.164	0.164
0.164	0.330	0.330	0.330	0.330
0.227	0.506	0.506	0.506	0.714
0.330	0.714	0.714	0.714	0.868
0.418	0.868	0.868	0.868	
0.506				
0.606				
0.714				
0.868				

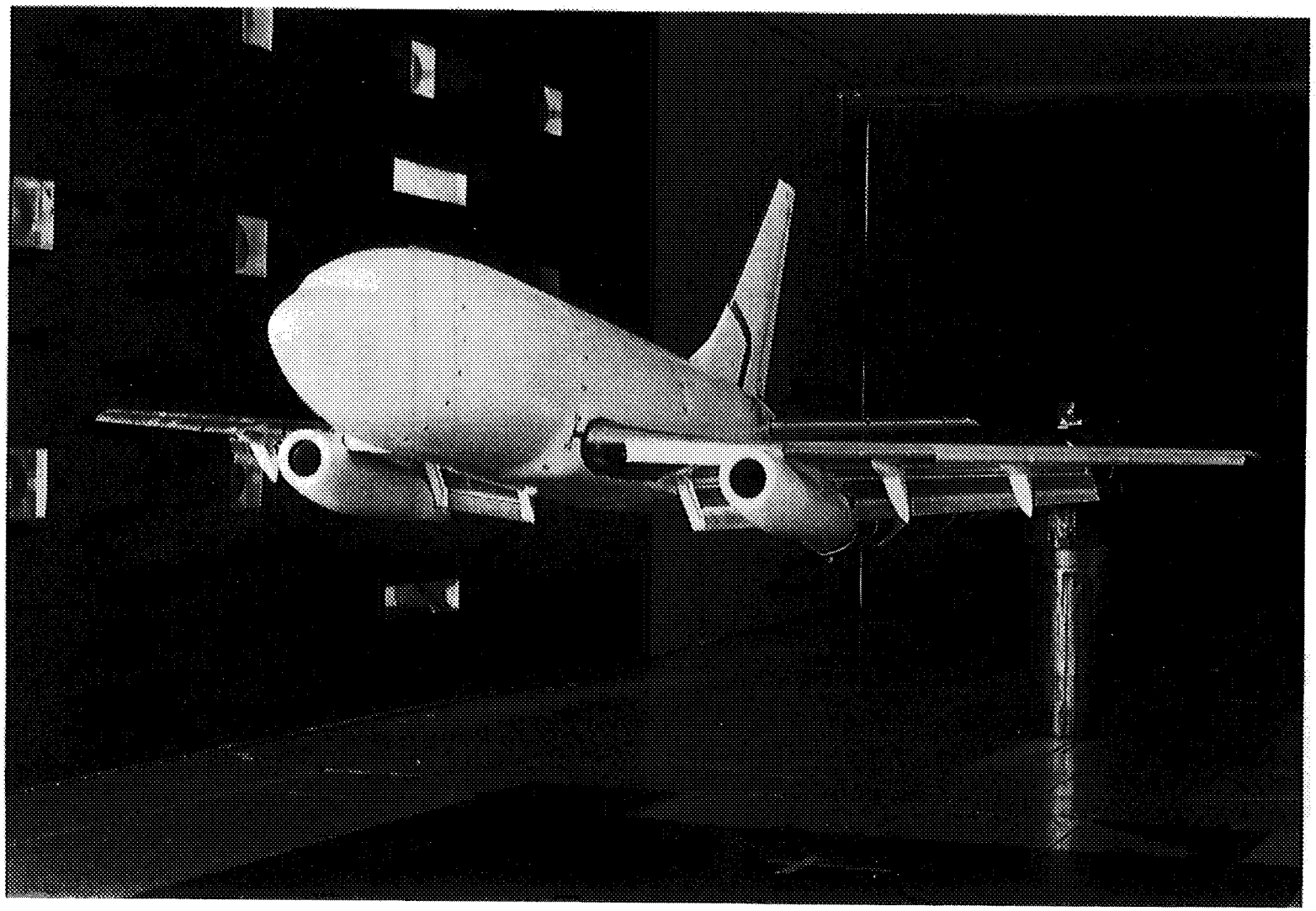

Figure 1. The 1/8-scale model of a twin-engine transport in the Langley 14- by 22-Foot Subsonic Tunnel.

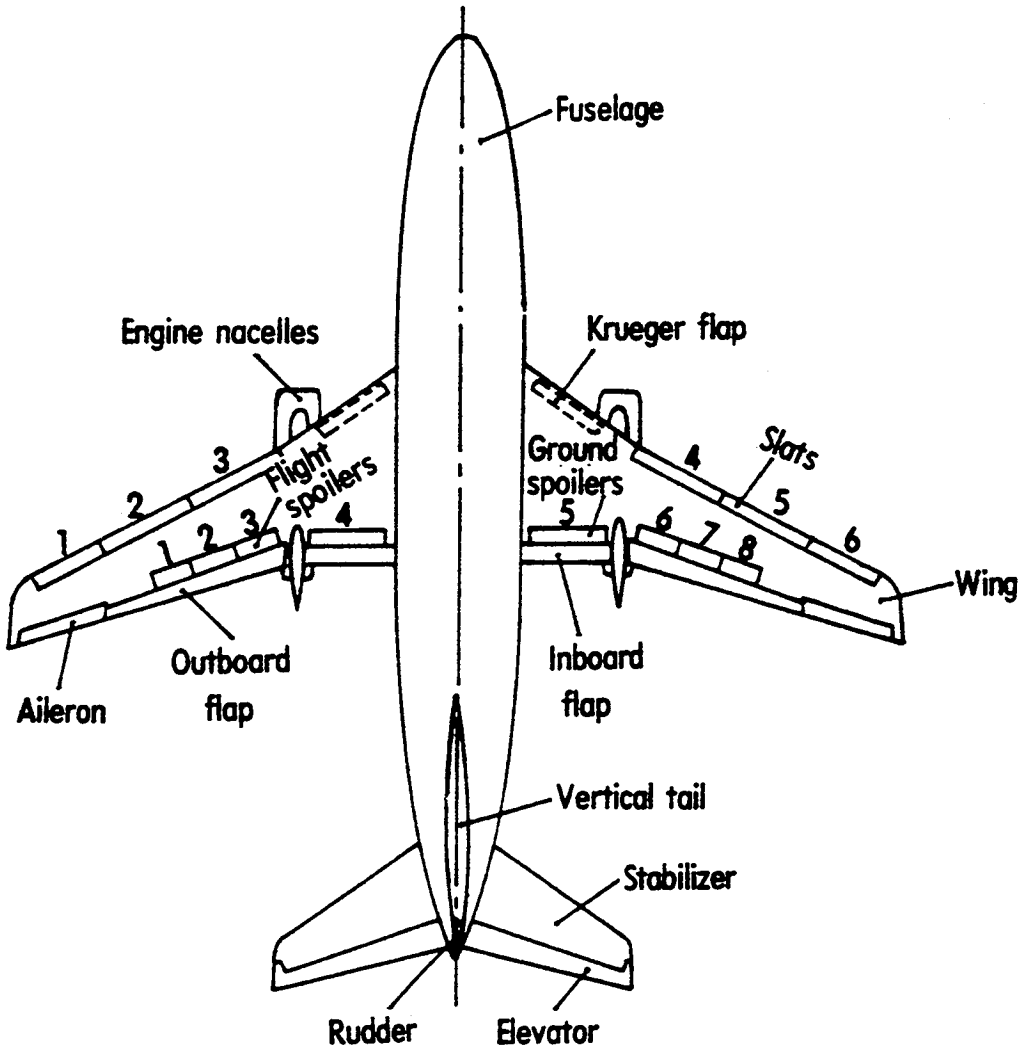

Figure 2. Planform of 1/8-scale twin-engine transport model showing component definition.

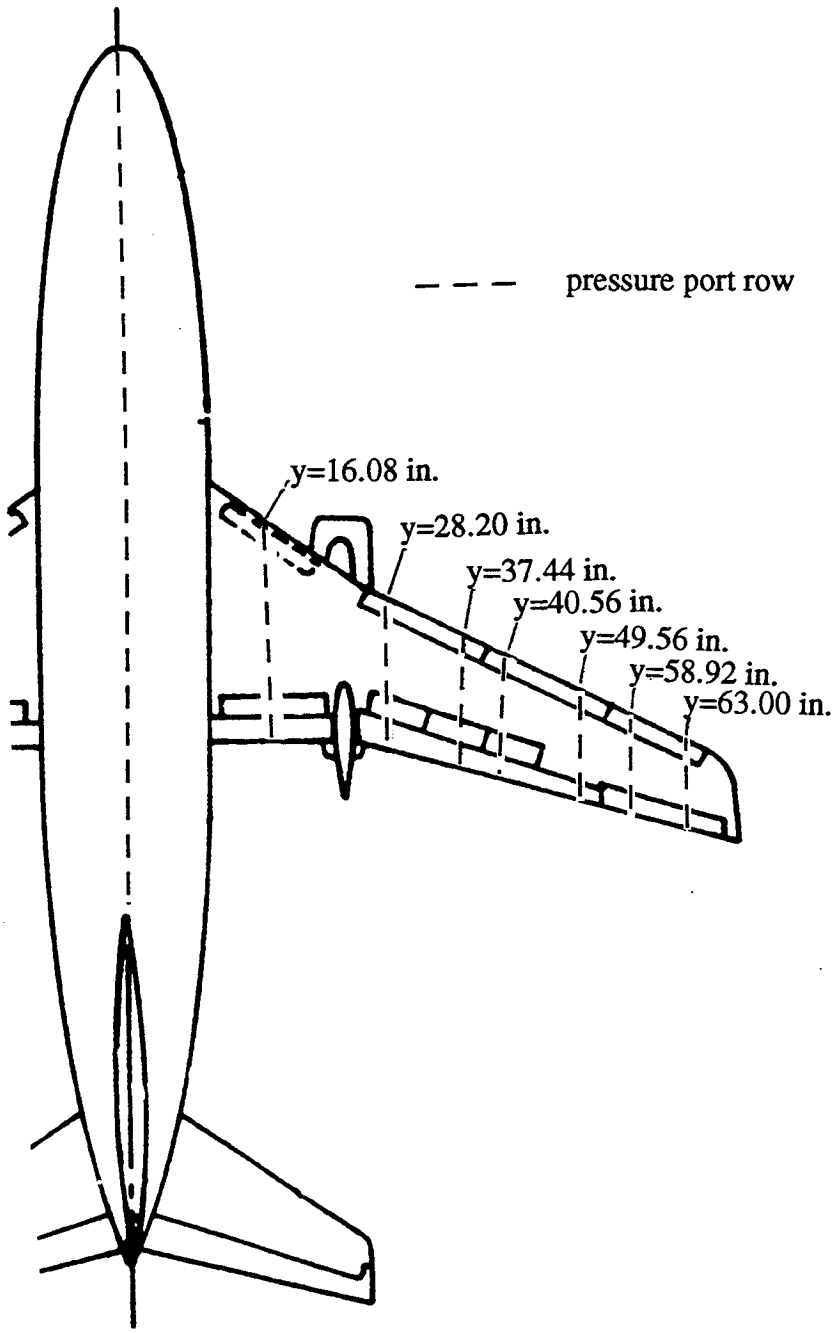

Figure 3. Planform of 1/8-scale twin-engine transport model showing pressure tap locations.

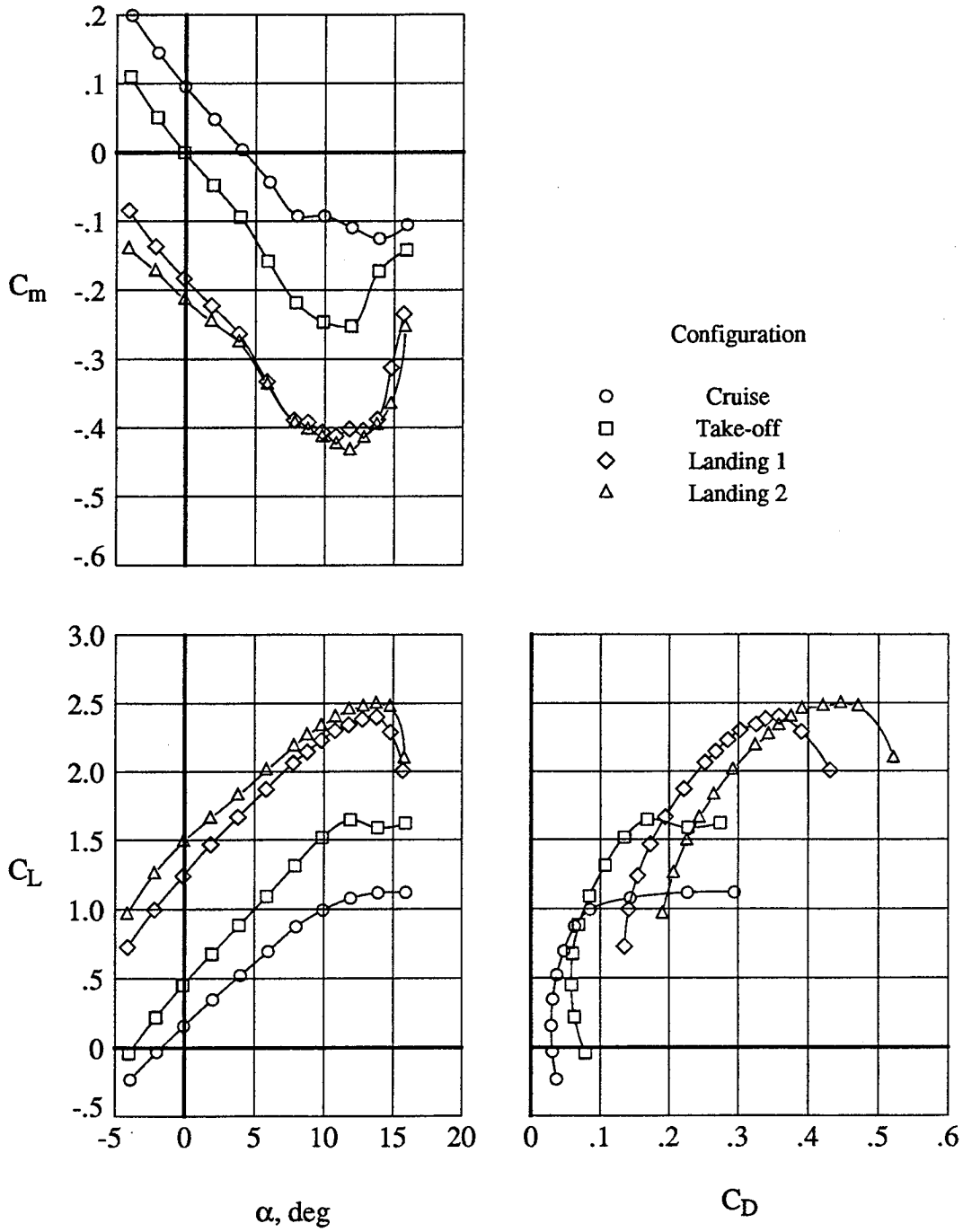

Figure 4. Effect of flap deflection on the longitudinal aerodynamic characteristics at $q_\infty = 40$ psf.

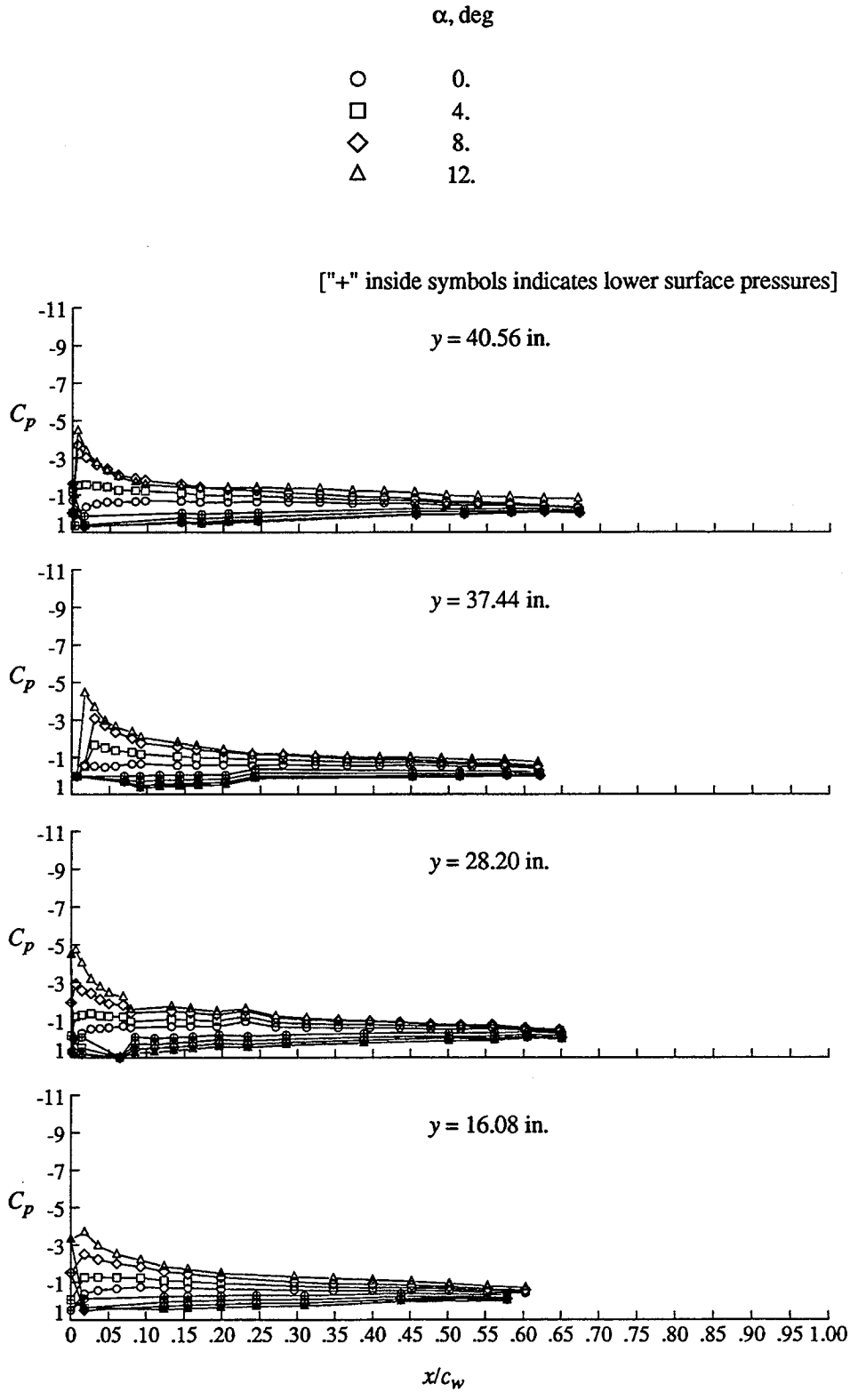

Figure 5. Wing pressure distributions for the Cruise configuration at $q_\infty = 40$ psf.

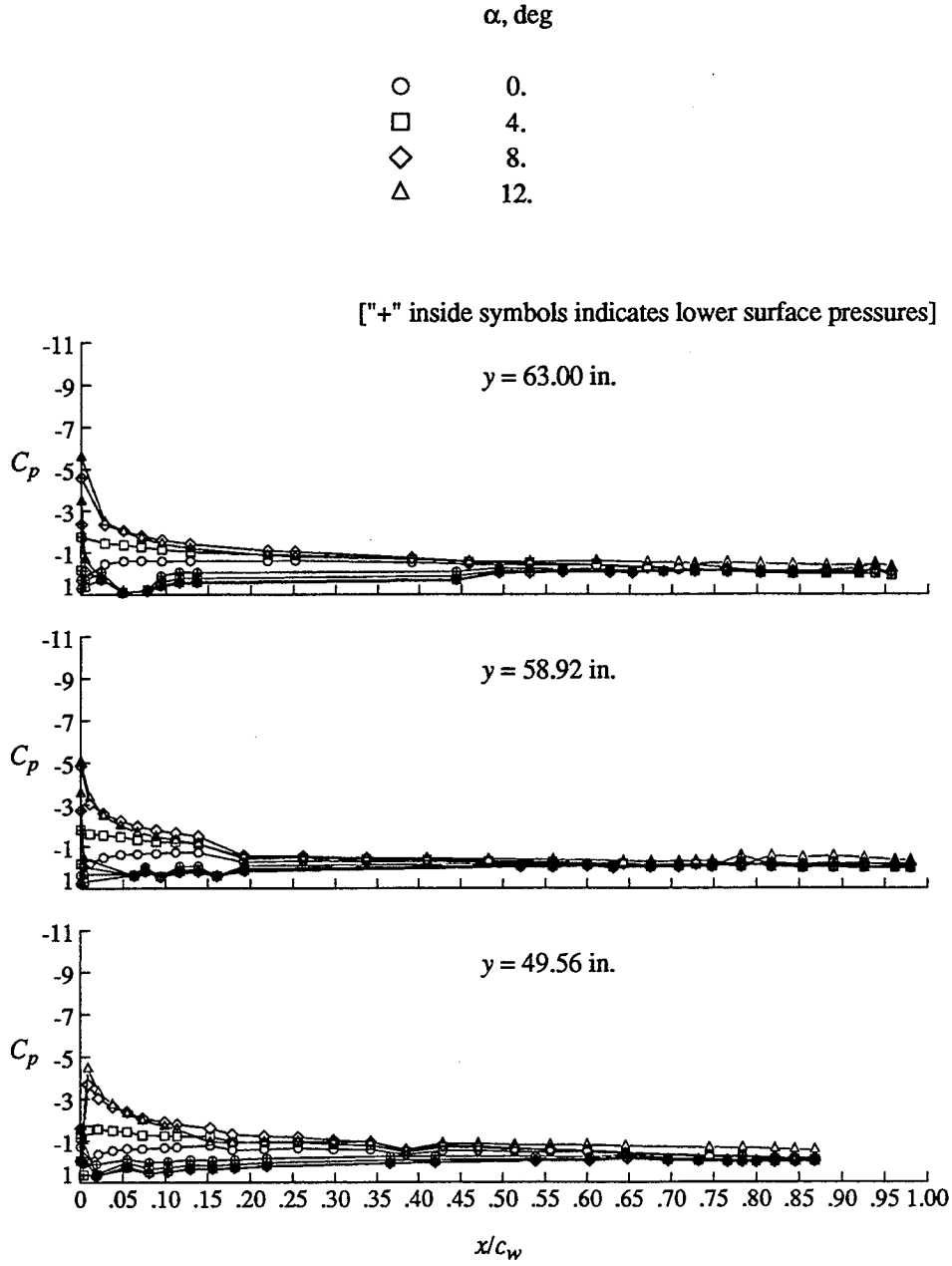

Figure 5. Continued.

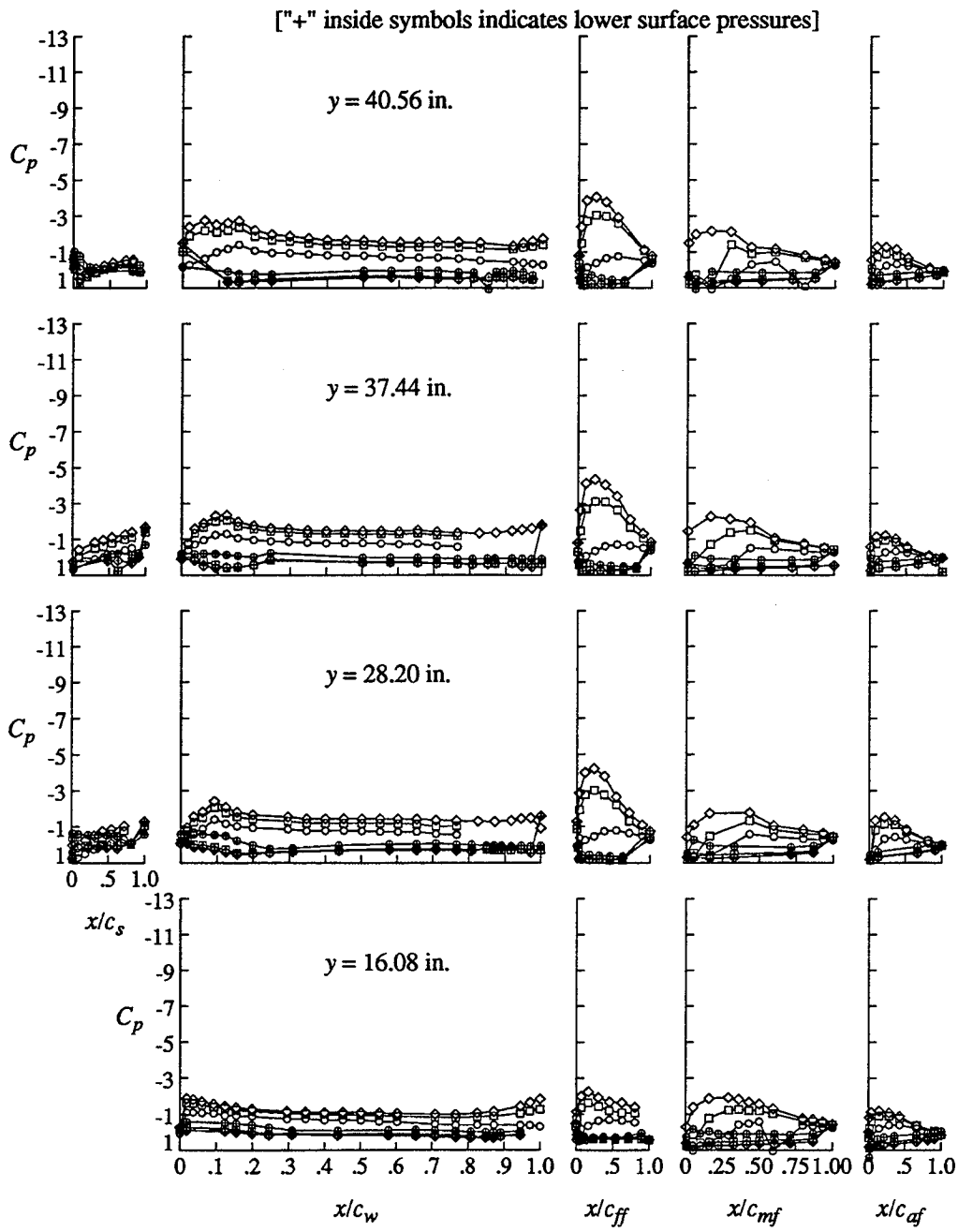

(a) $\alpha = 0°$.

Figure 6. Effect of flap deflection on the wing pressure distributions.

$q_\infty = 40$ psf.

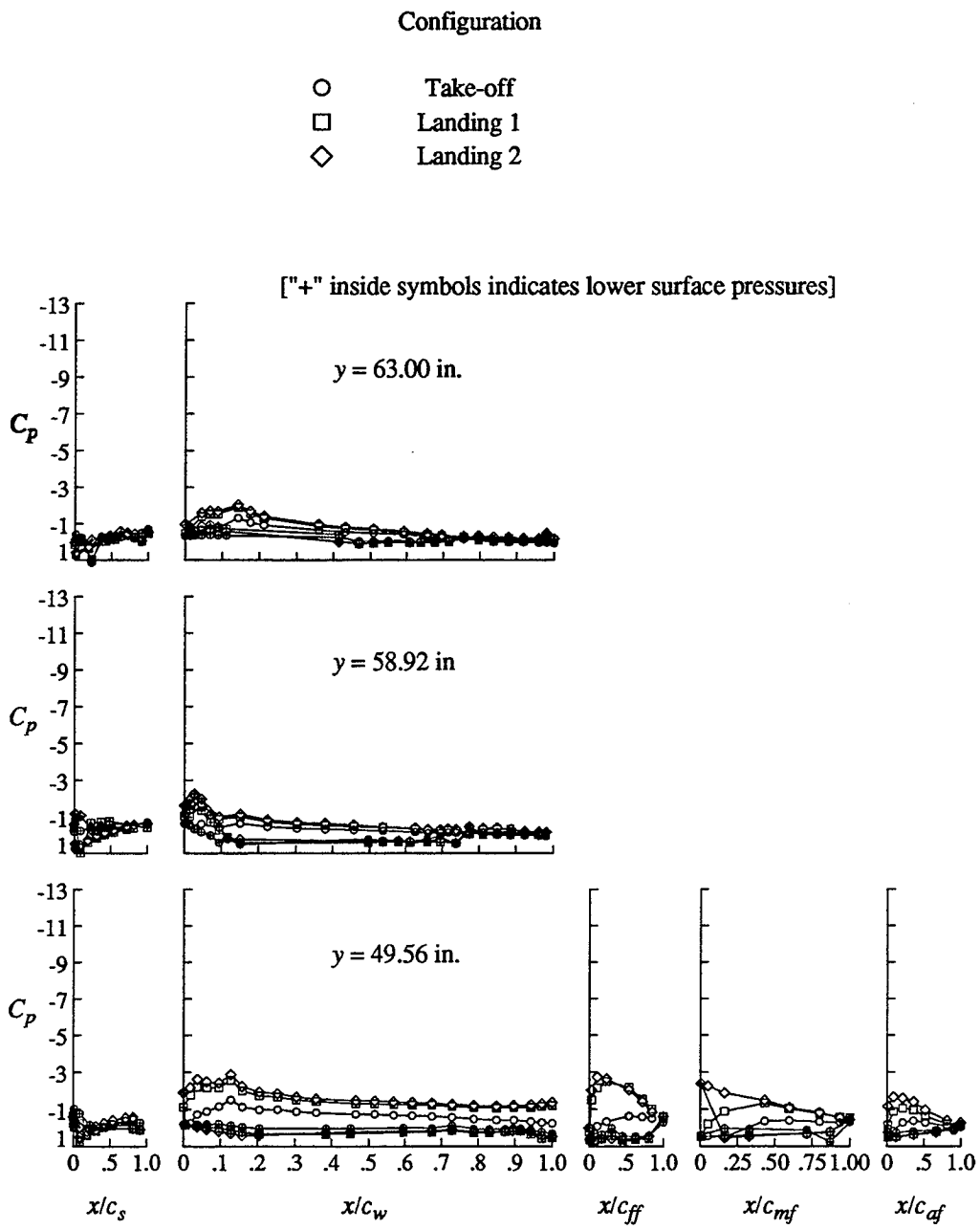

(a) $\alpha = 0°$.

Figure 6. Continued.

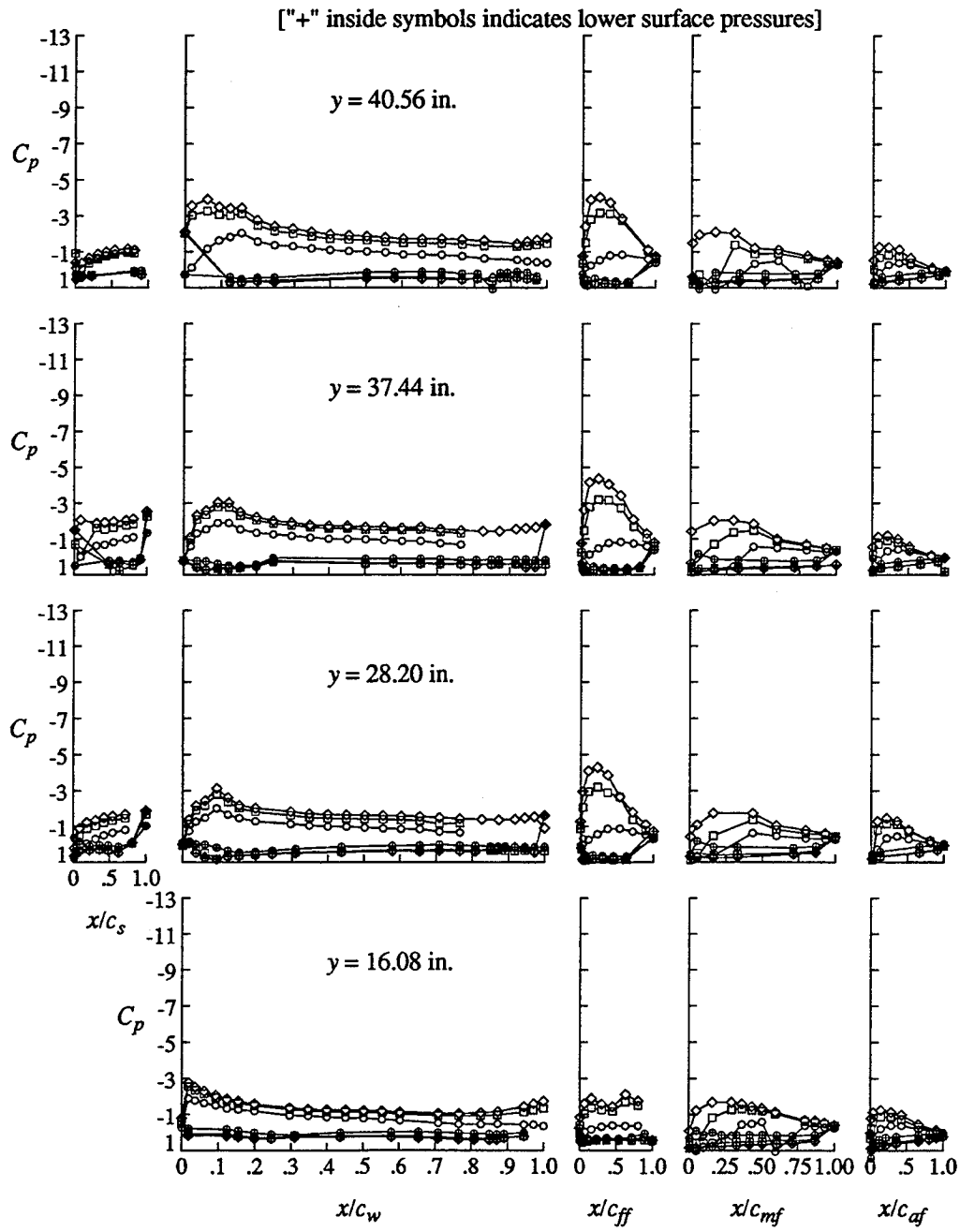

(b) $\alpha = 4°$.

Figure 6. Continued.

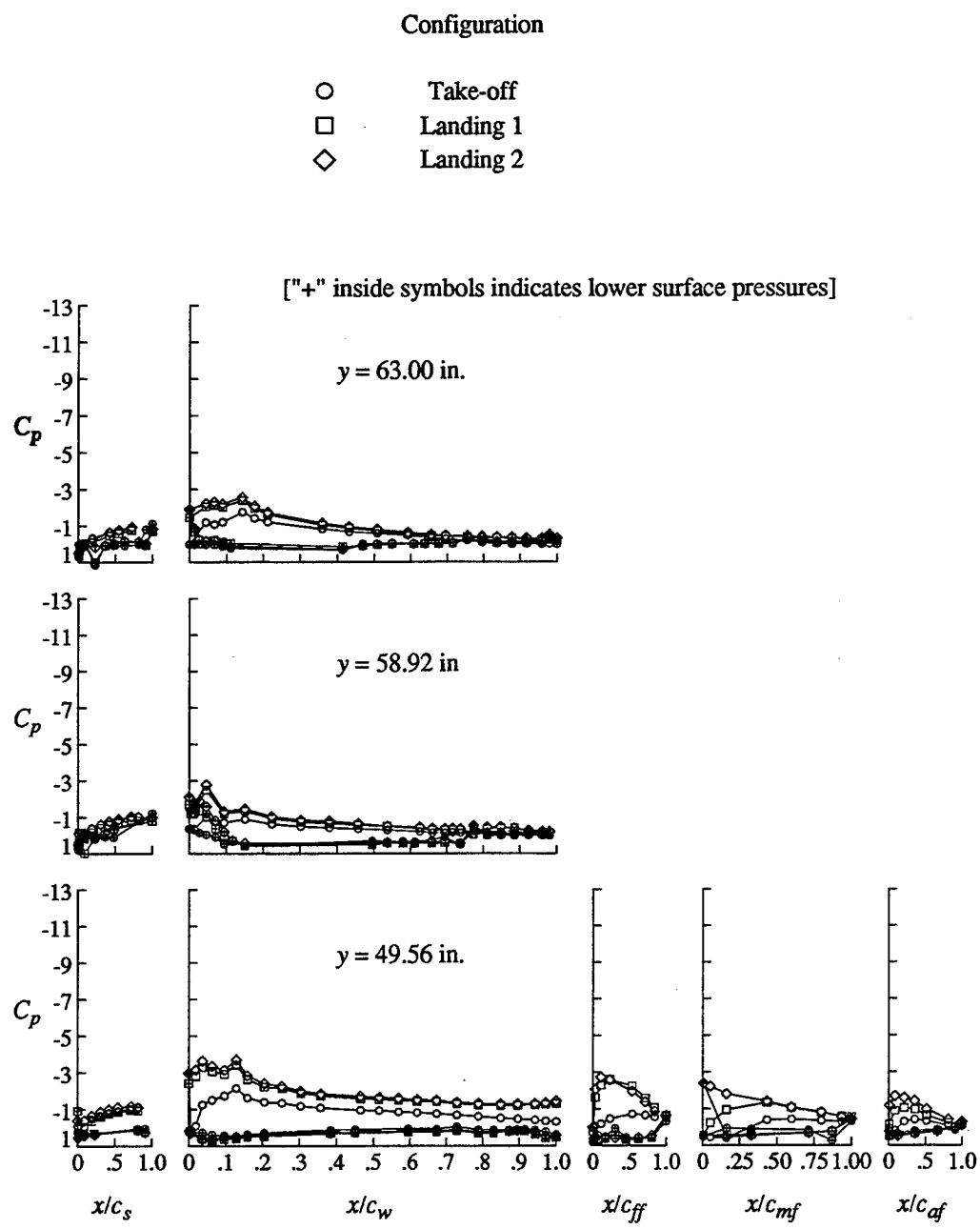

(b) $\alpha = 4°$.

Figure 6. Continued.

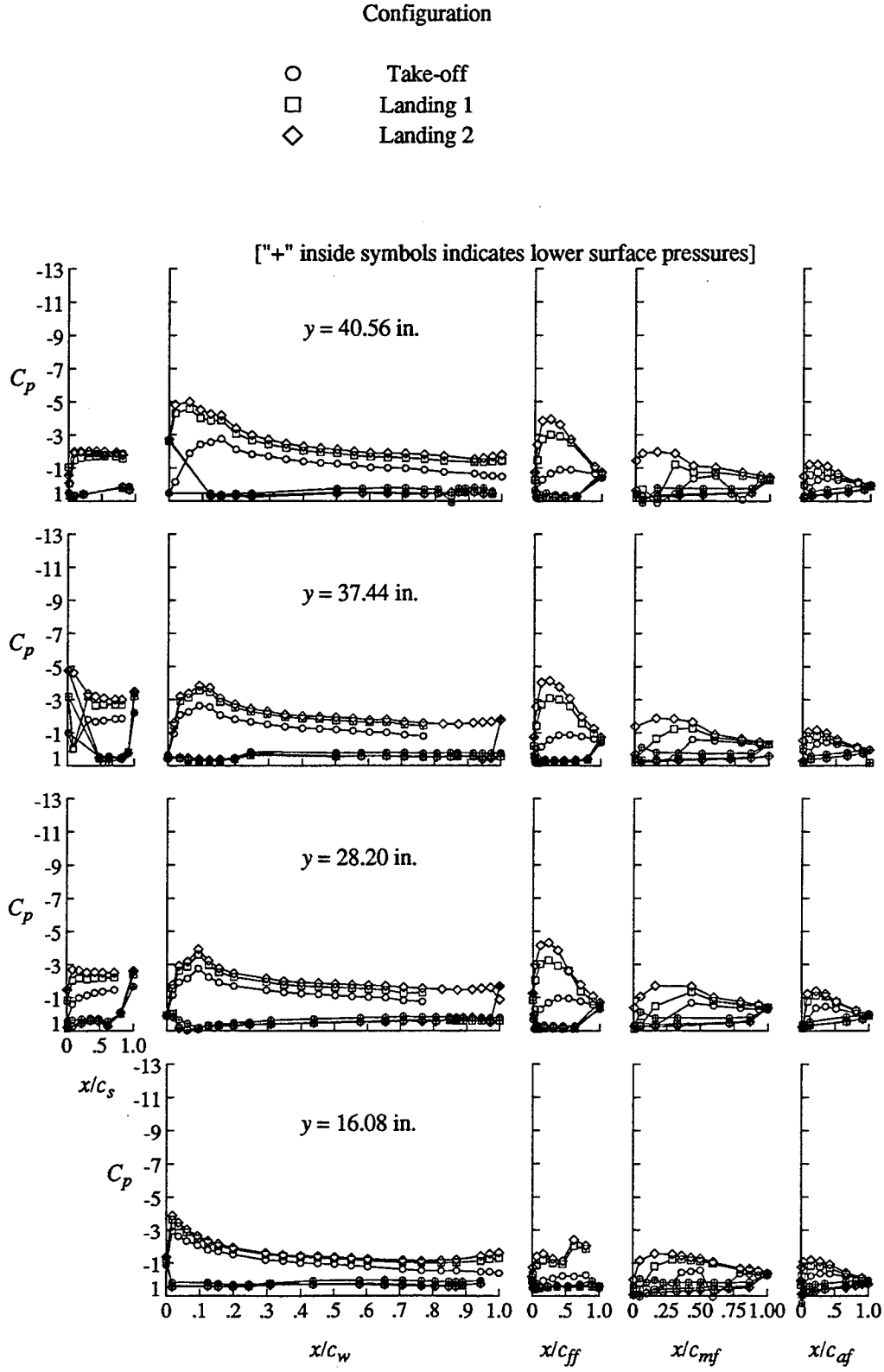

(c) $\alpha = 8°$.

Figure 6. Continued.

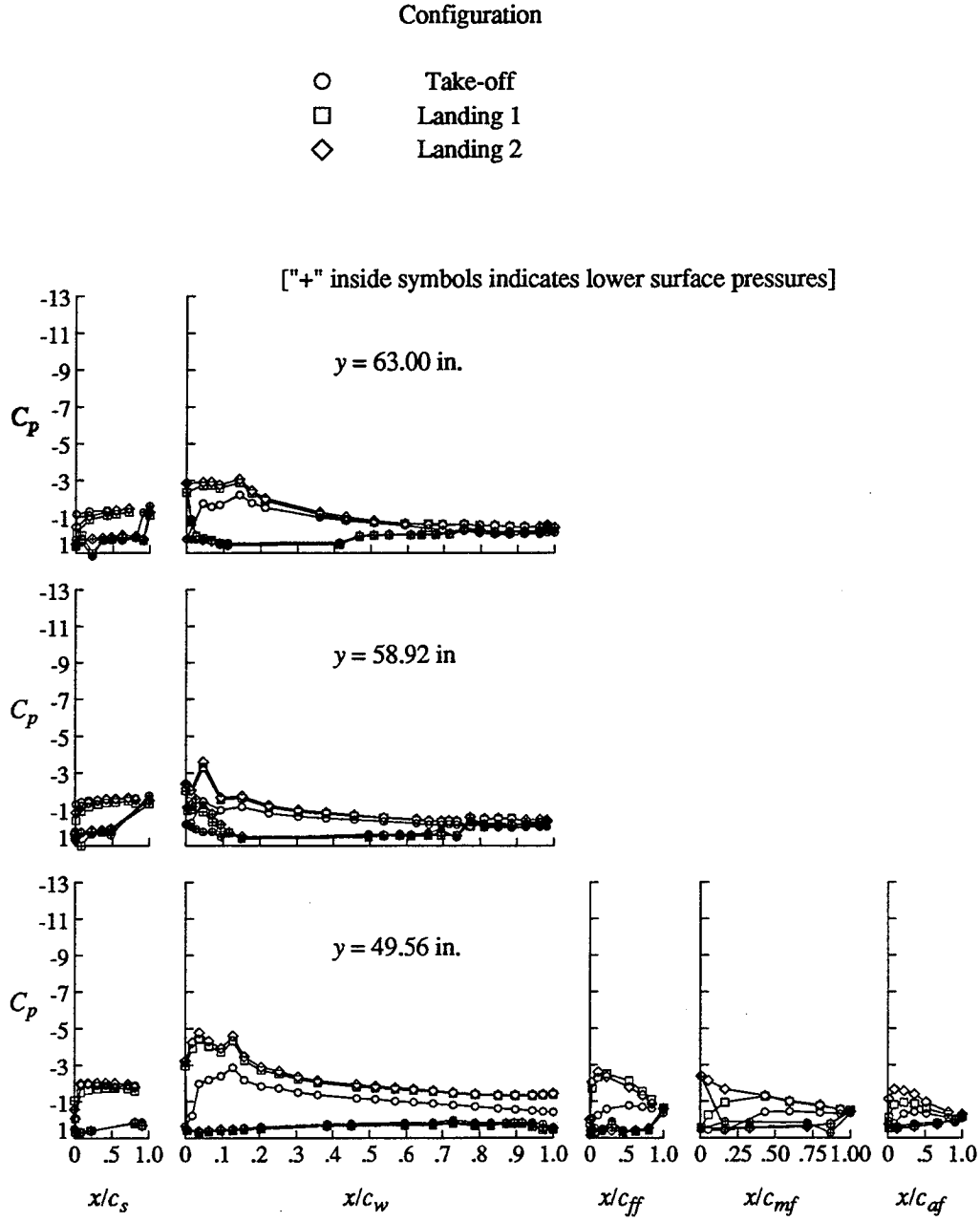

(c) $\alpha = 8°$.

Figure 6. Continued.

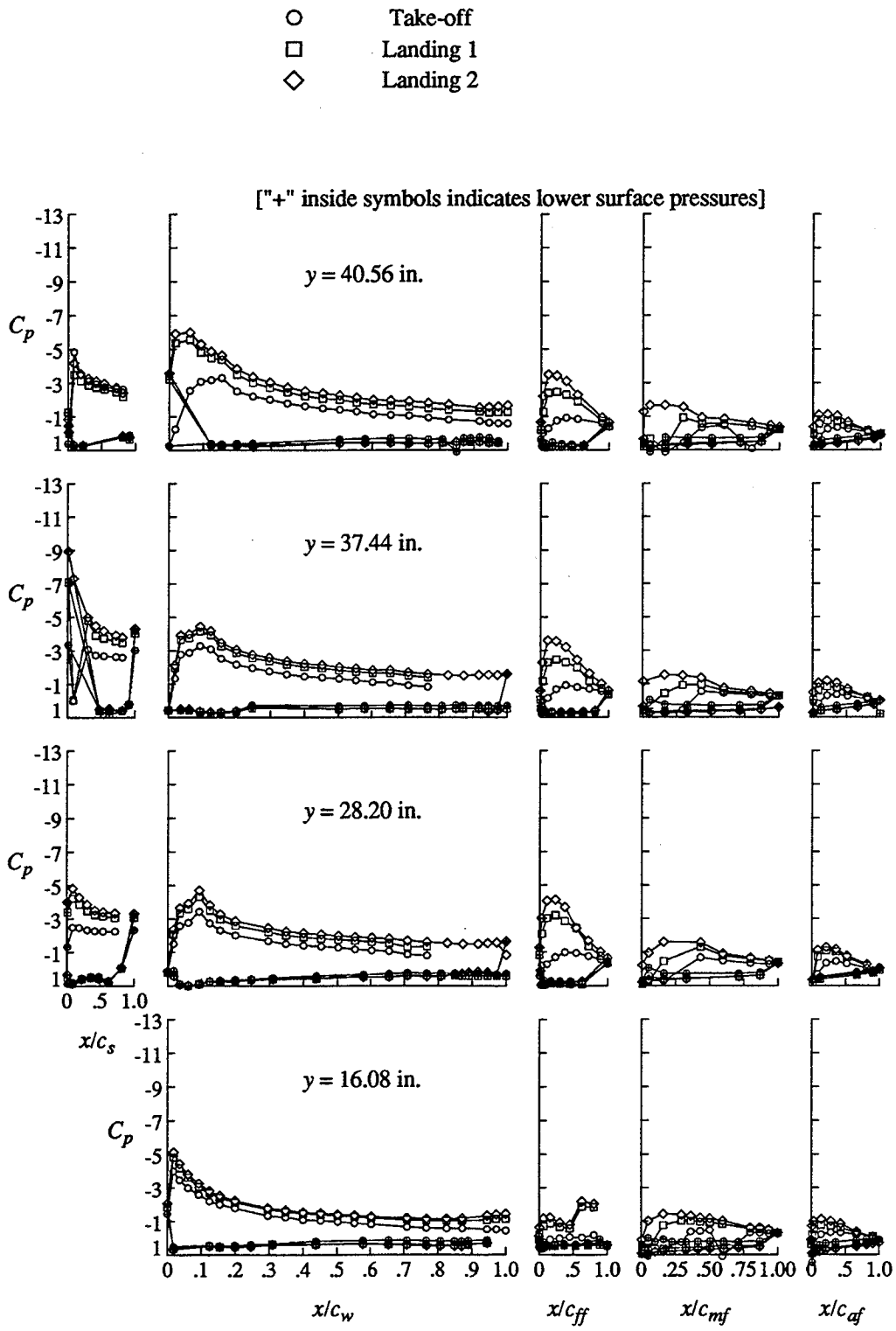

(d) $\alpha = 12°$.

Figure 6. Concluded.

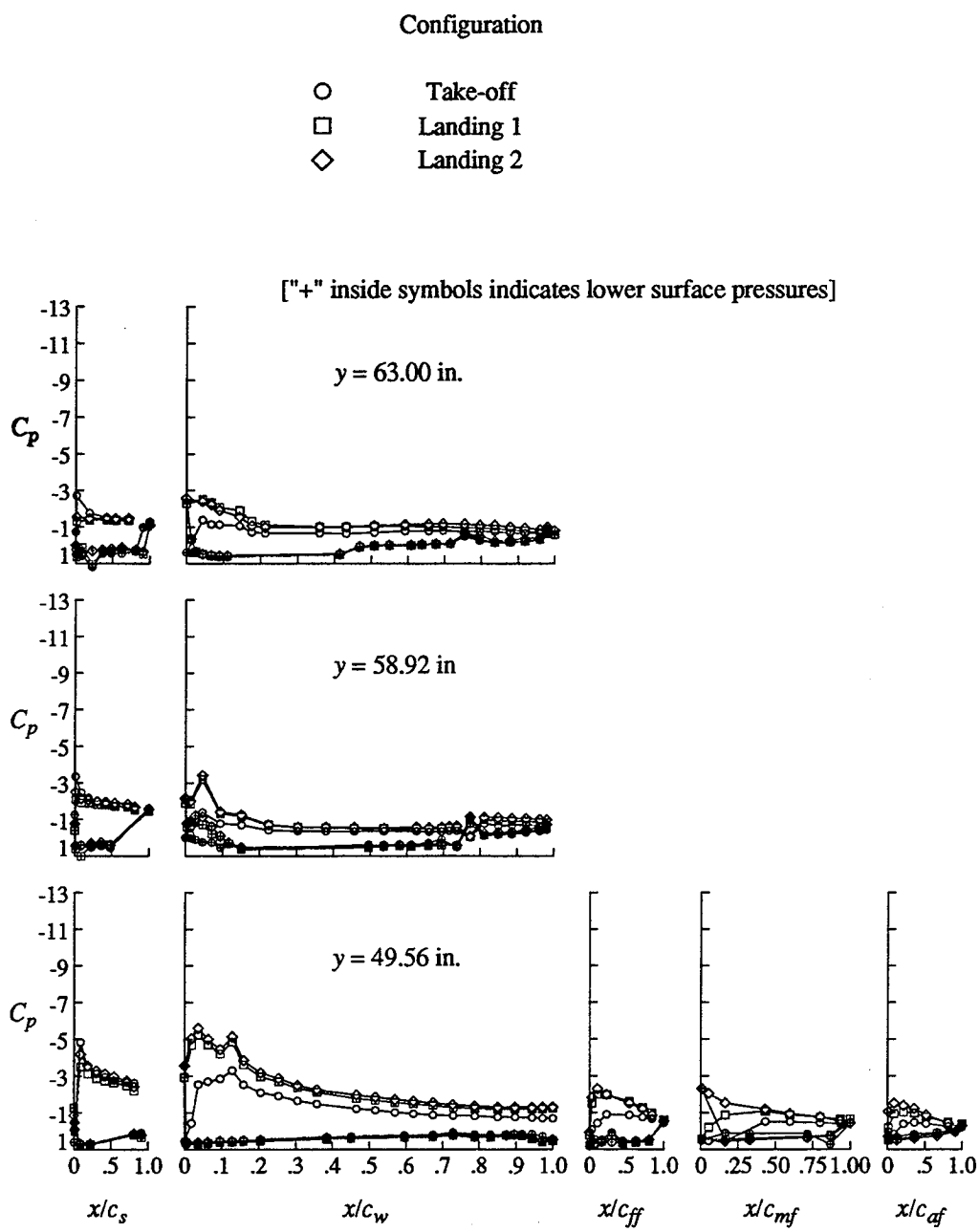

(d) $\alpha = 12°$.

Figure 6. Concluded.

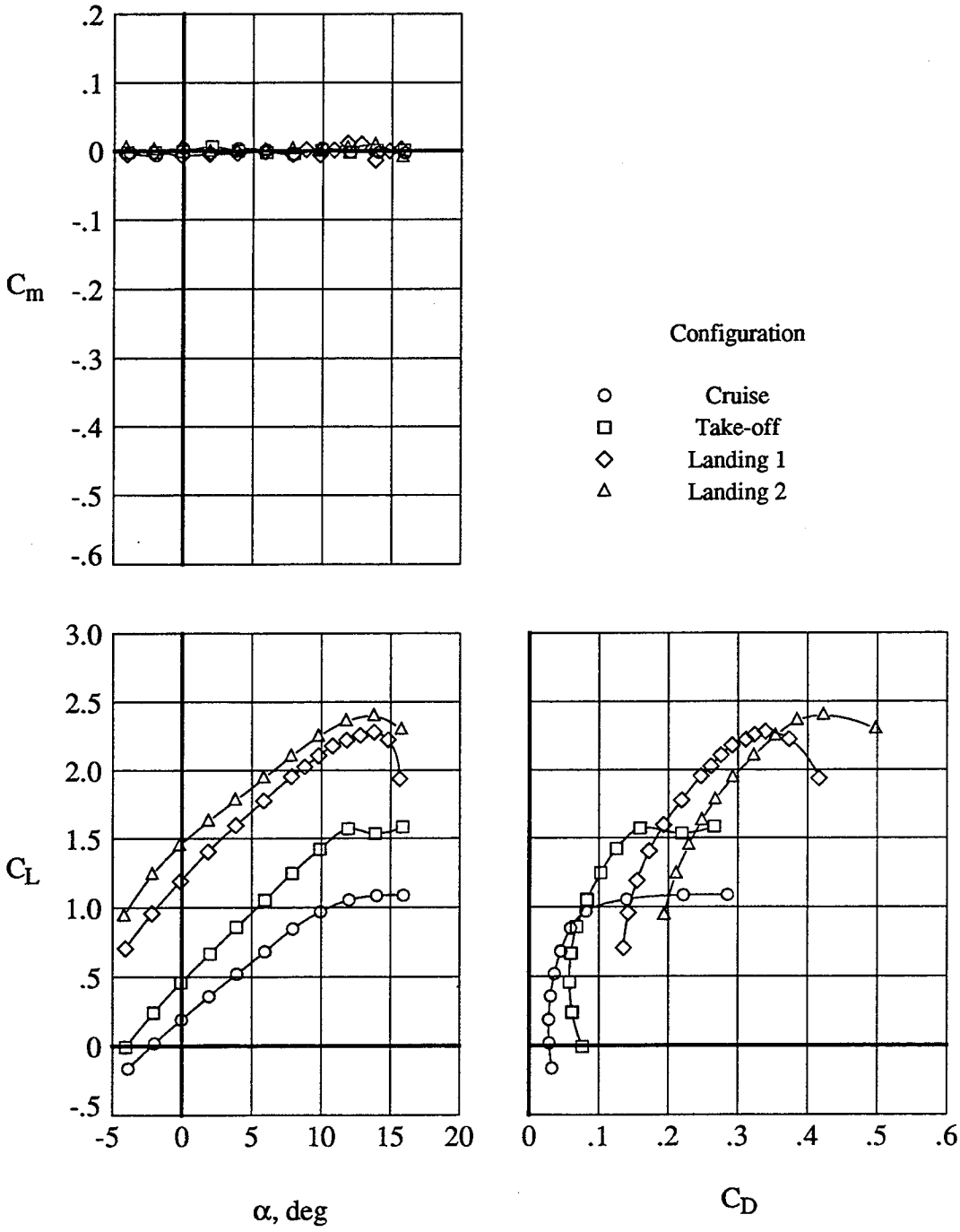

Figure 7. Trimmed longitudinal aerodynamic characteristics at $q_\infty = 40$ psf.

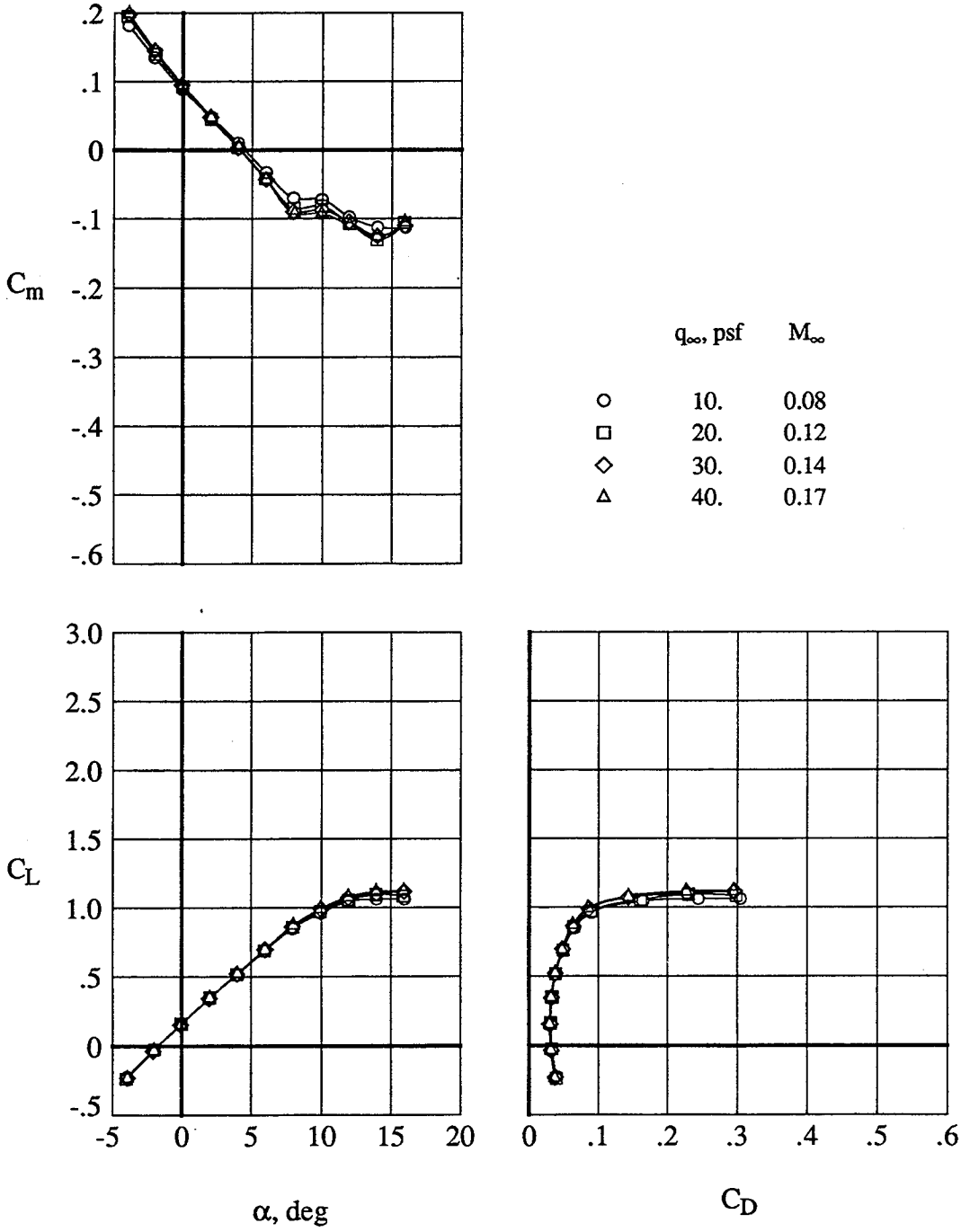

(a) Cruise configuration

Figure 8. Effect of tunnel speed on the longitudinal aerodynamic characteristics.

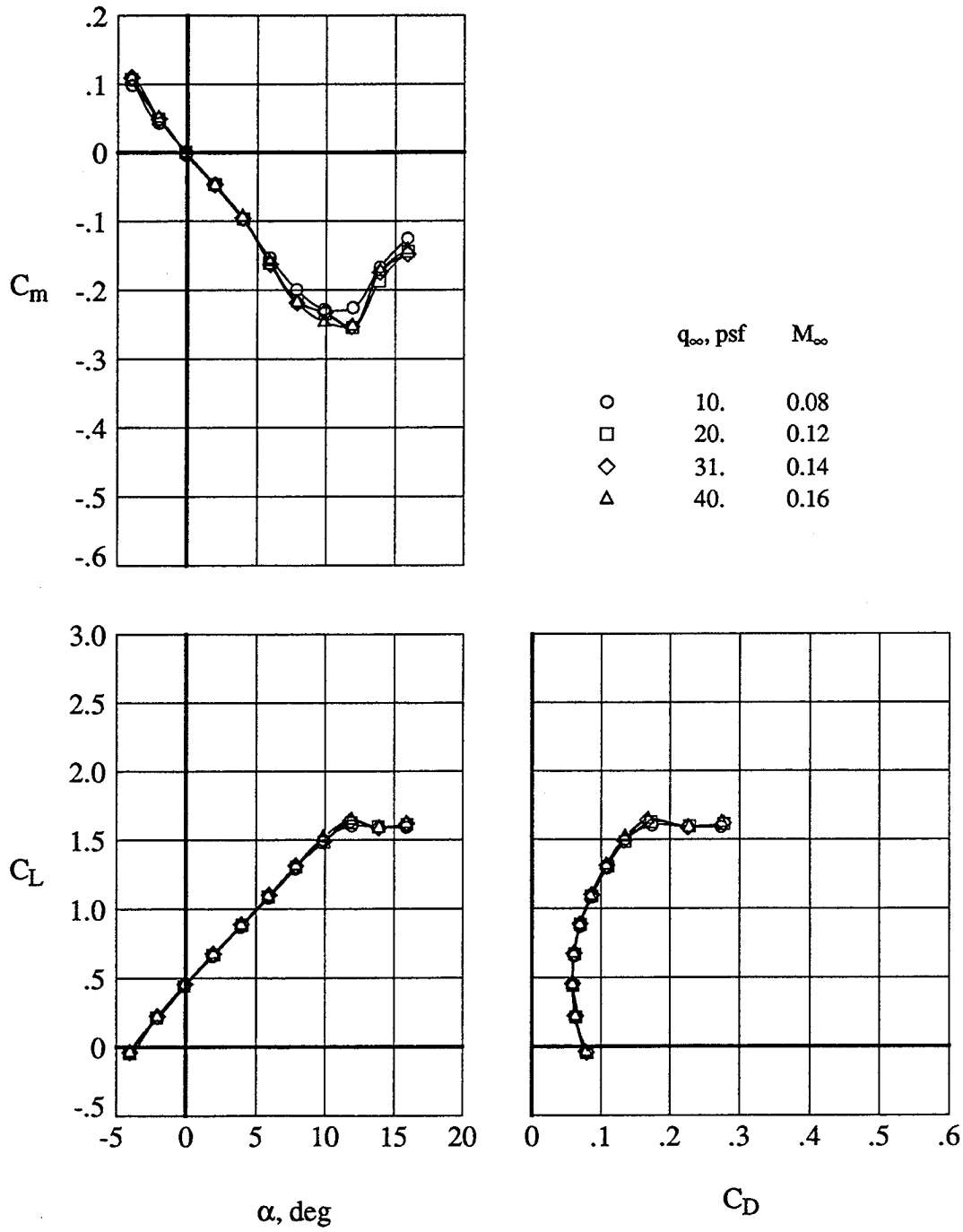

(b) Take-off configuration

Figure 8. Continued.

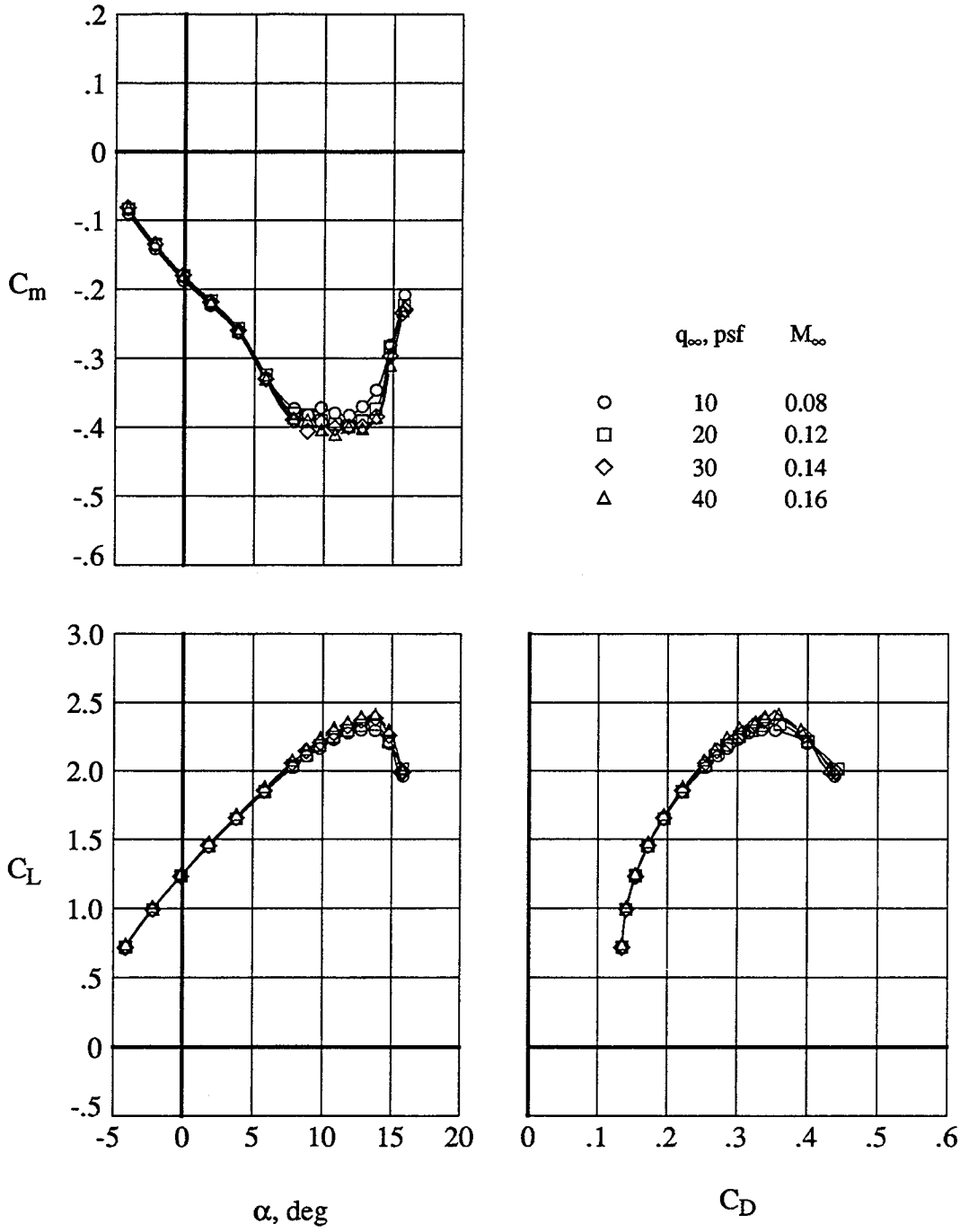

(c) Landing 1 configuration

Figure 8. Continued.

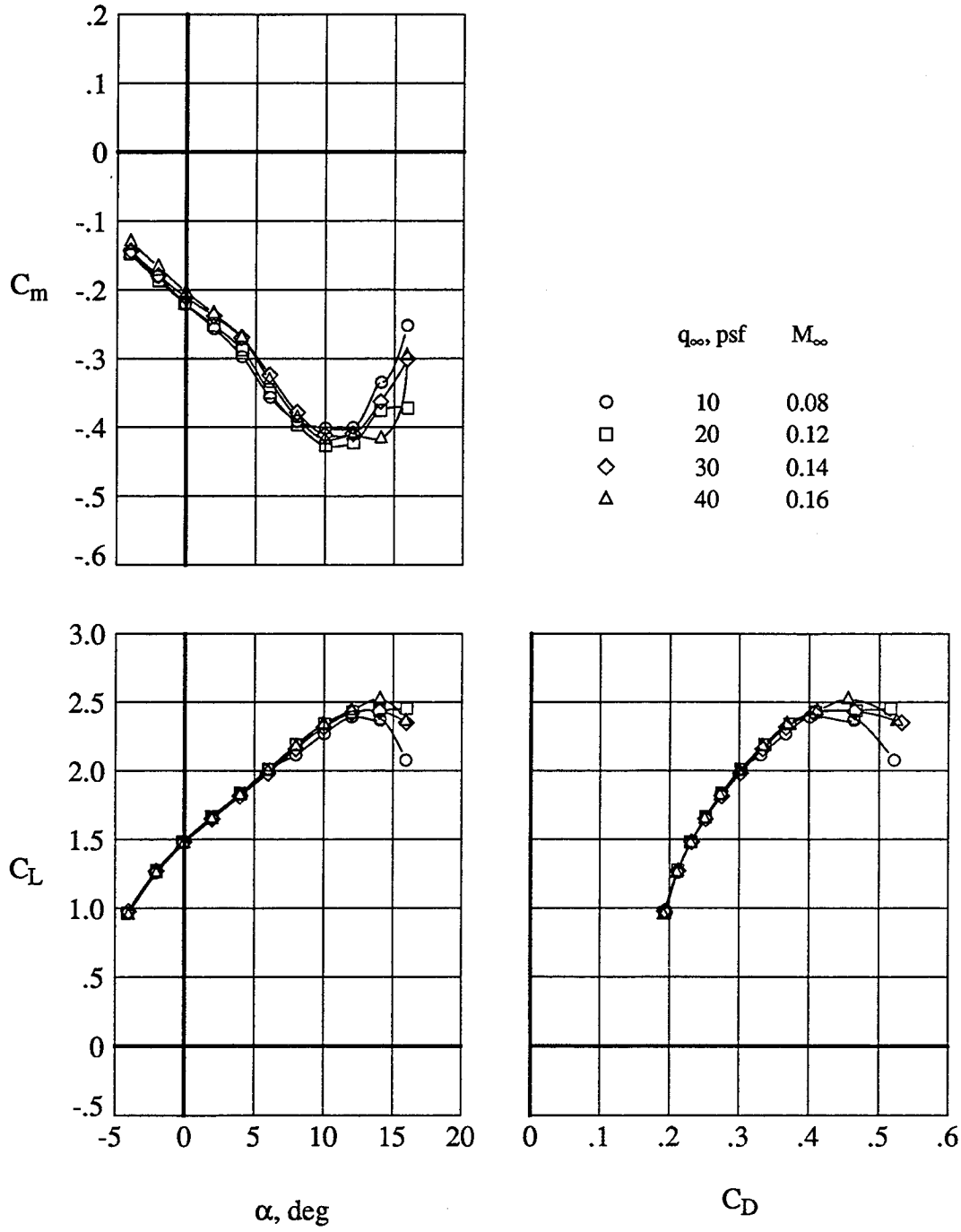

(d) Landing 2 configuration

Figure 8. Concluded.

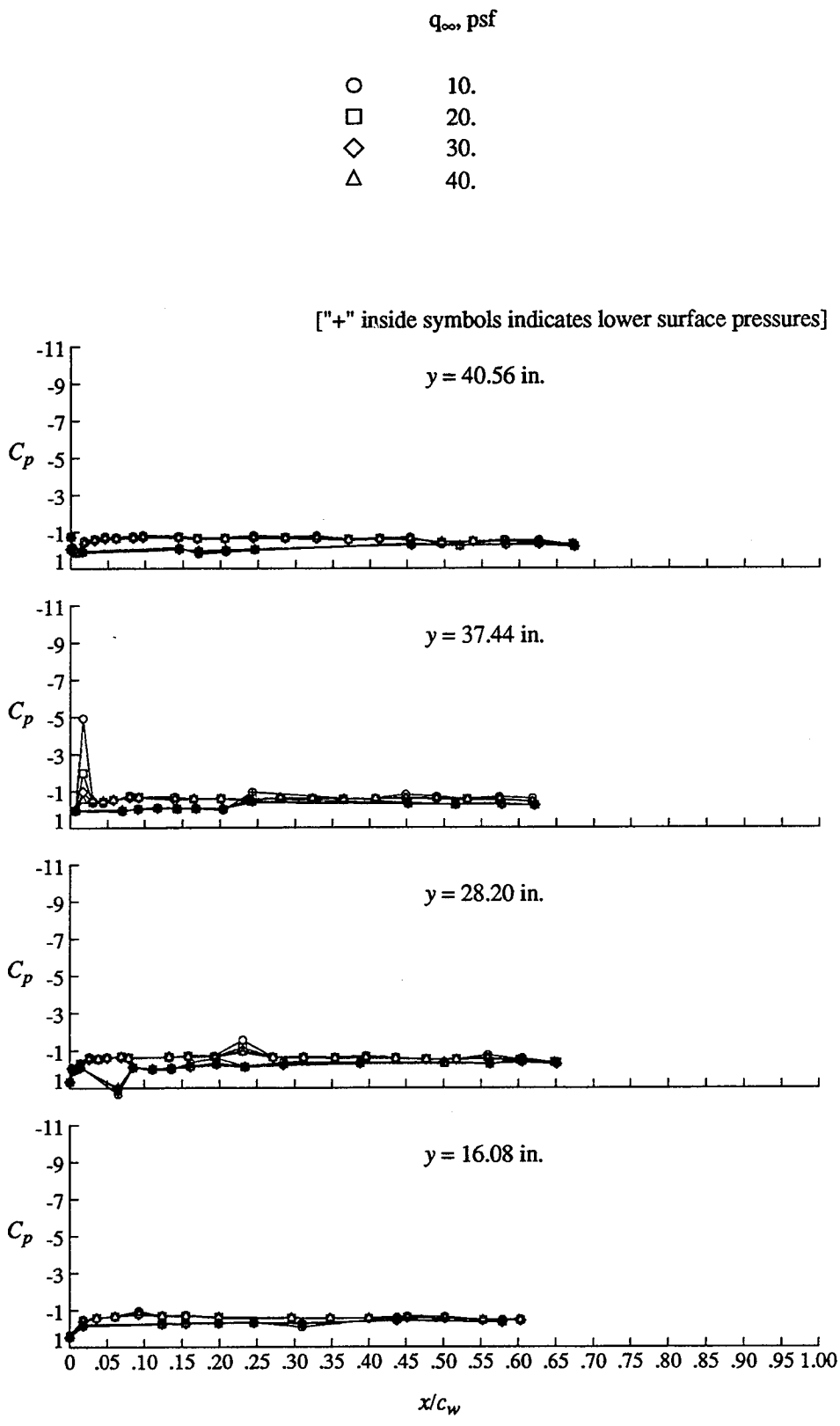

(a) $\alpha = 0°$.

Figure 9. Effect of tunnel speed on wing pressure distributions for Cruise configuration.

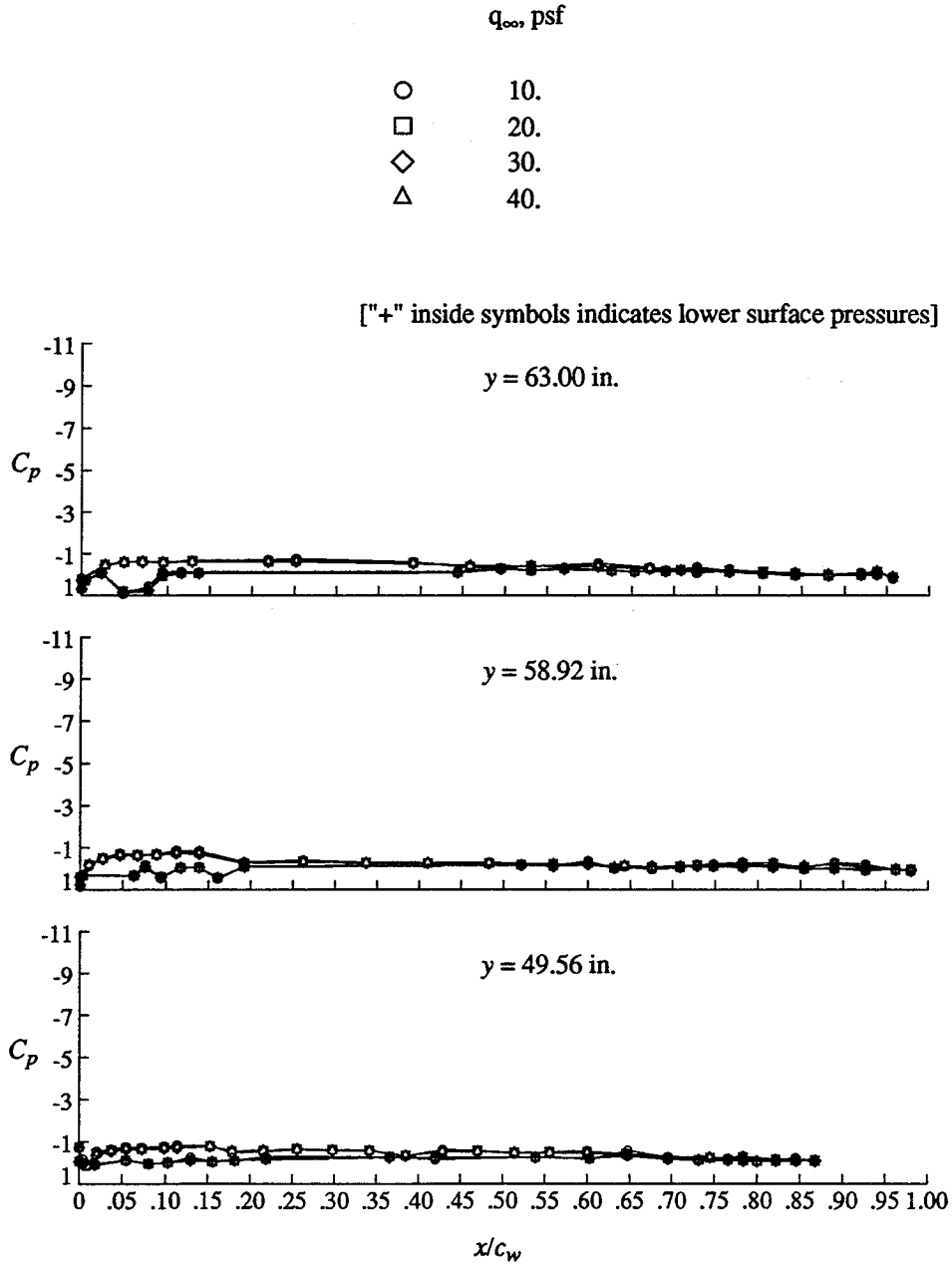

(a) $\alpha = 0°$.

Figure 9. Continued.

q_∞, psf

○	10.
□	20.
◇	30.
△	40.

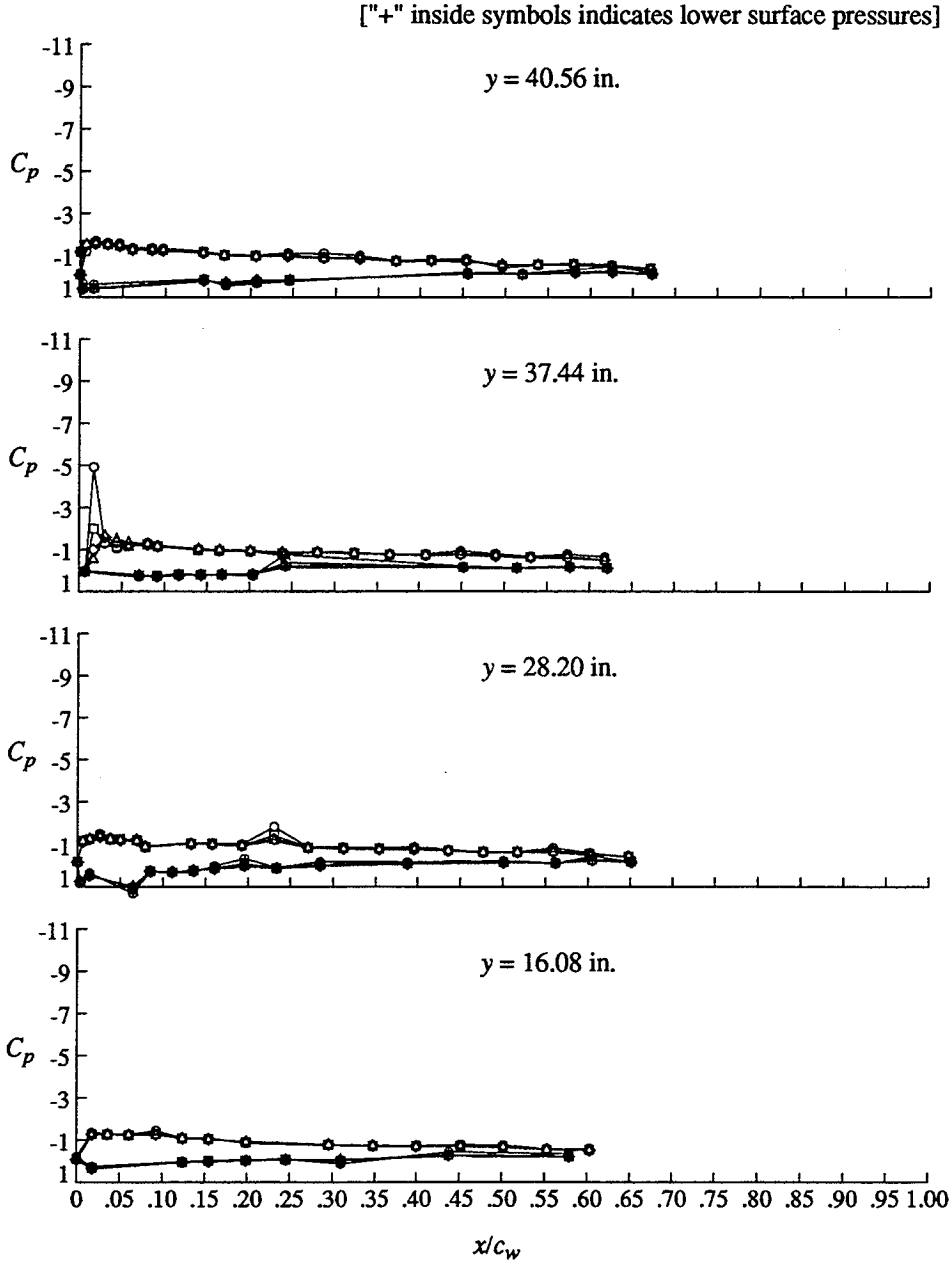

(b) $\alpha = 4°$.

Figure 9. Continued.

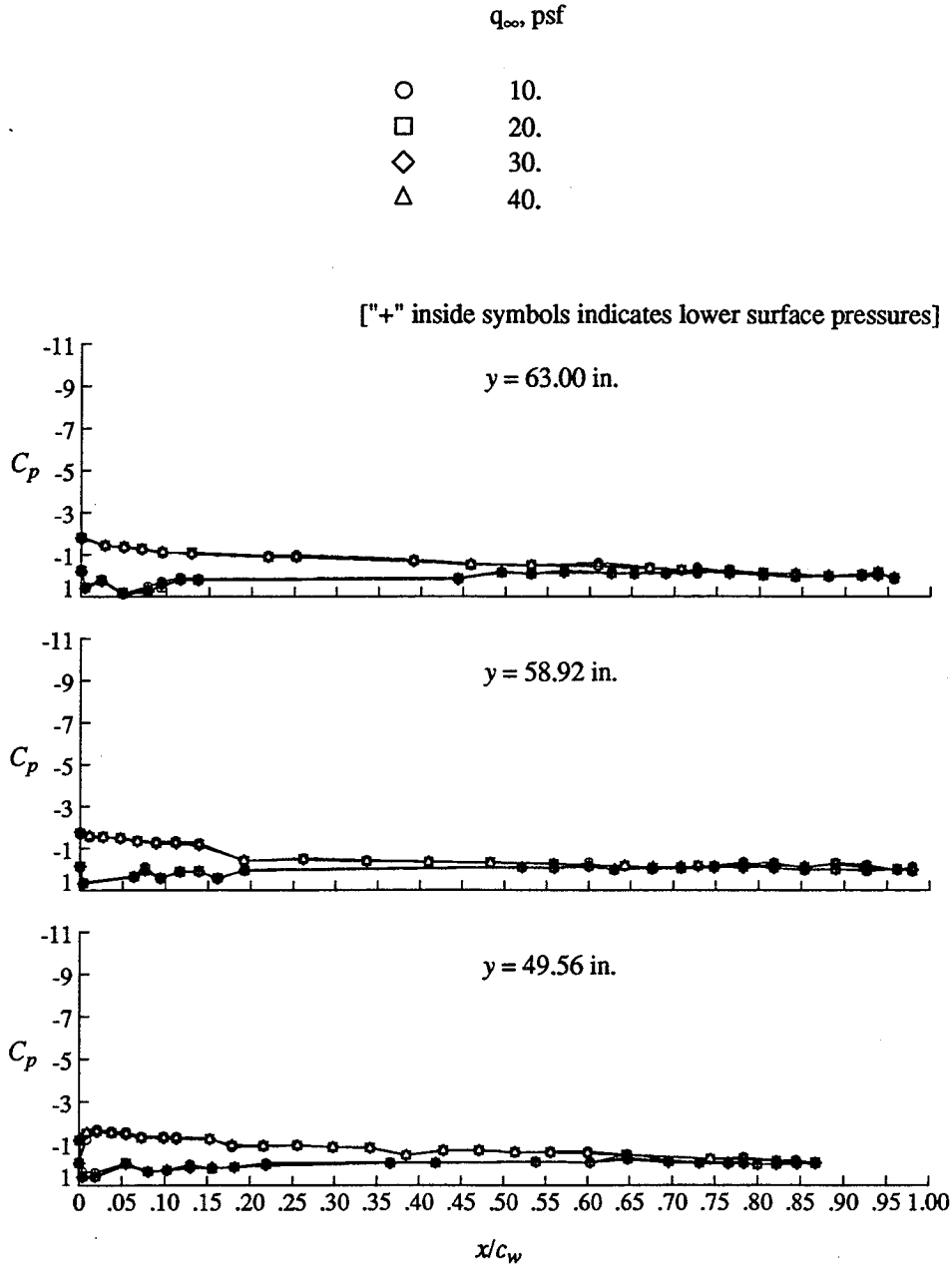

(b) $\alpha = 4°$.

Figure 9. Continued.

q_∞, psf

○	10.
□	20.
◇	30.
△	40.

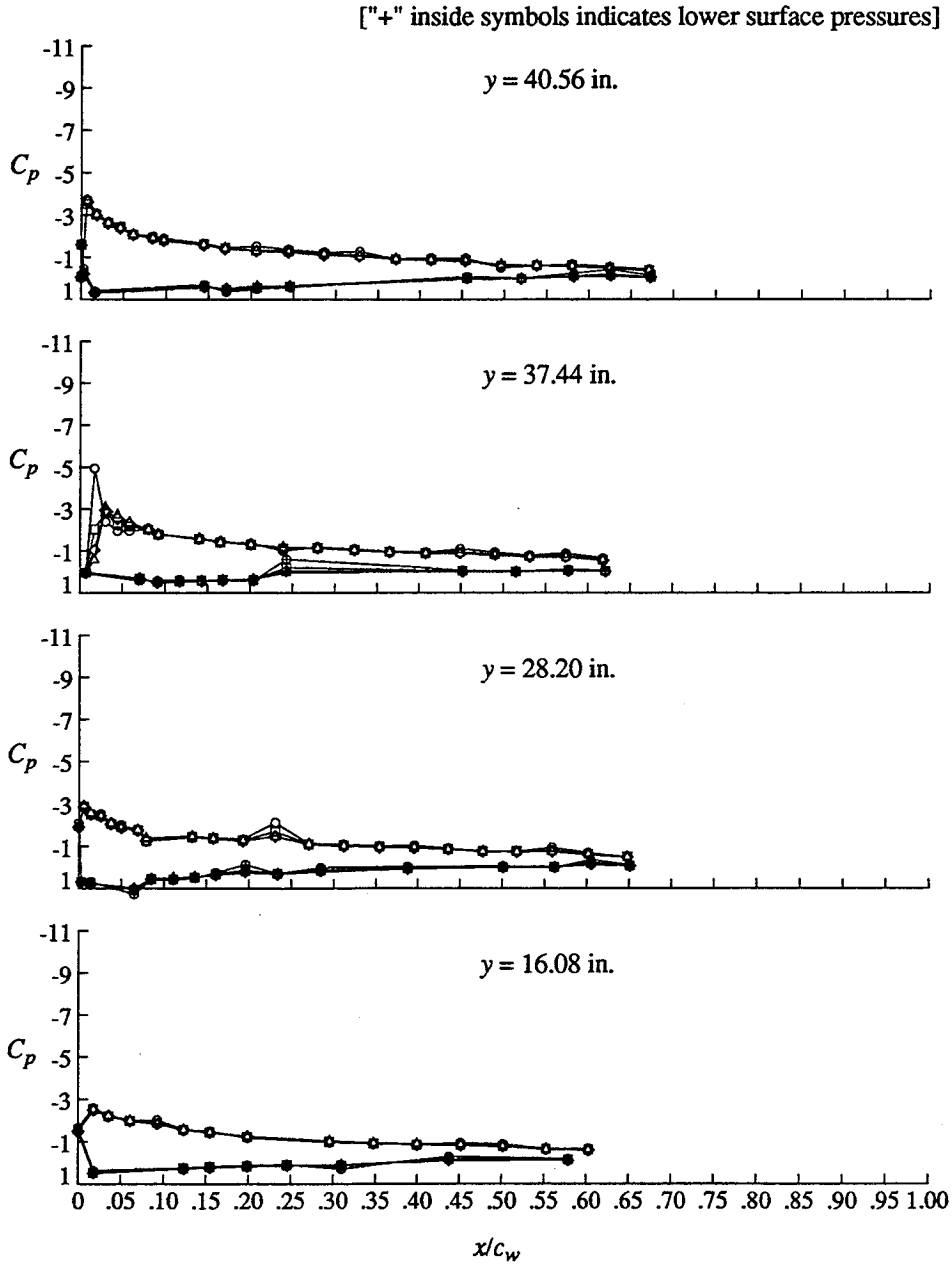

(c) $\alpha = 8°$.

Figure 9. Continued.

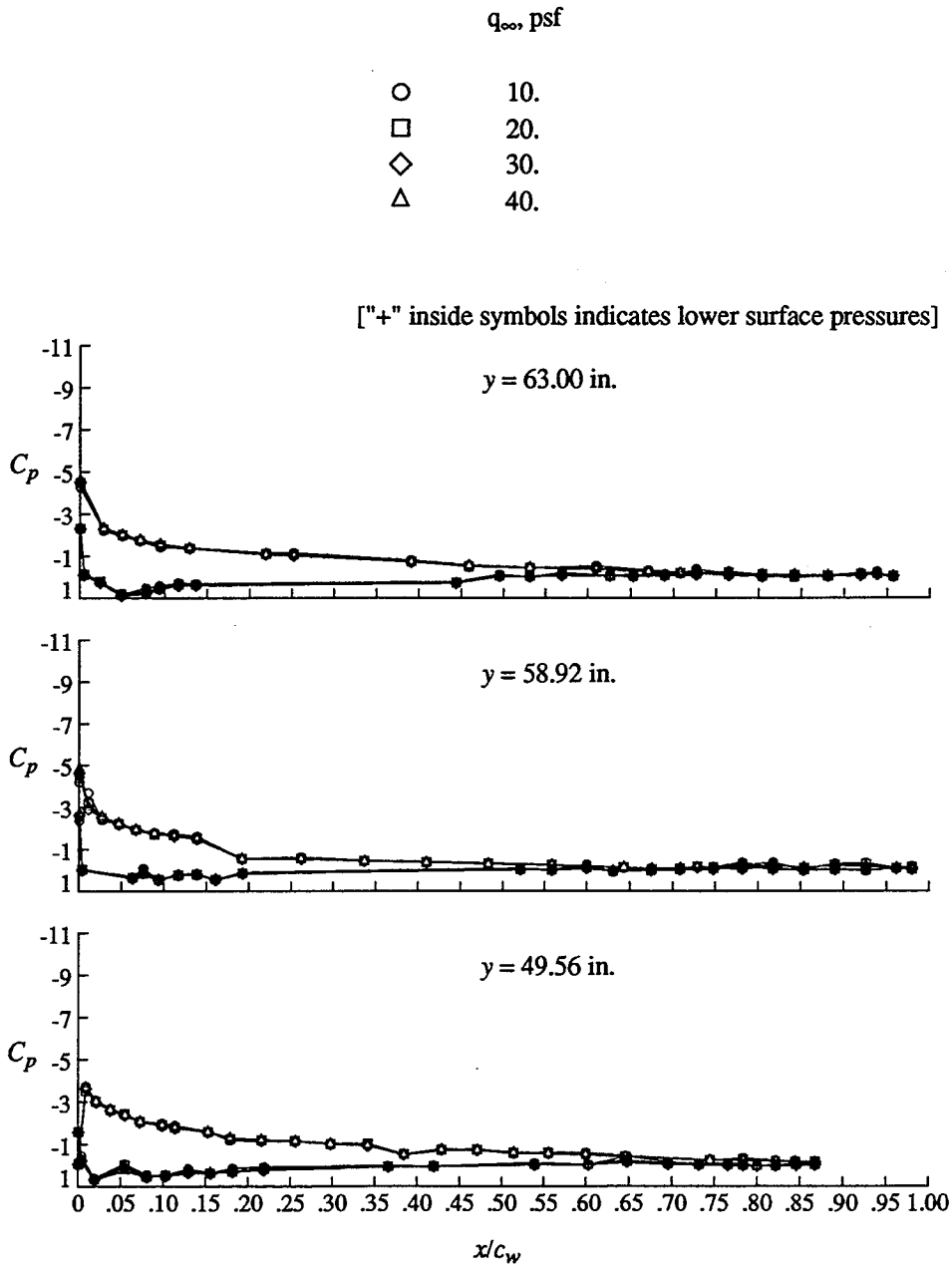

(c) $\alpha = 8°$.

Figure 9. Continued.

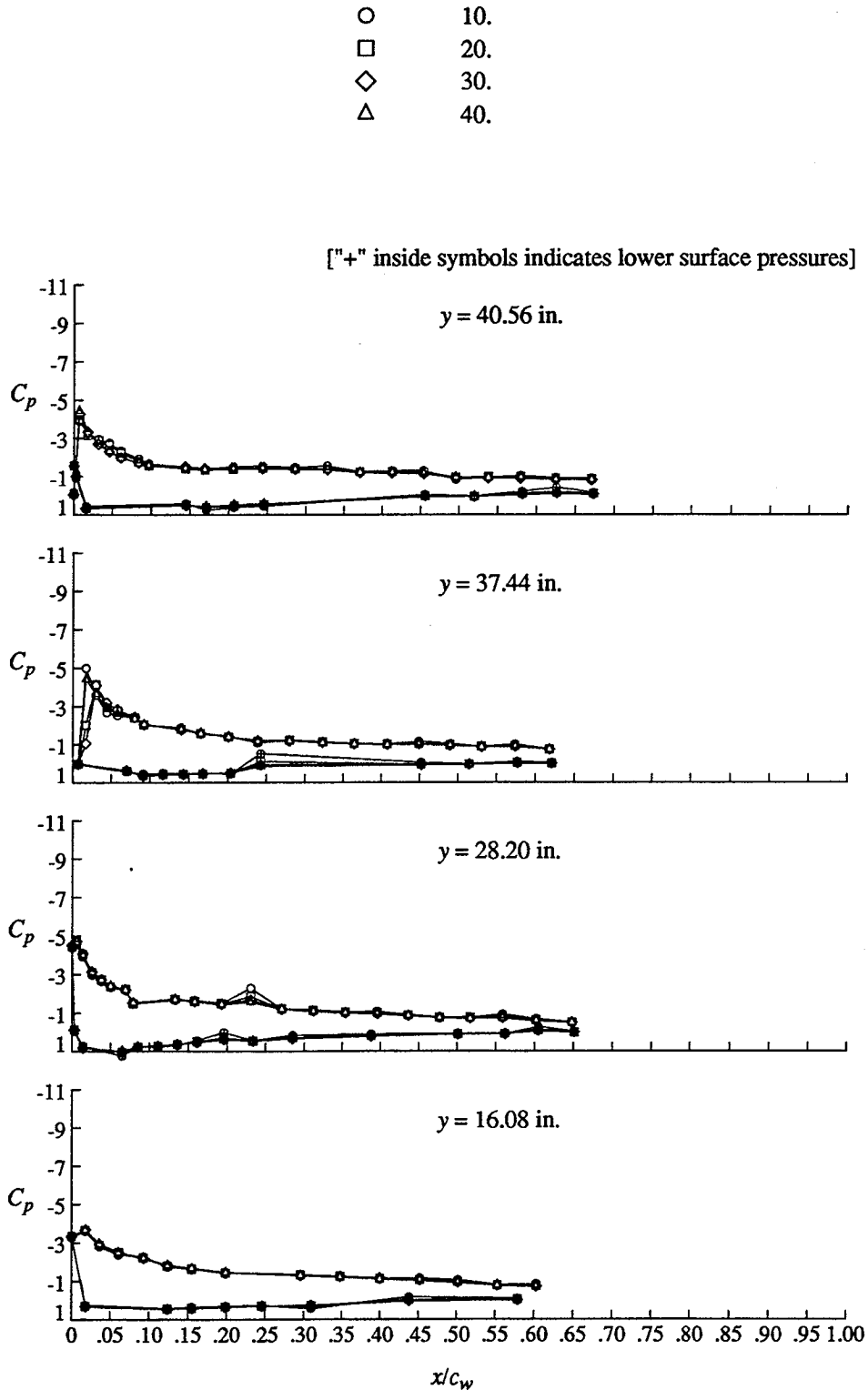

(d) $\alpha = 12°$.

Figure 9. Concluded.

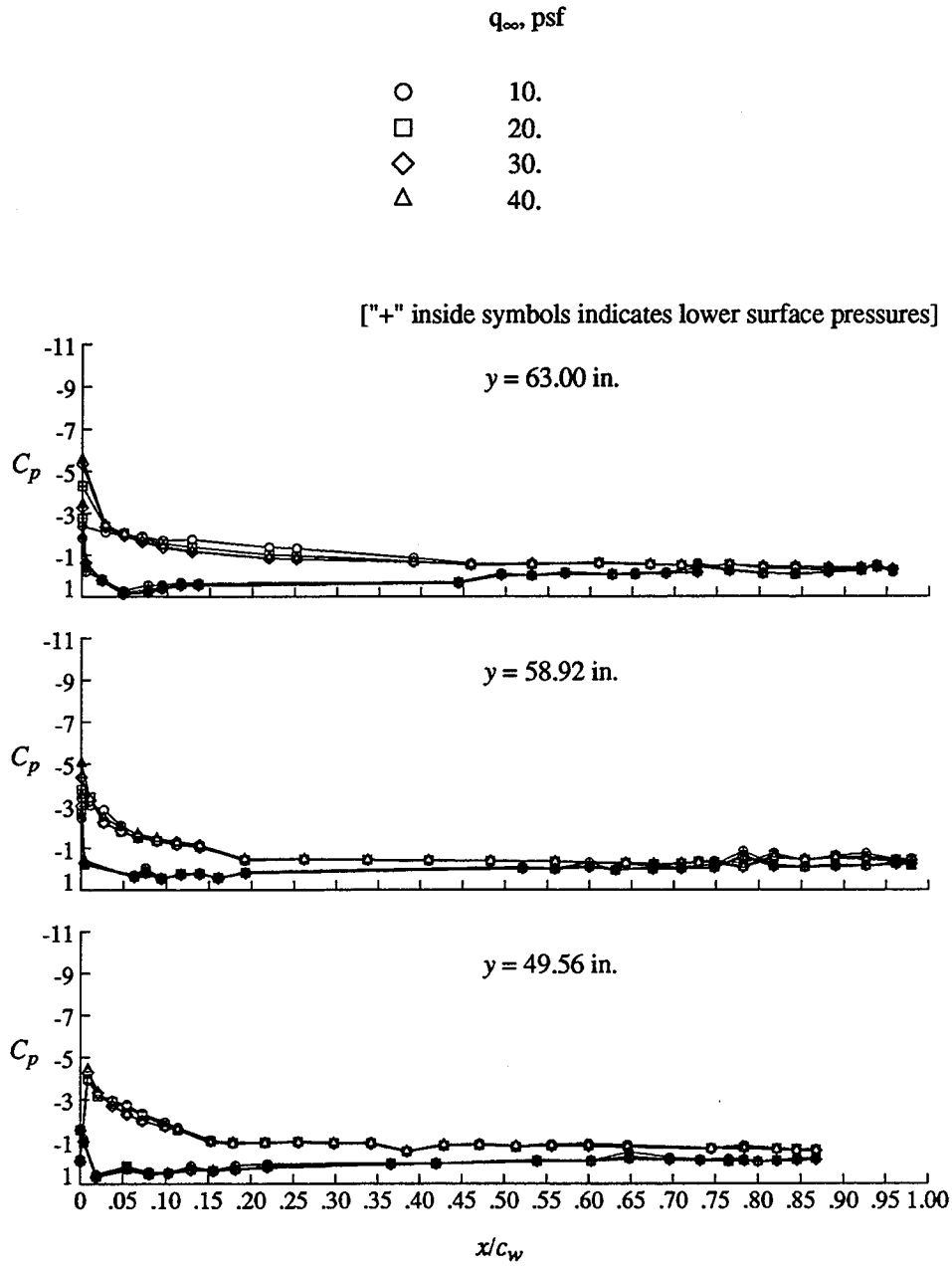

(d) $\alpha = 12°$.

Figure 9. Concluded.

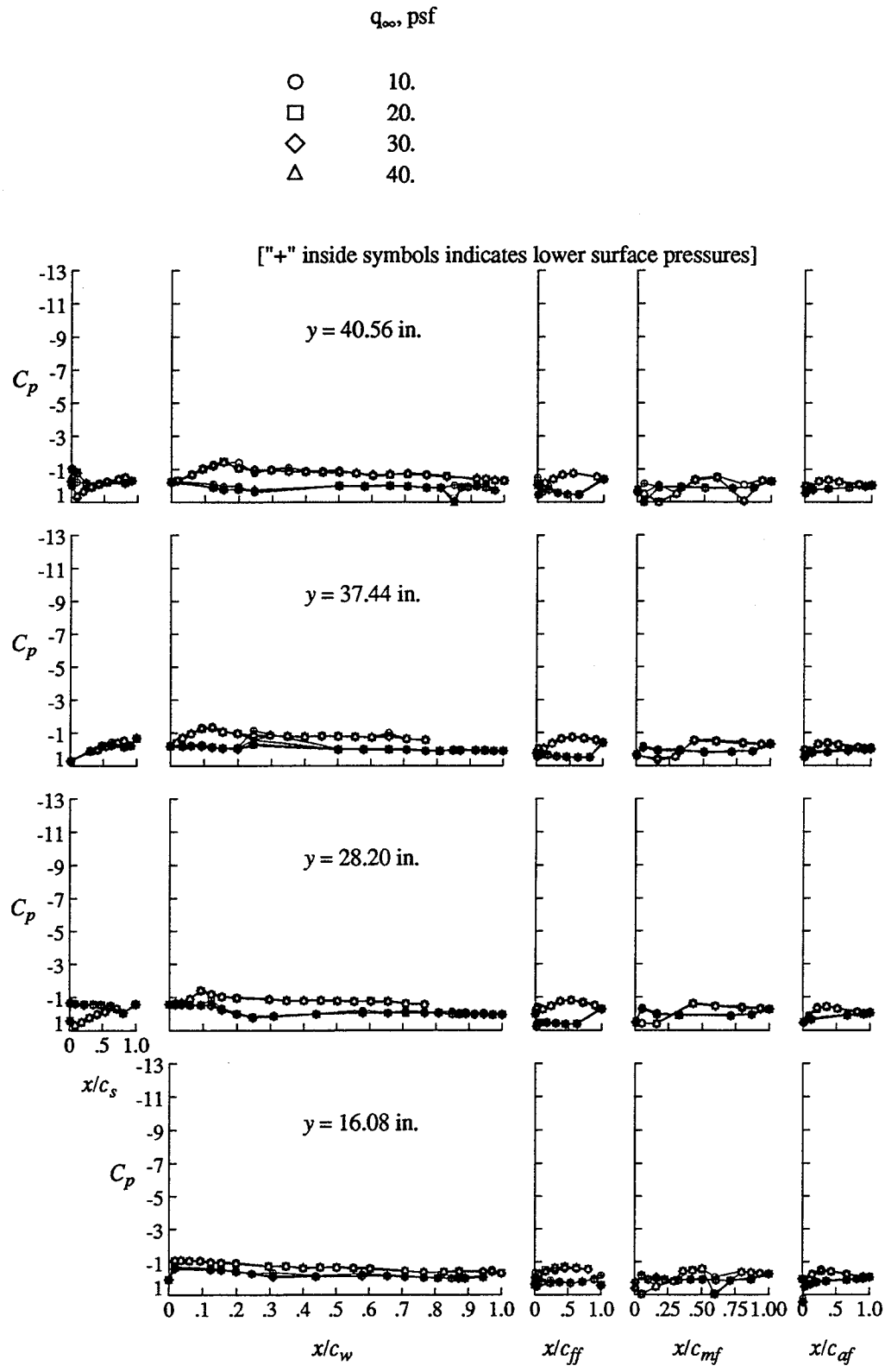

(a) $\alpha = 0°$.

Figure 10. Effect of tunnel speed on the wing pressure distributions of Take-off configuration.

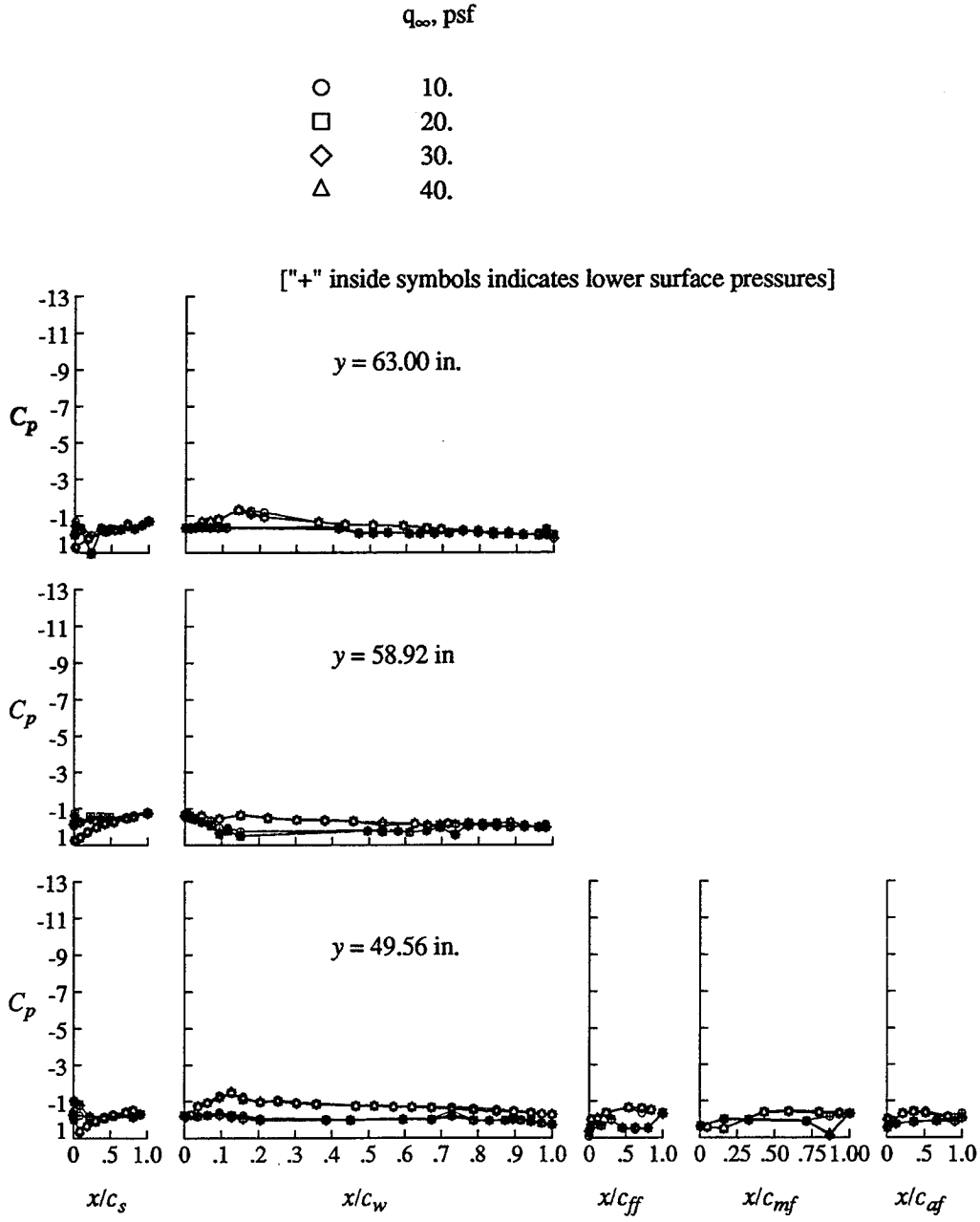

(a) $\alpha = 0°$.

Figure 10. Continued.

q_∞, psf

○	10.
□	20.
◇	30.
△	40.

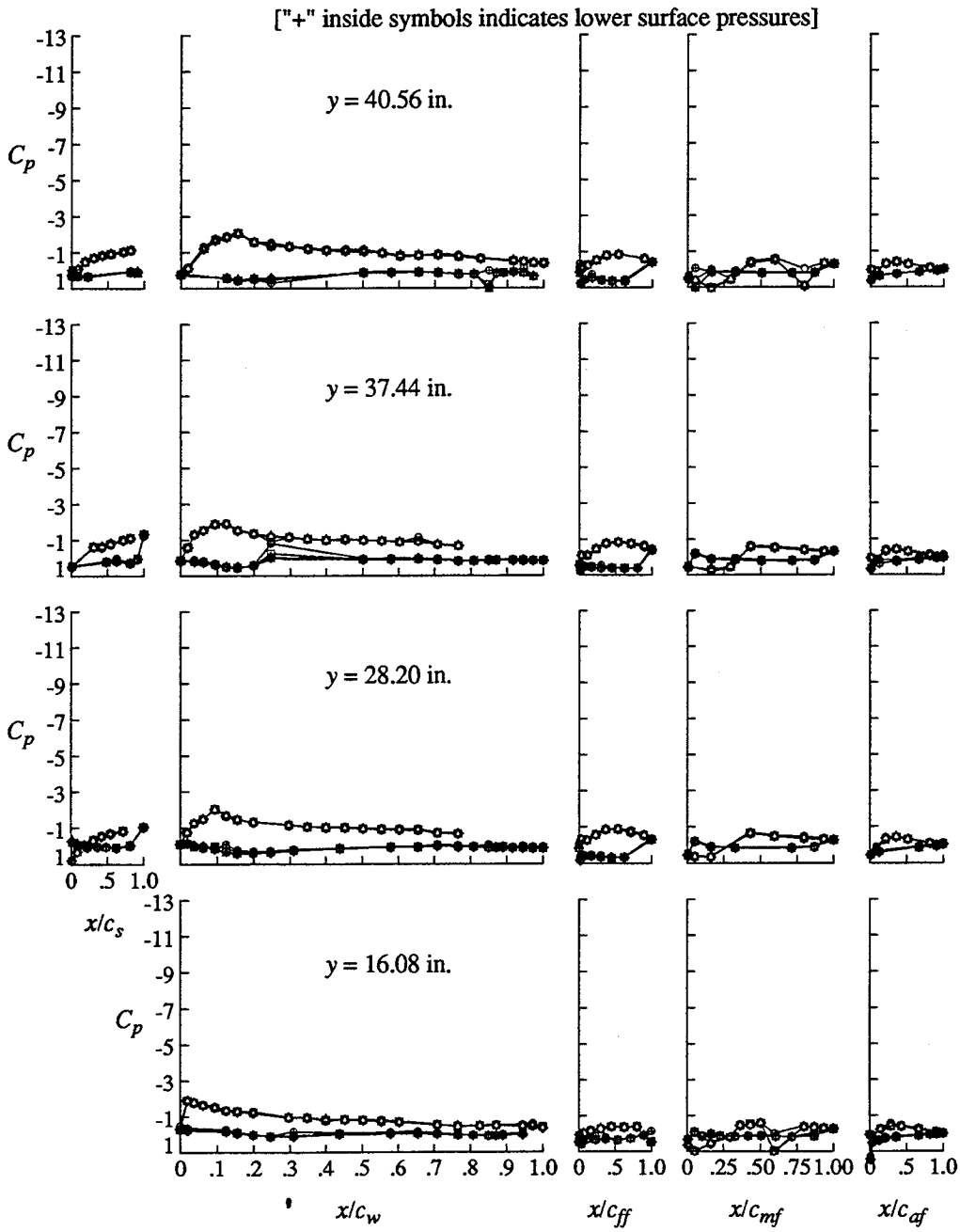

(b) $\alpha = 4°$.

Figure 10. Continued.

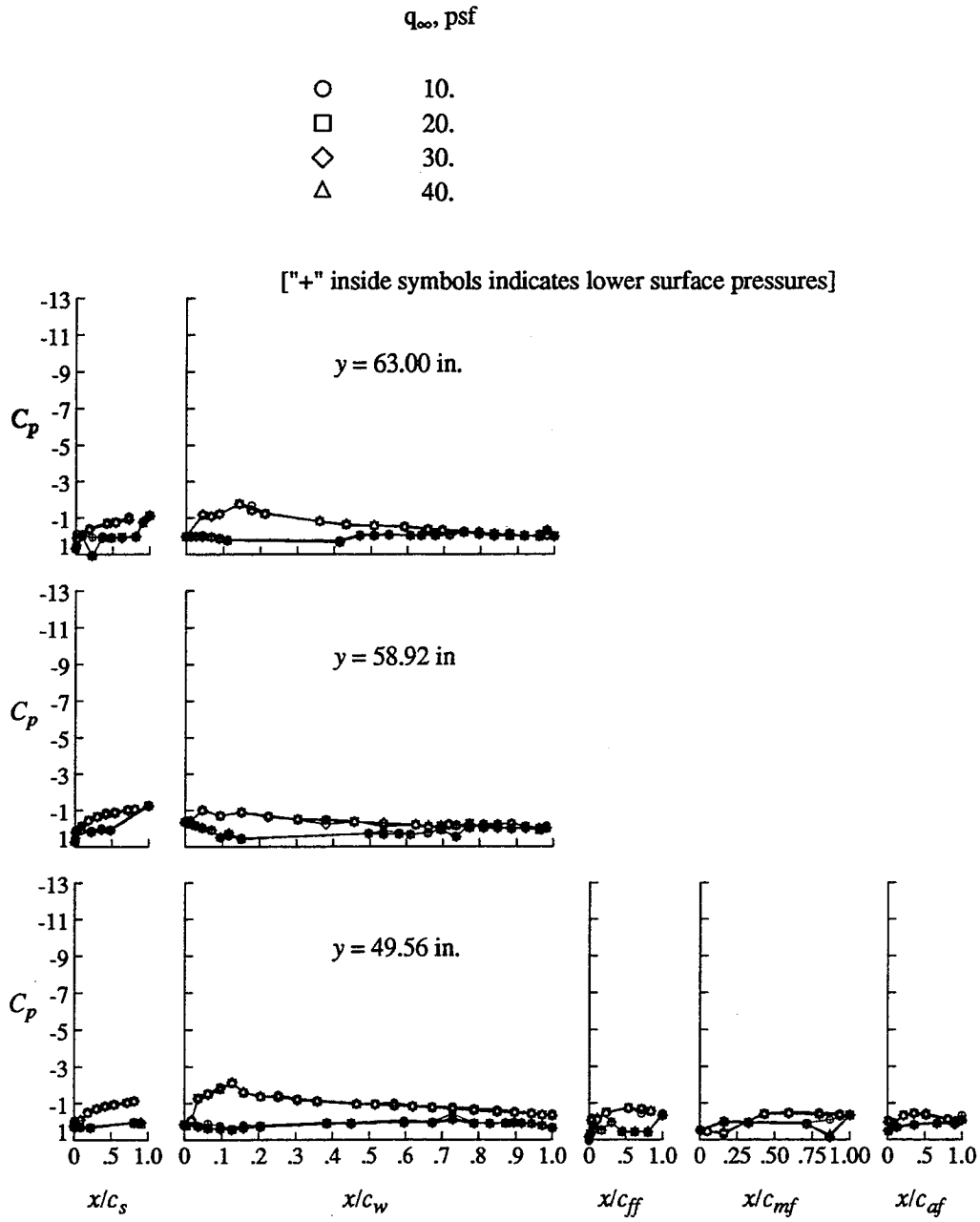

(b) $\alpha = 4°$.

Figure 10. Continued.

q_∞, psf

○	10.
□	20.
◇	30.
△	40.

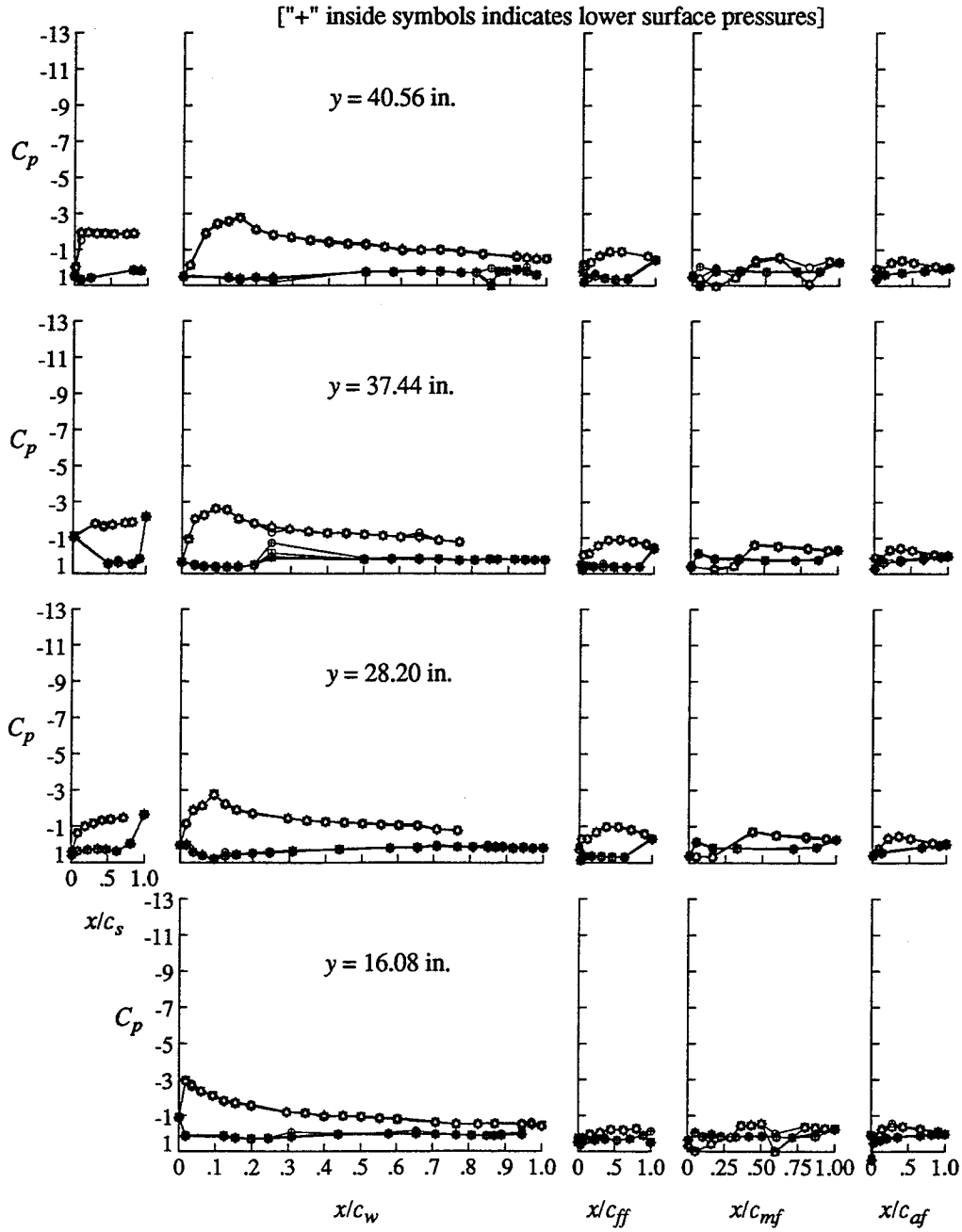

(c) $\alpha = 8°$.

Figure 10. Continued.

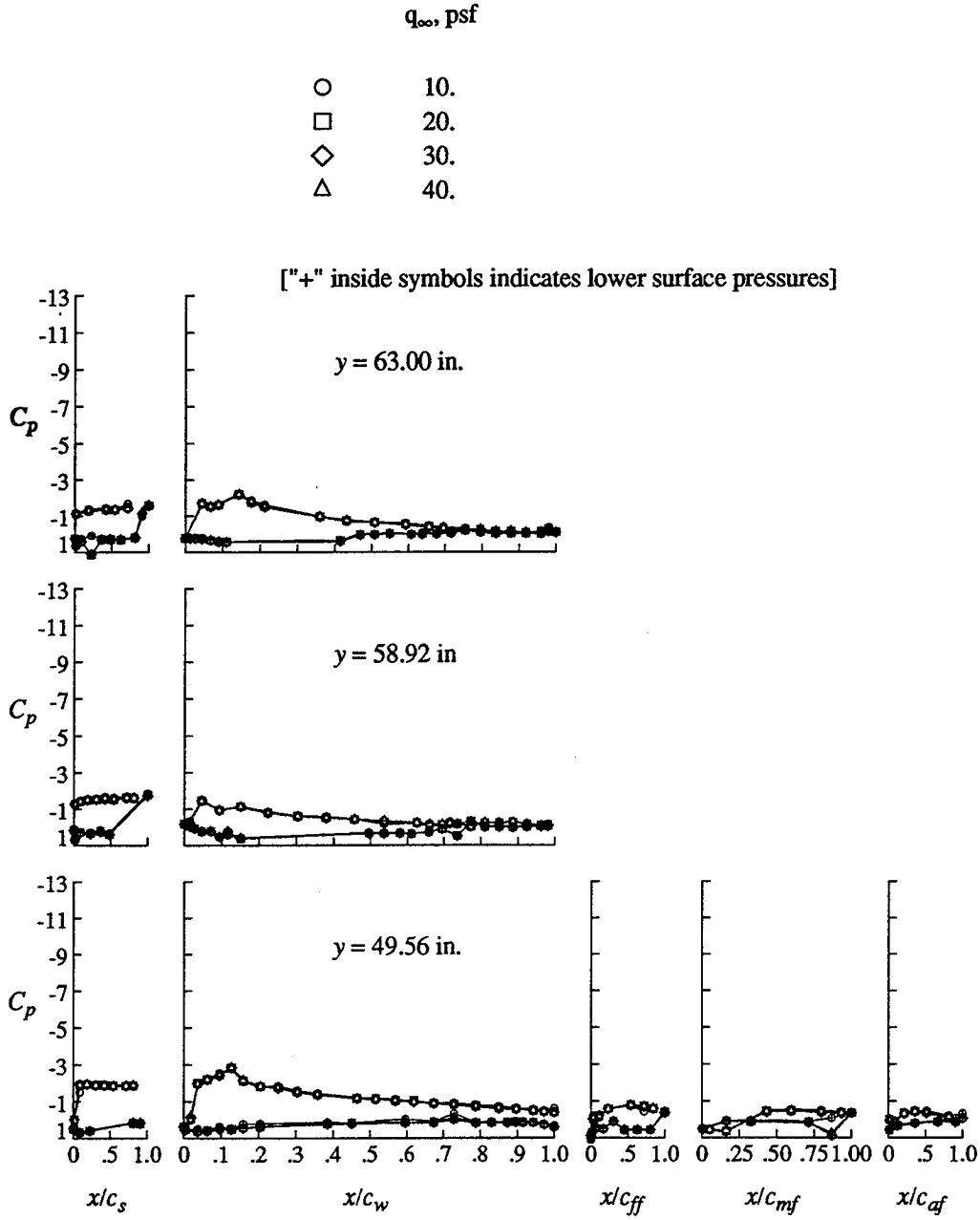

(c) $\alpha = 8°$.

Figure 10. Continued.

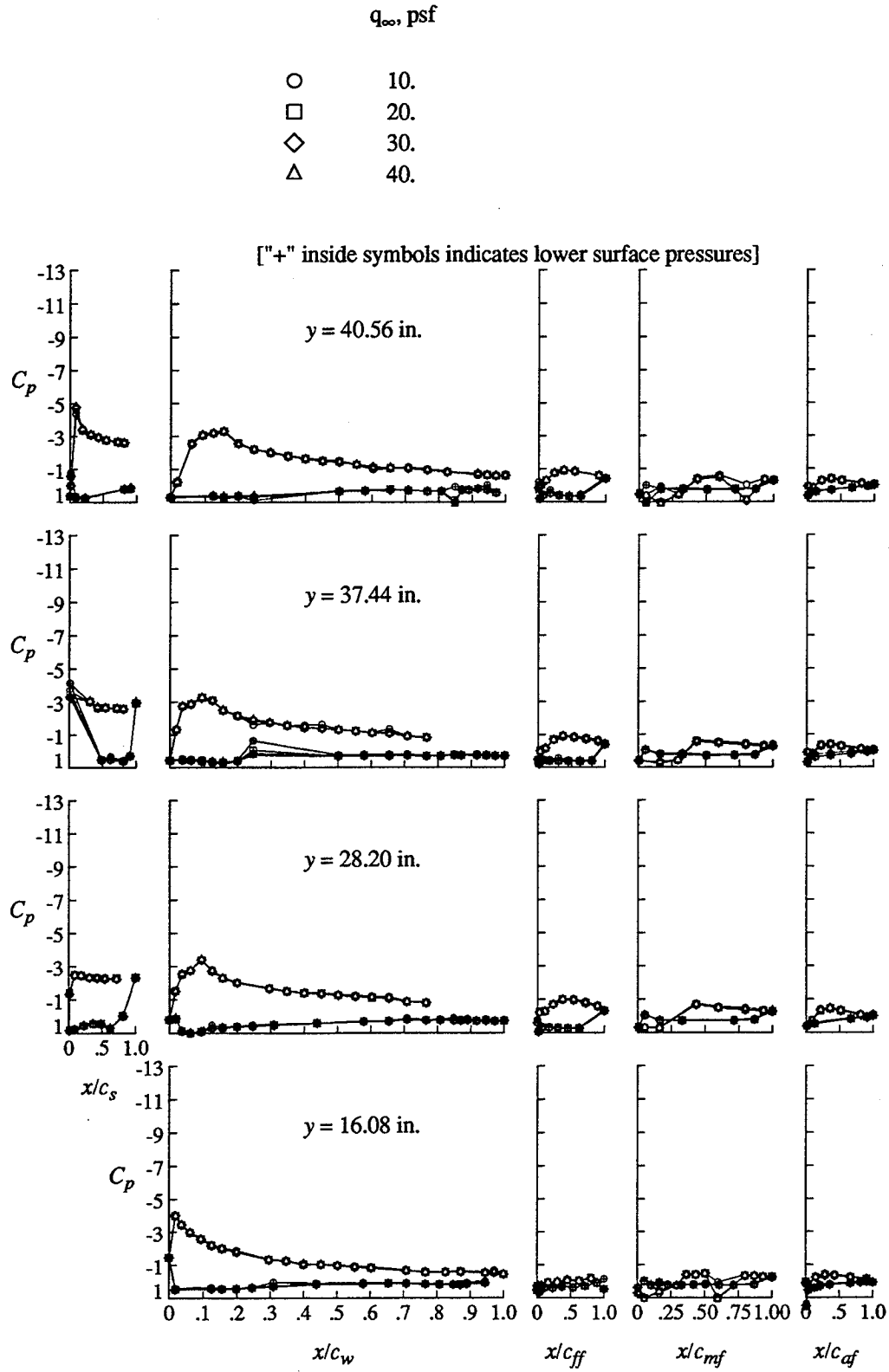

(d) $\alpha = 12°$.

Figure 10. Concluded.

q_∞, psf

○	10.
□	20.
◇	30.
△	40.

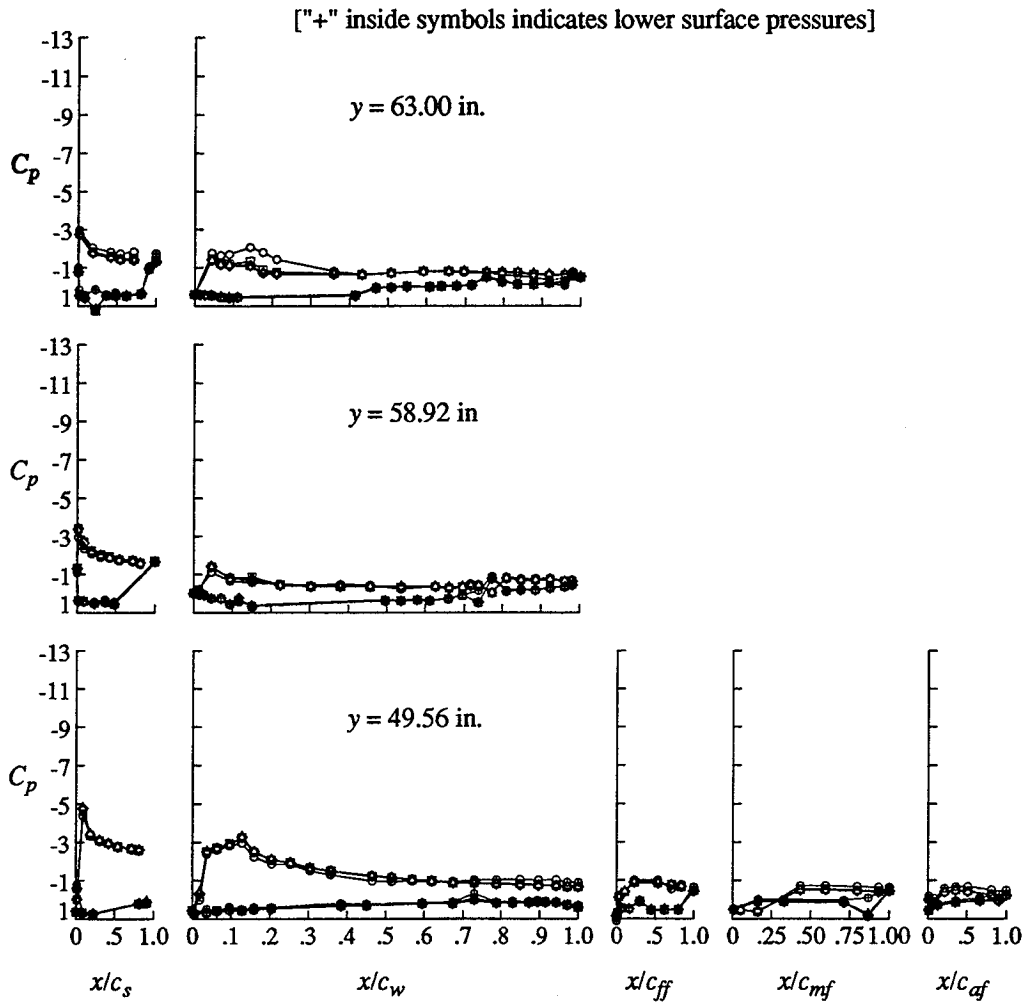

(d) $\alpha = 12°$.

Figure 10. Concluded.

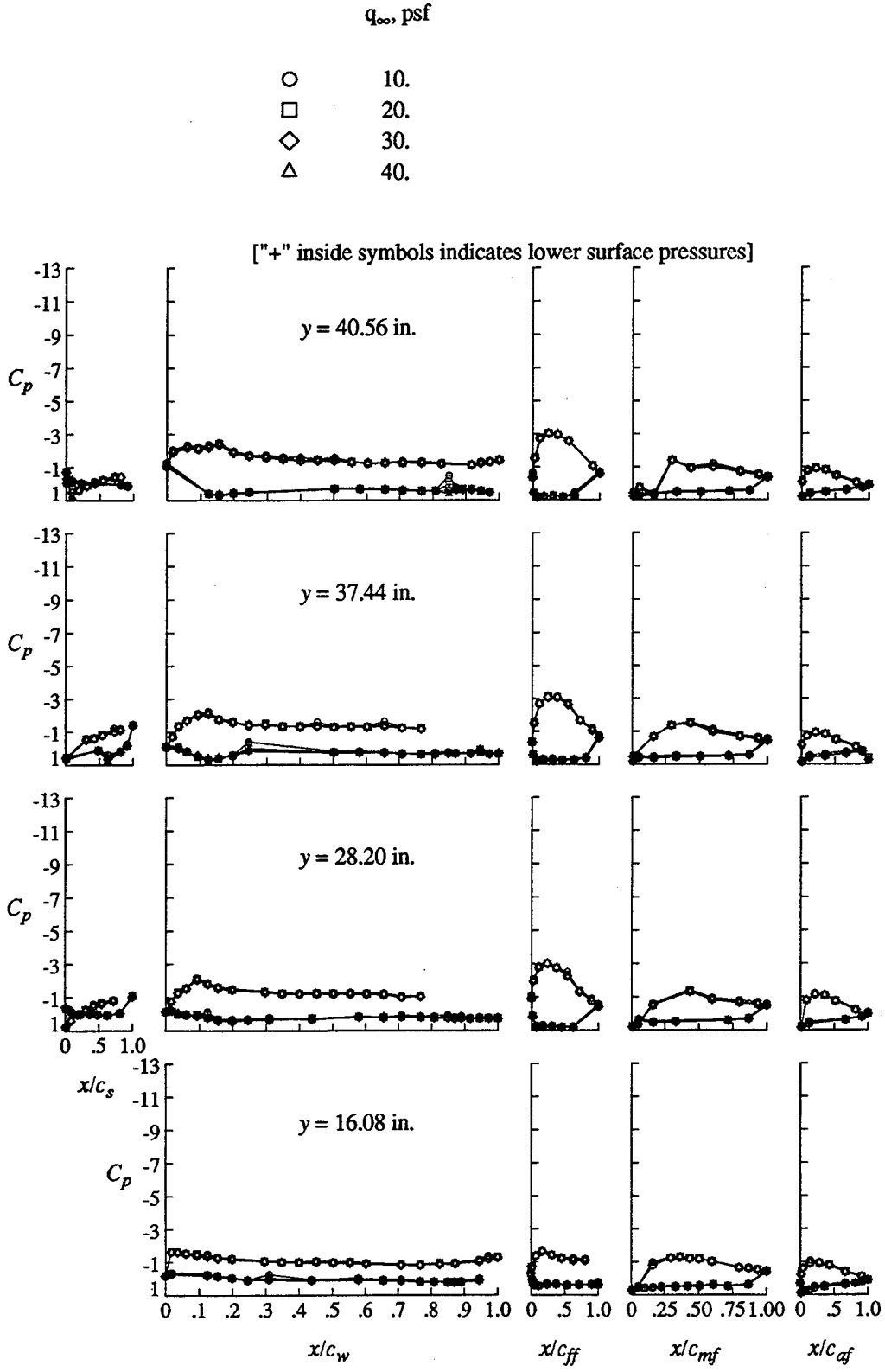

(a) $\alpha = 0°$.

Figure 11. Effect of tunnel speed on the wing pressure distributions of Landing 1 configuration.

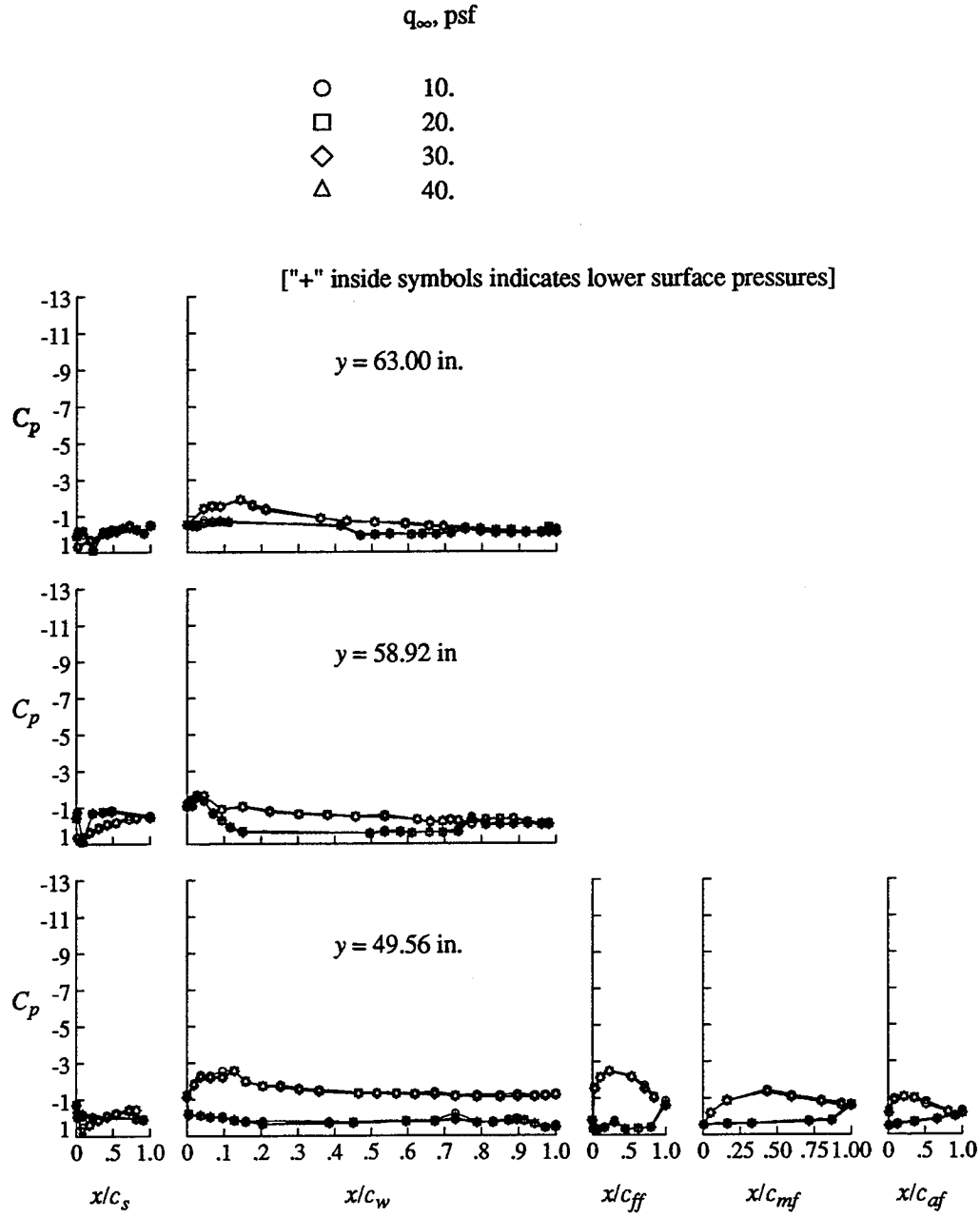

(a) $\alpha = 0°$.

Figure 11. Continued.

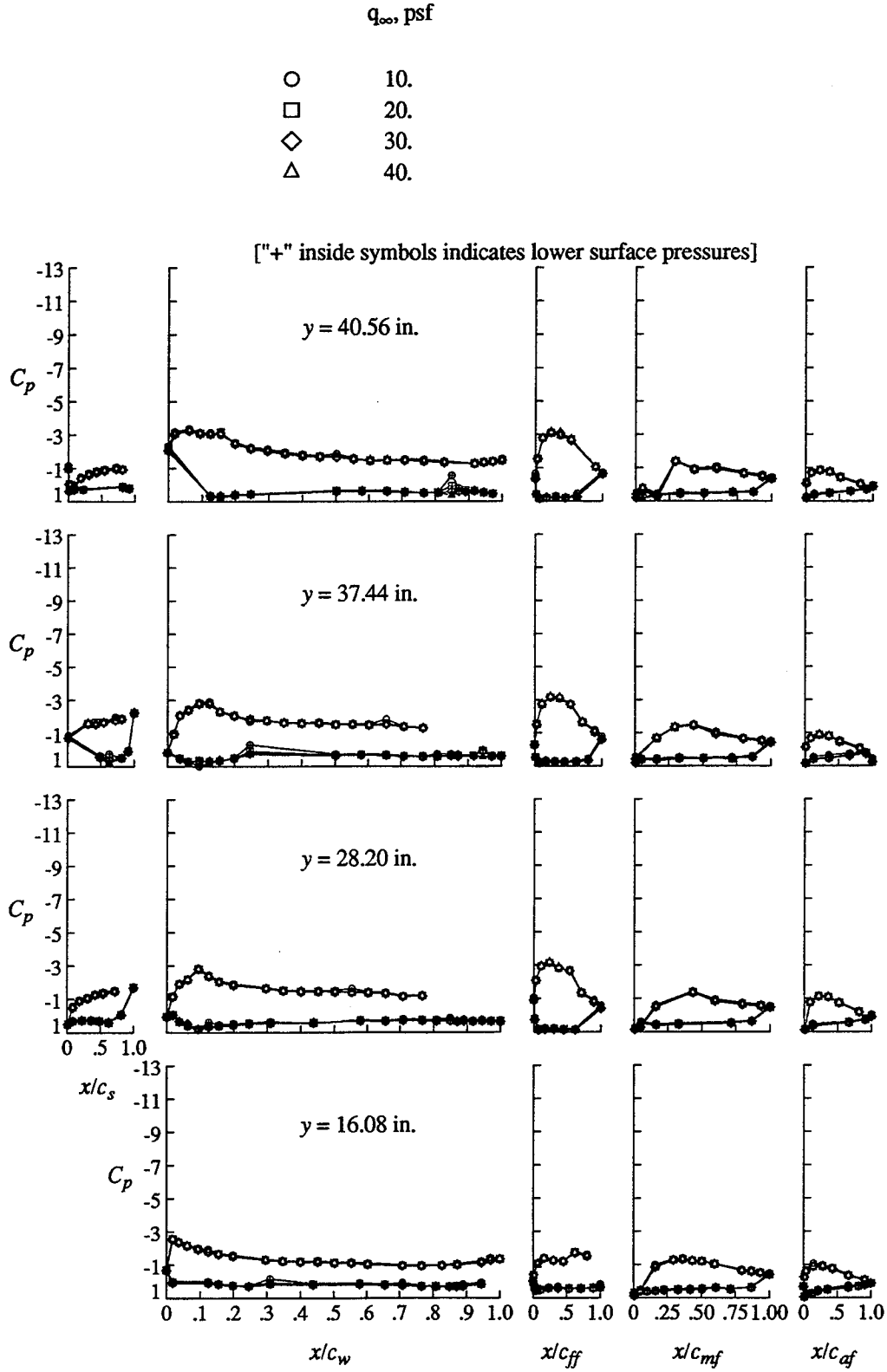

(b) $\alpha = 4°$.

Figure 11. Continued.

q_∞, psf

○	10.
□	20.
◇	30.
△	40.

["+" inside symbols indicates lower surface pressures]

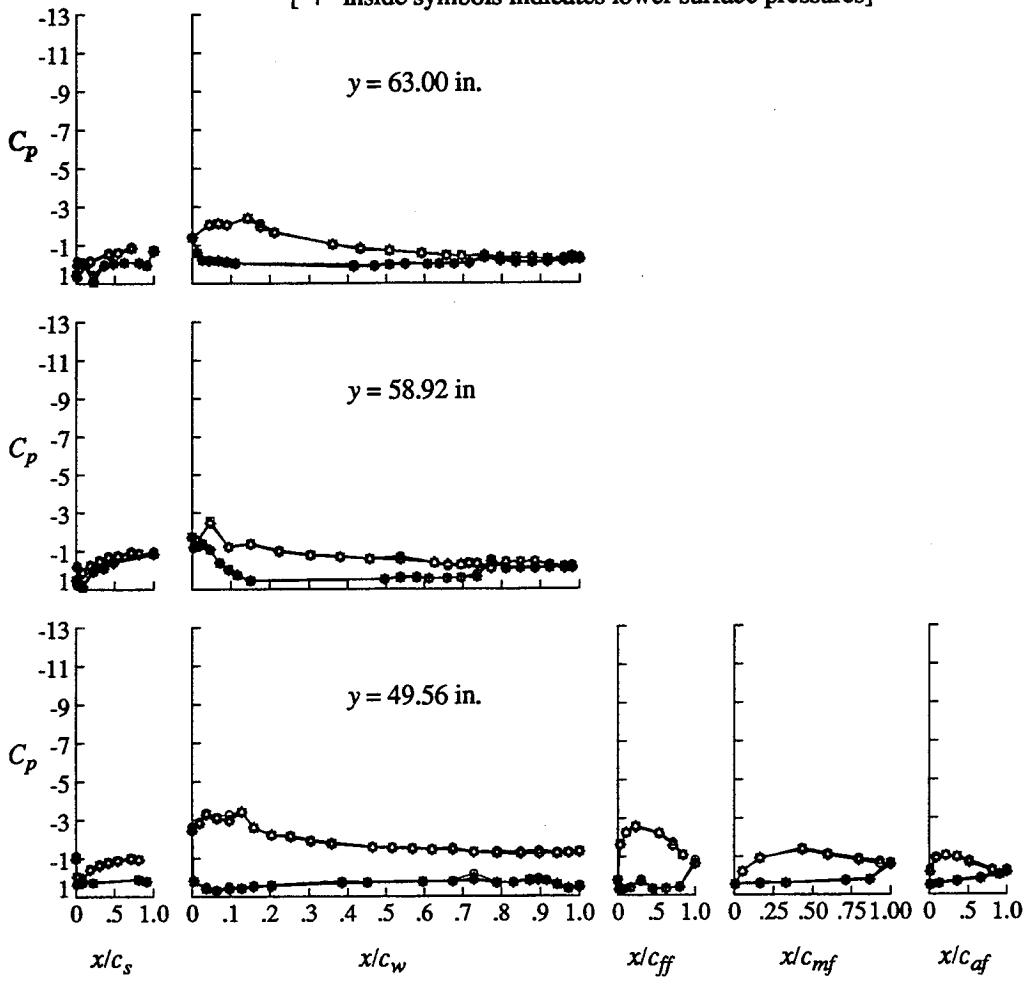

(b) $\alpha = 4°$.

Figure 11. Continued.

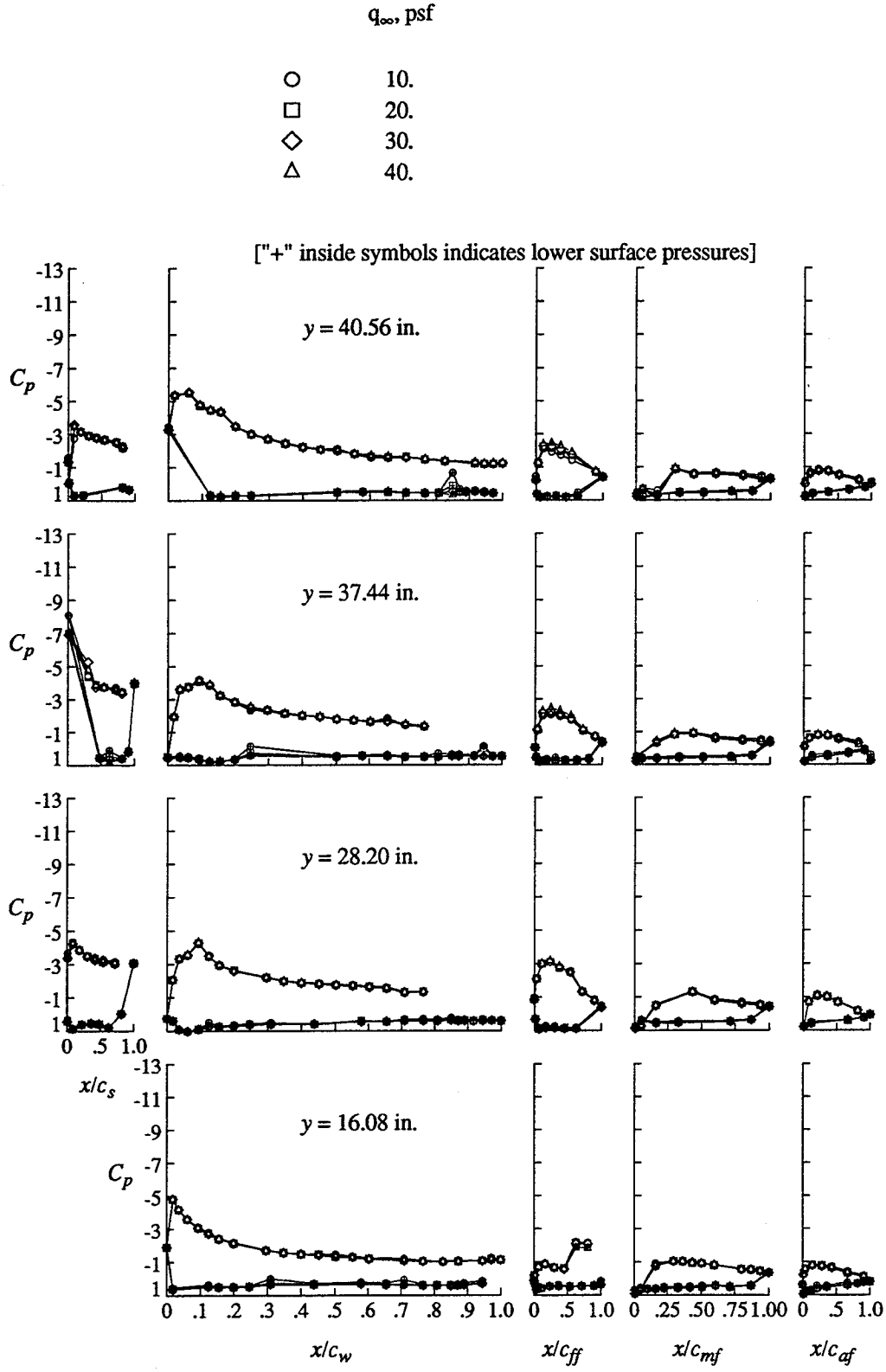

(c) $\alpha = 8°$.

Figure 11. Continued.

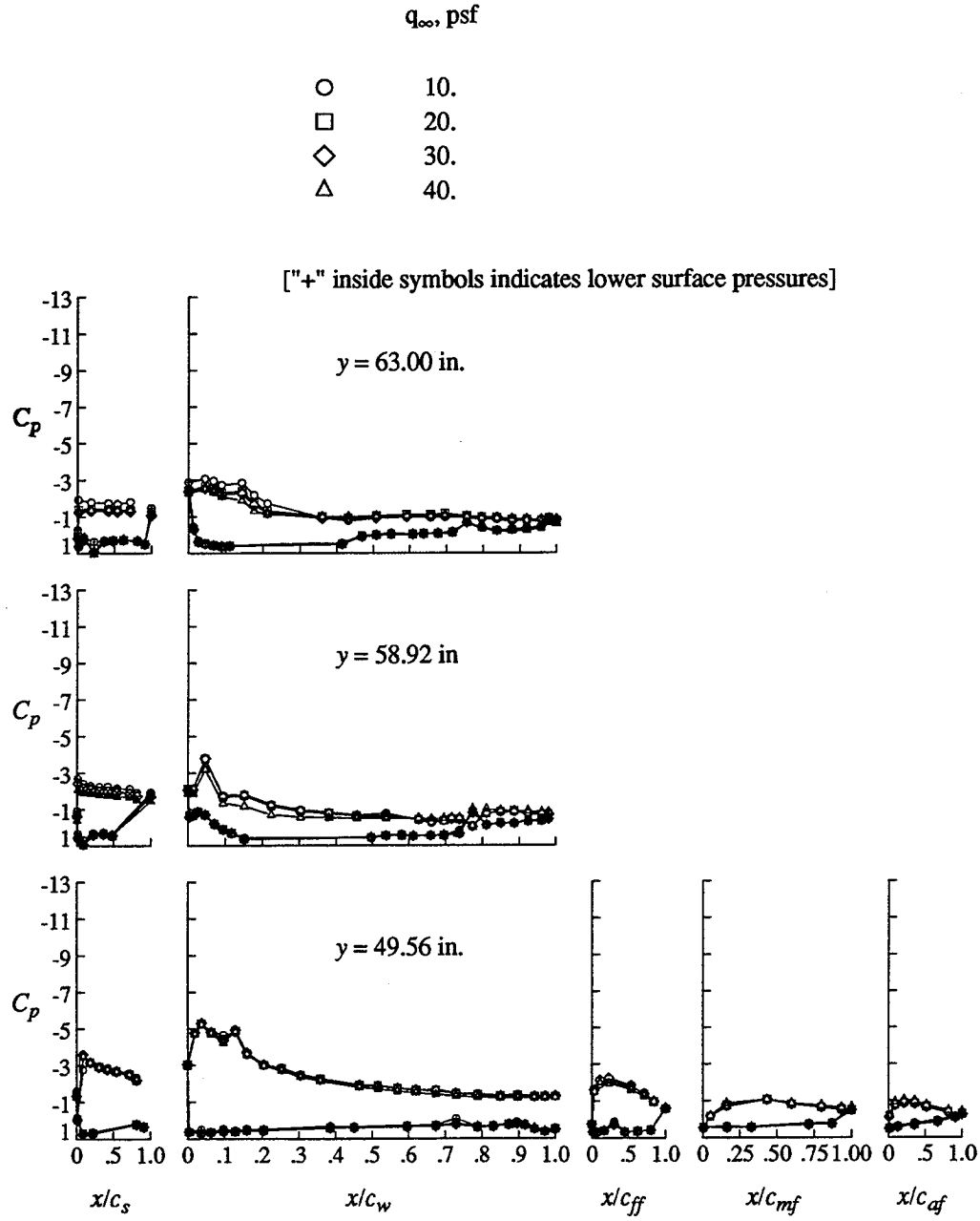

(c) $\alpha = 8°$.

Figure 11. Continued.

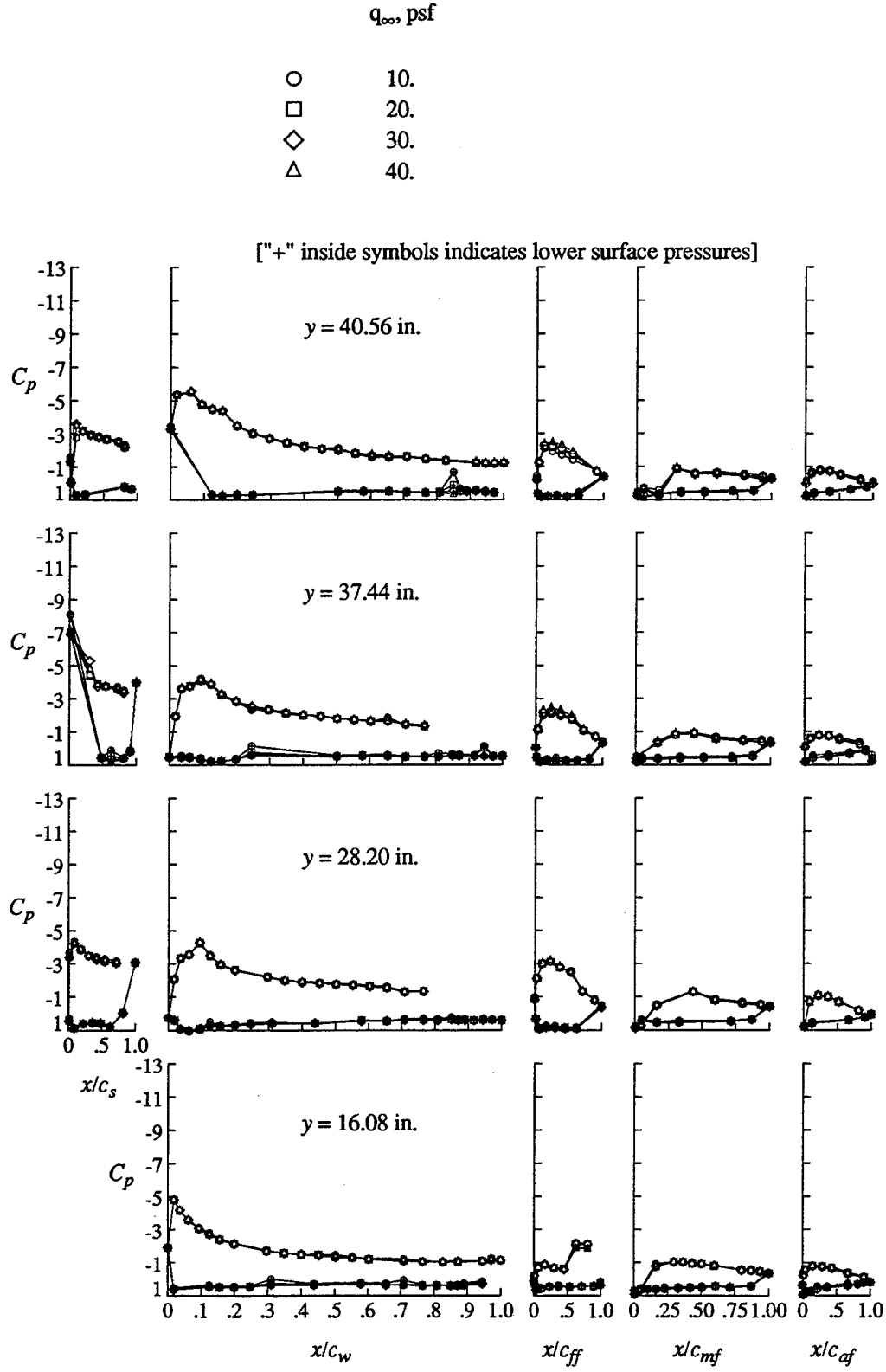

(d) $\alpha = 12°$.

Figure 11. Concluded.

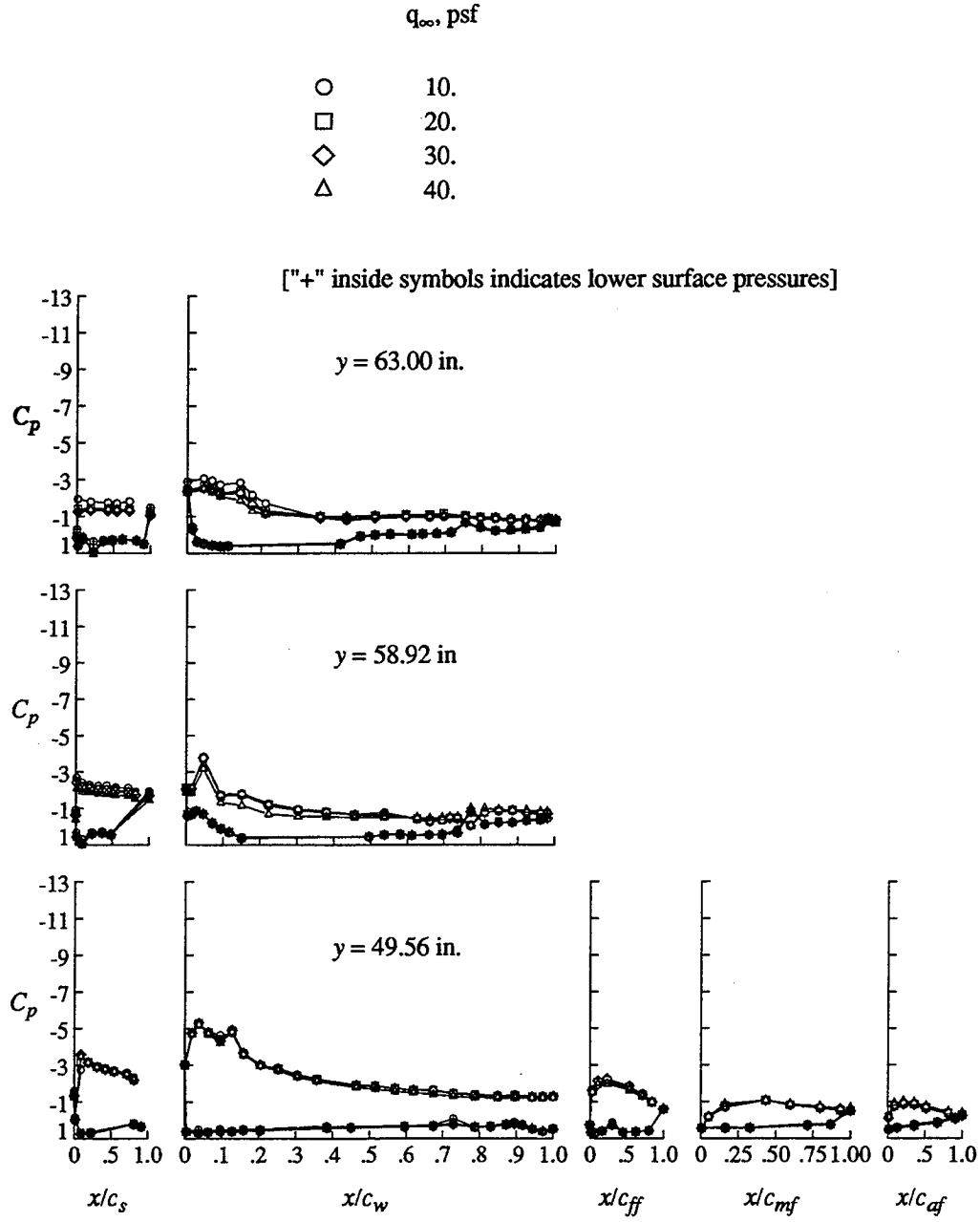

(d) $\alpha = 12°$.

Figure 11. Concluded.

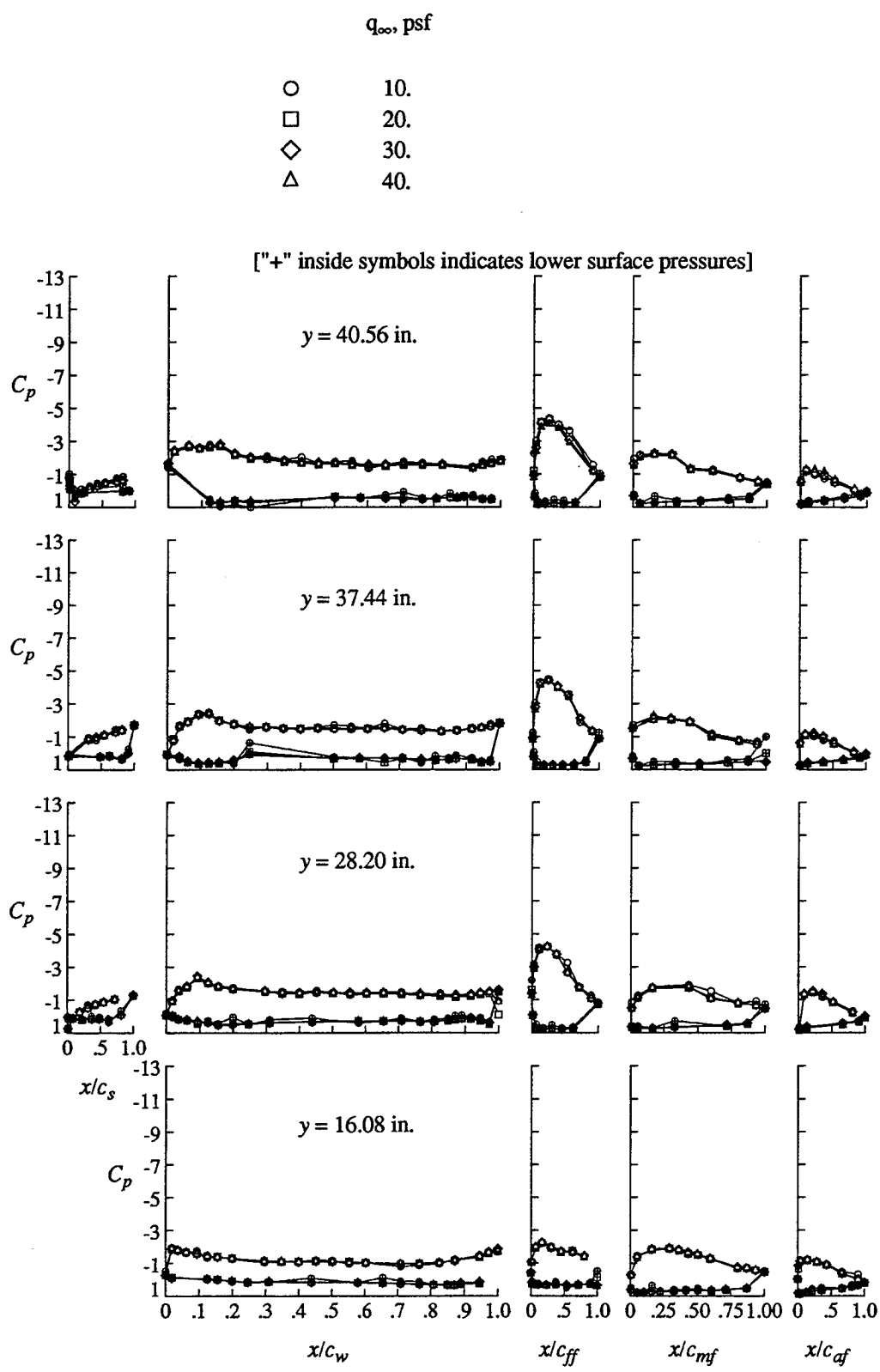

(a) $\alpha = 0°$.

Figure 12. Effect of tunnel speed on the wing pressure distributions of Landing 2 configuration.

q_∞, psf

○	10.
□	20.
◇	30.
△	40.

["+" inside symbols indicates lower surface pressures]

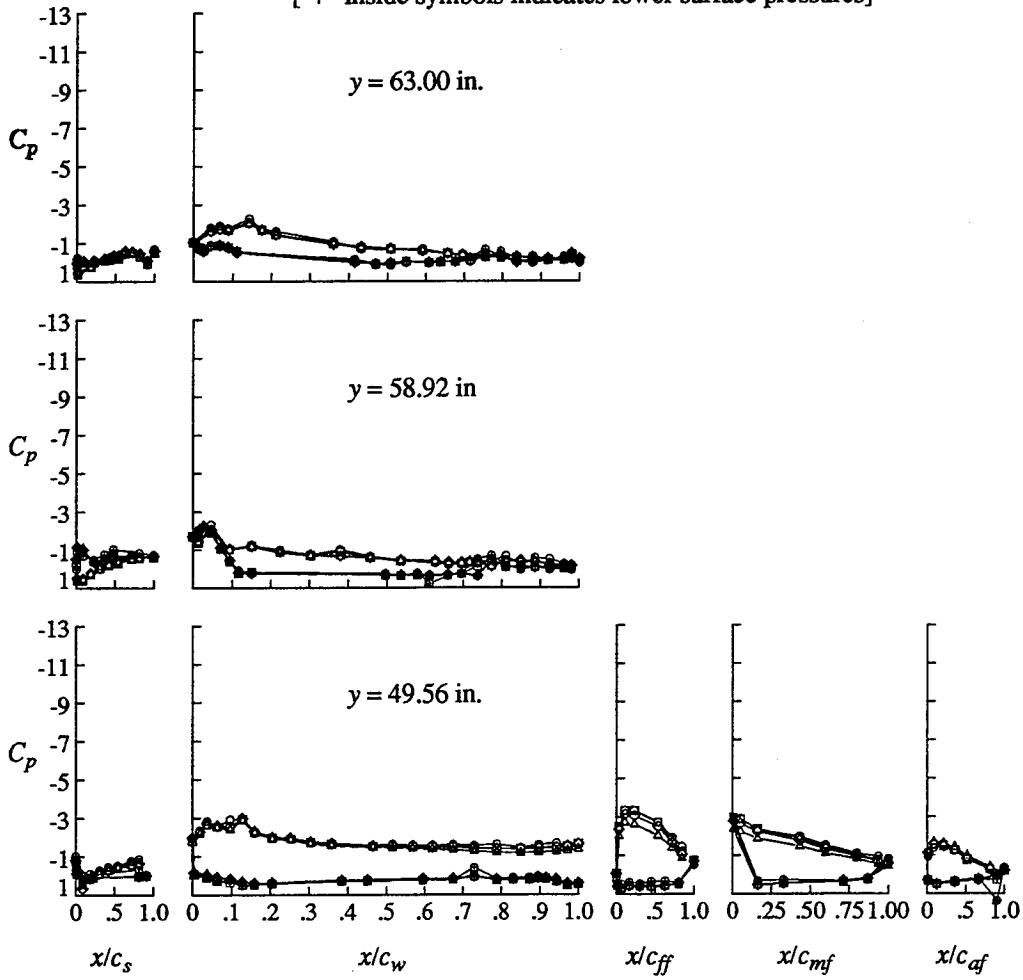

(a) $\alpha = 0°$.

Figure 12. Continued.

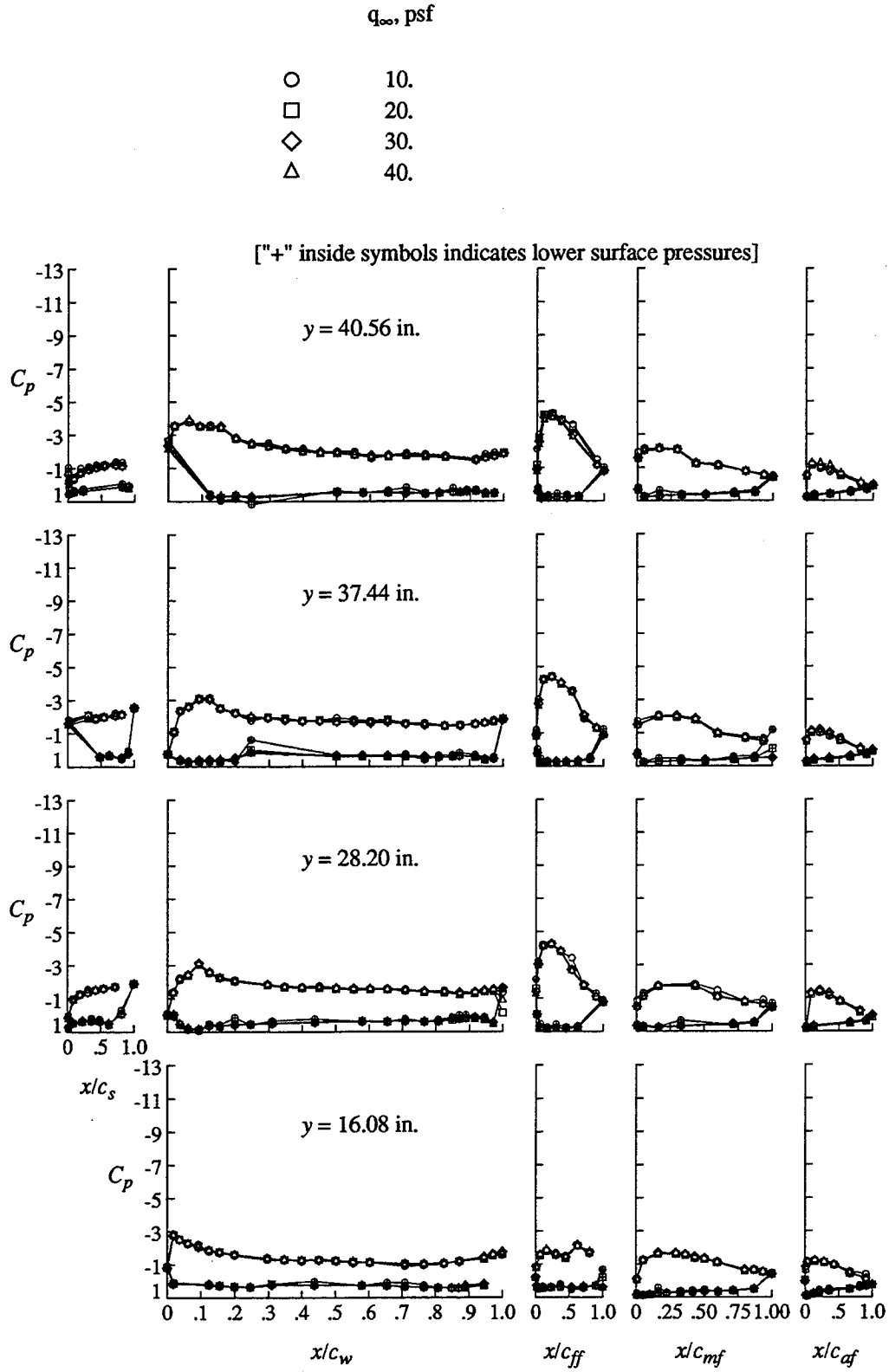

(b) $\alpha = 4°$.

Figure 12. Continued.

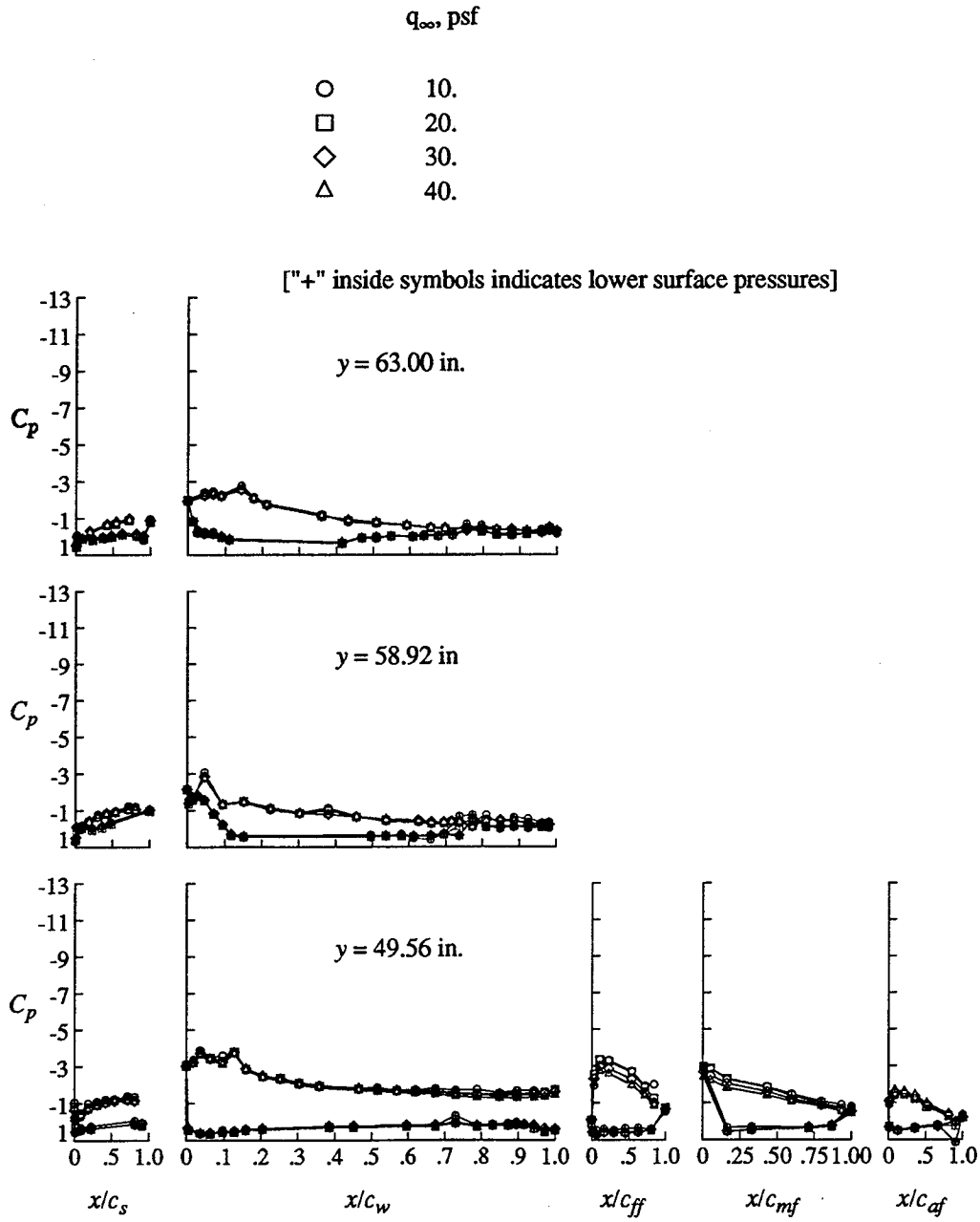

(b) $\alpha = 4°$.

Figure 12. Continued.

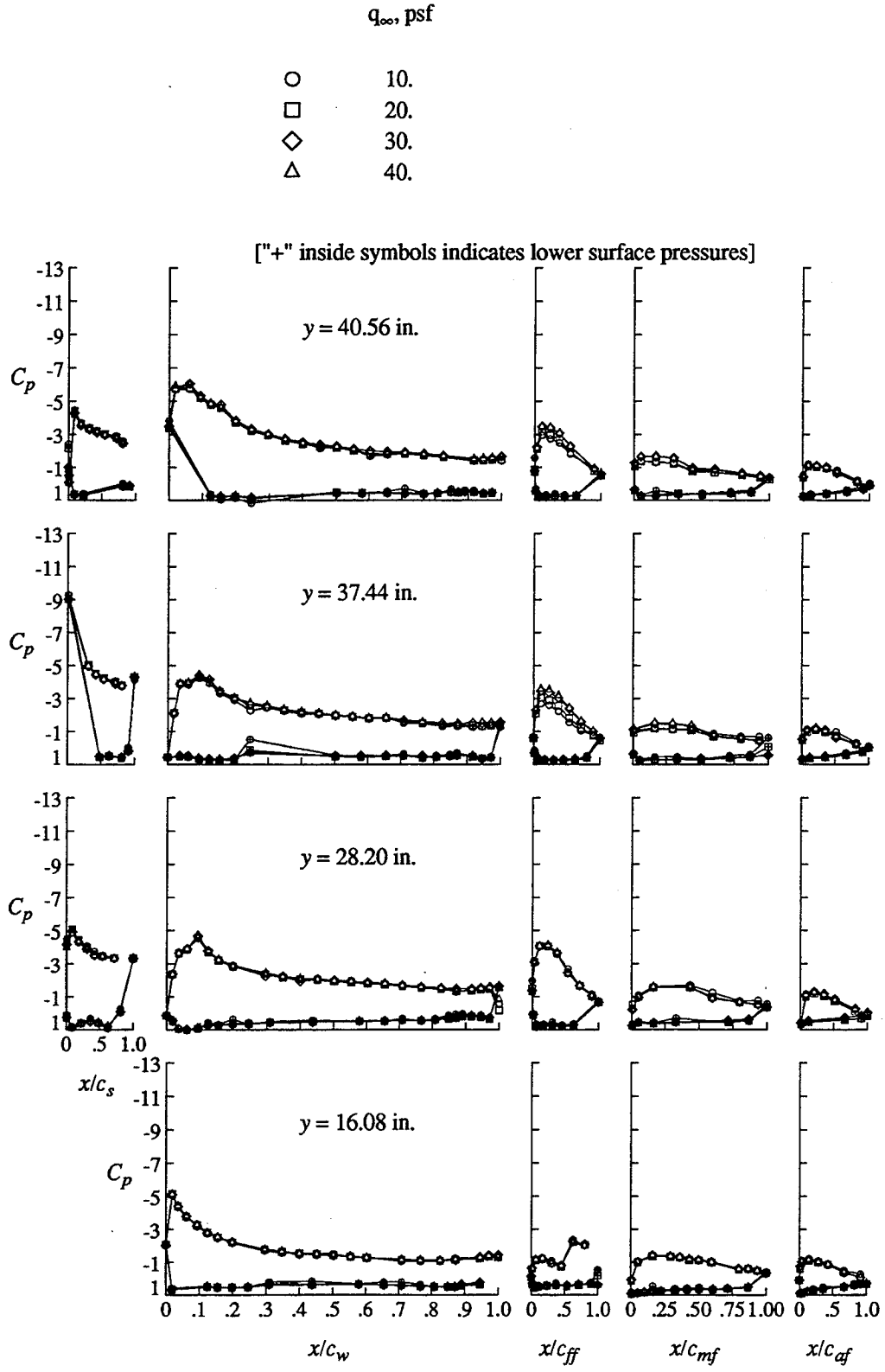

(c) $\alpha = 8°$.

Figure 12. Continued.

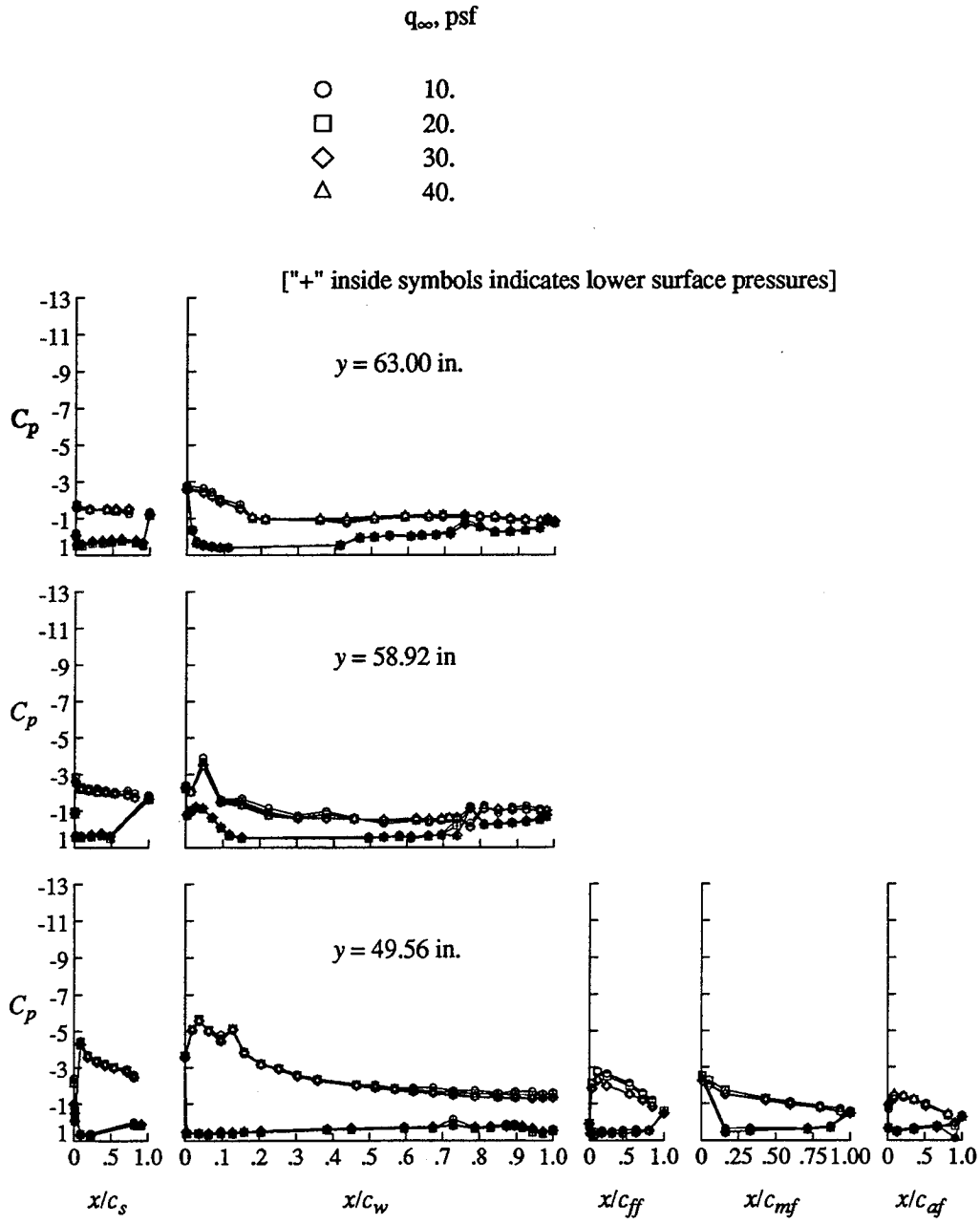

(c) $\alpha = 8°$.

Figure 12. Continued.

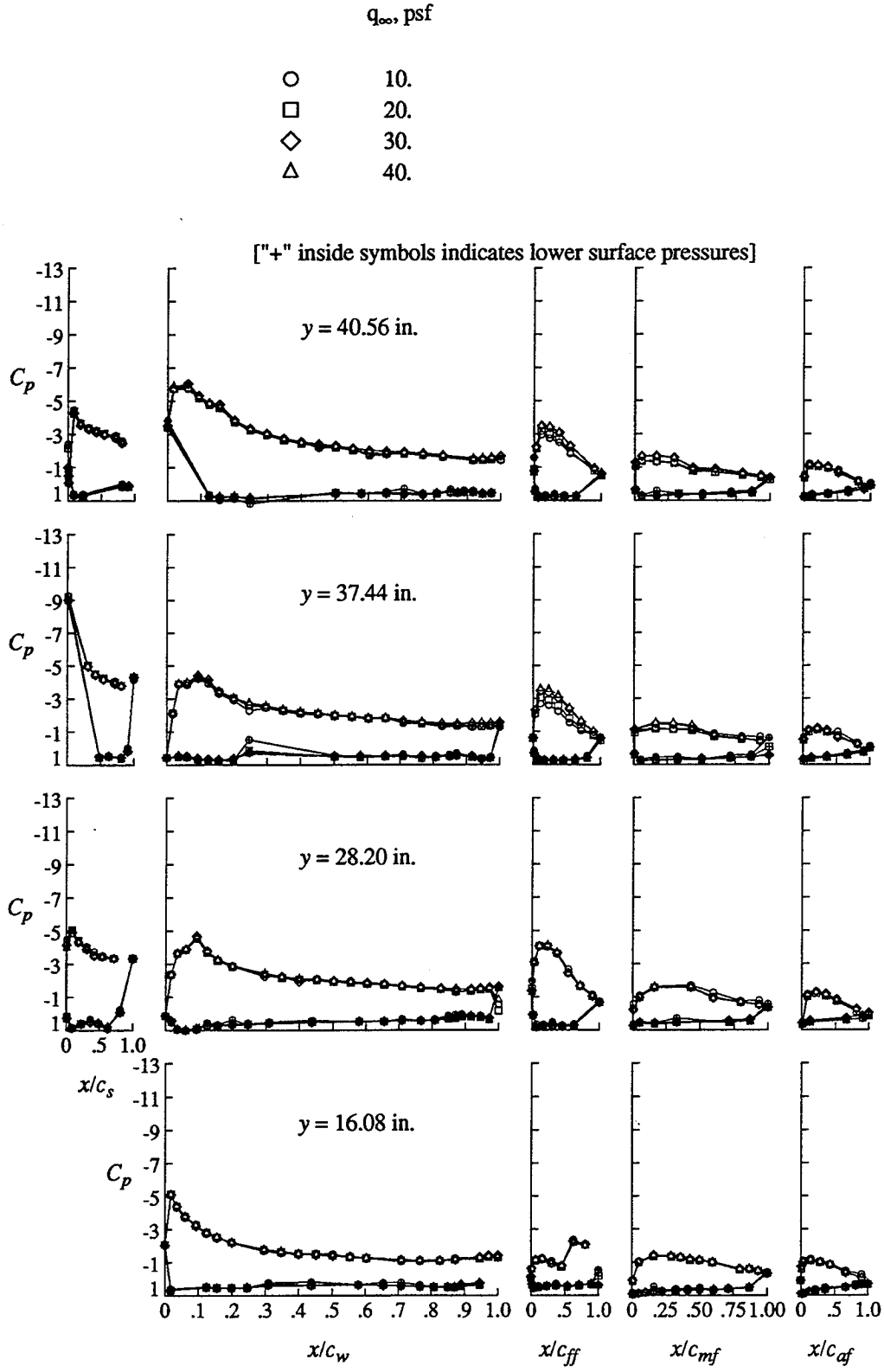

(d) $\alpha = 12°$.

Figure 12. Concluded.

q_∞, psf

○	10.
□	20.
◇	30.
△	40.

["+" inside symbols indicates lower surface pressures]

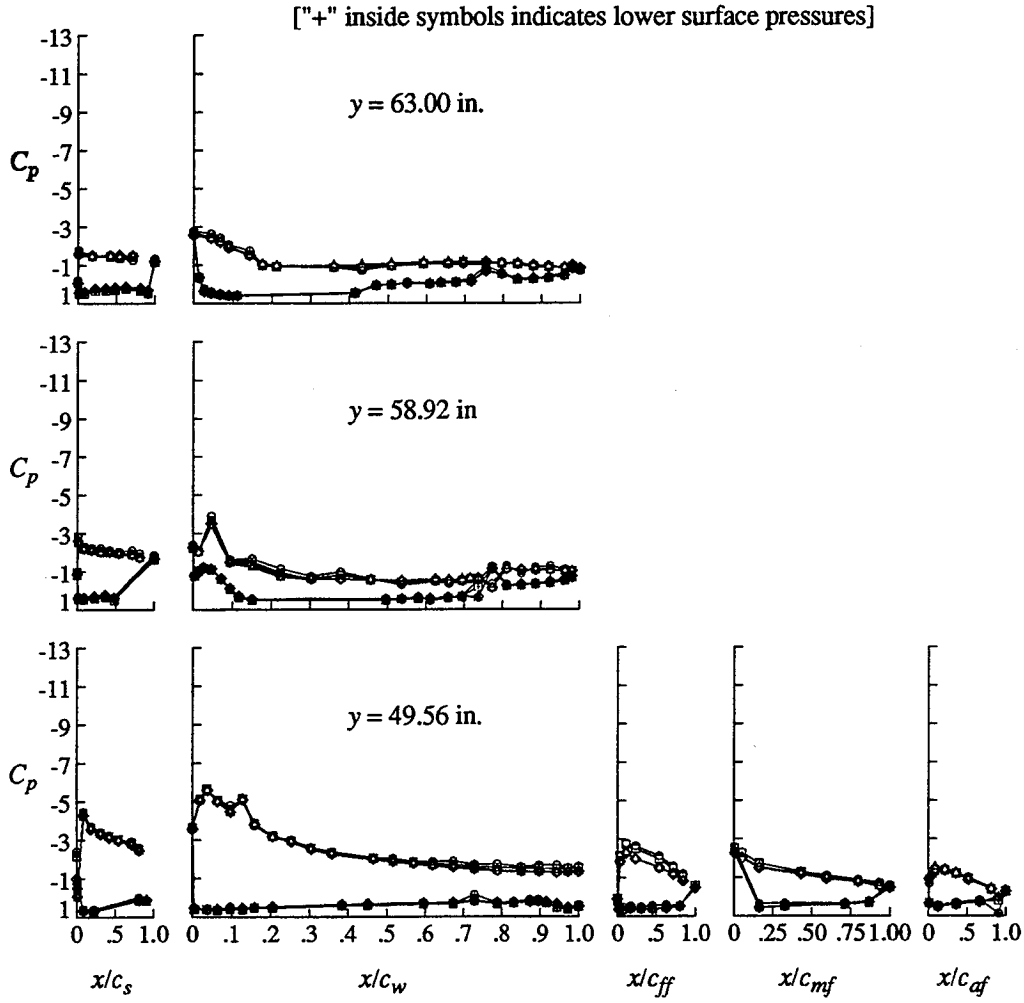

(d) $\alpha = 12°$.

Figure 12. Concluded.

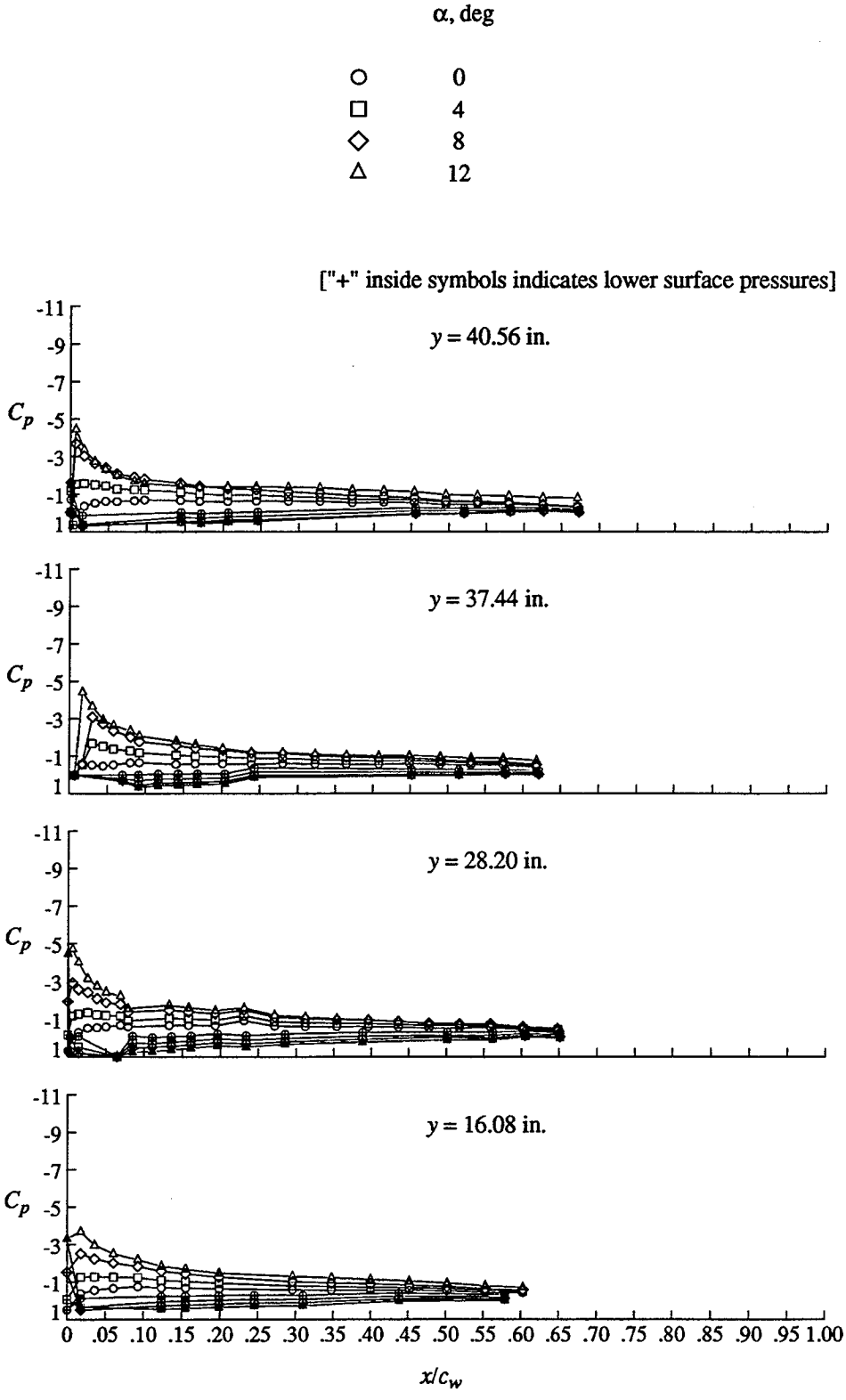

(a) Cruise configuration.

Figure 13. Effect of alpha on the wing pressure distributions.

q_∞ = 40 psf.

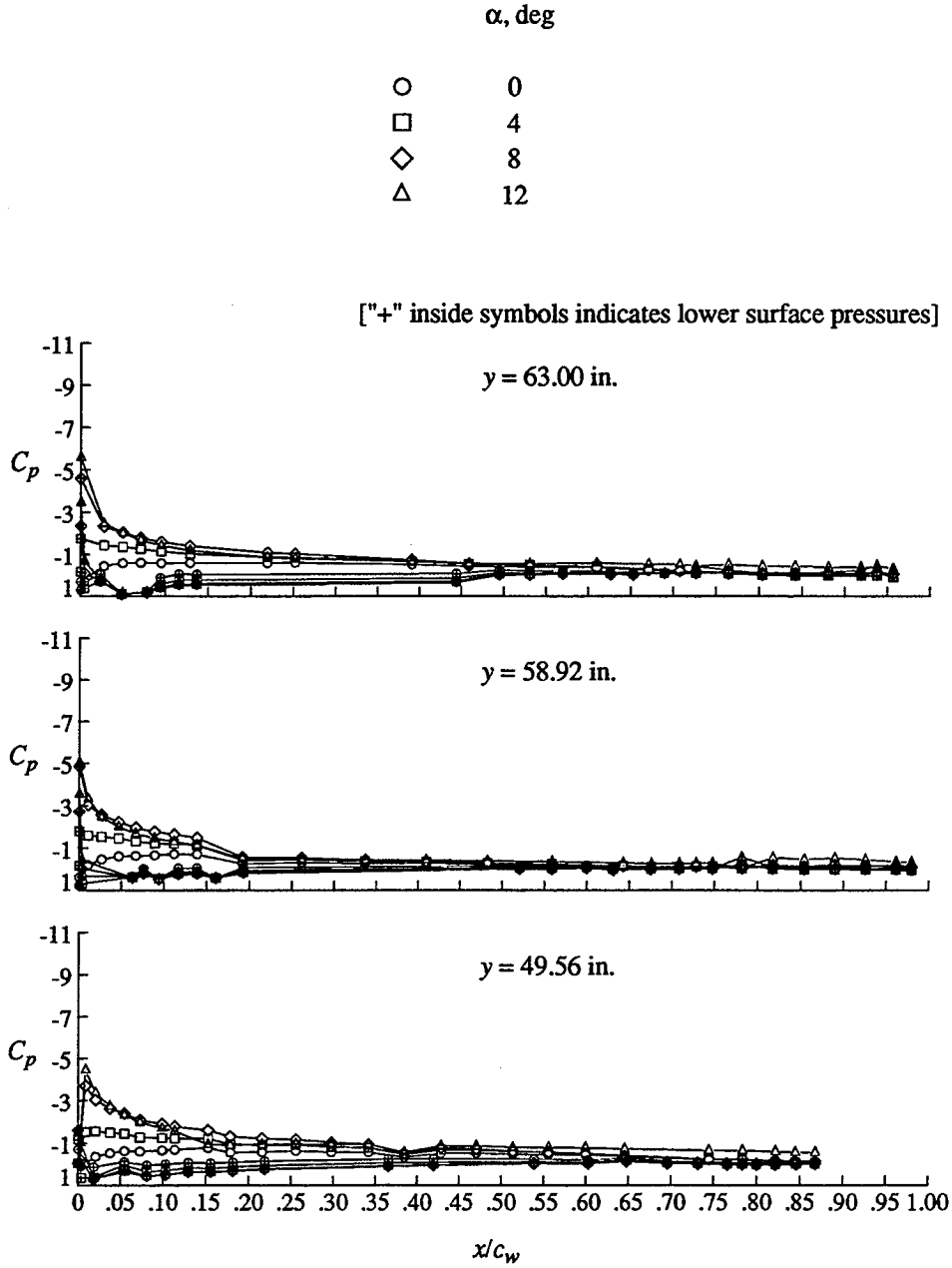

(a) Cruise configuration.

Figure 13. Continued.

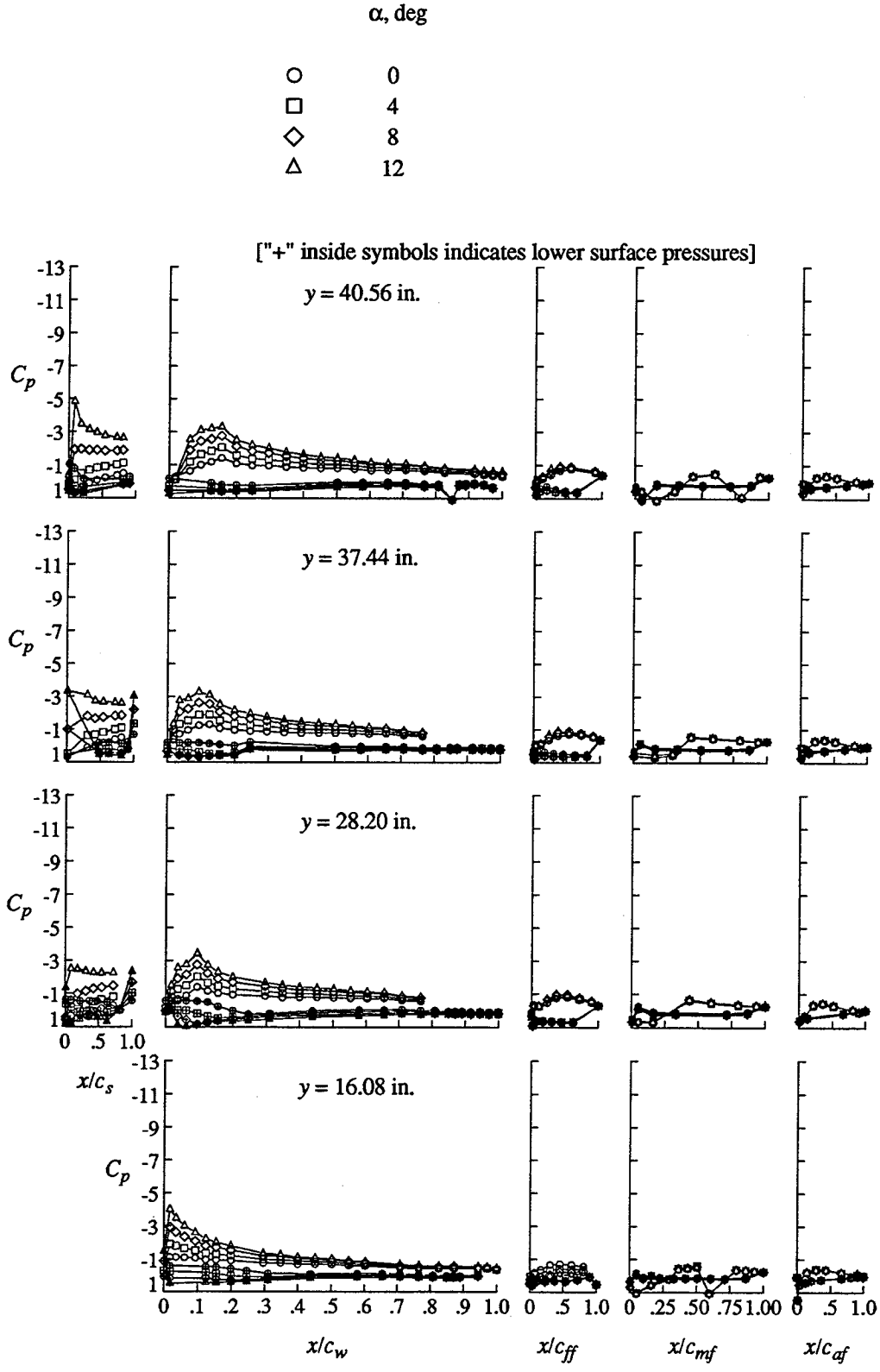

(b) Take-off configuration.

Figure 13. Continued.

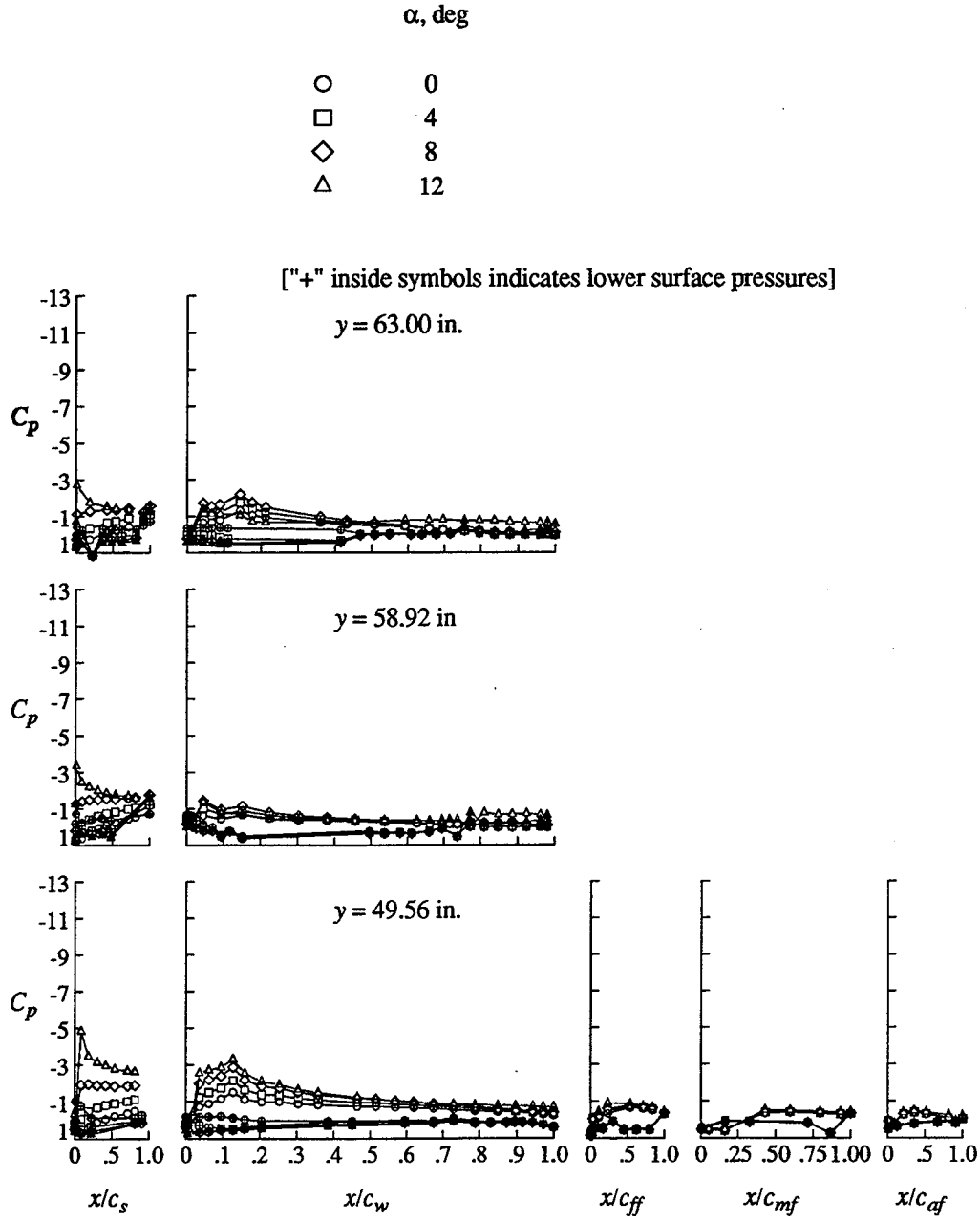

(b) Take-off configuration.

Figure 13. Continued.

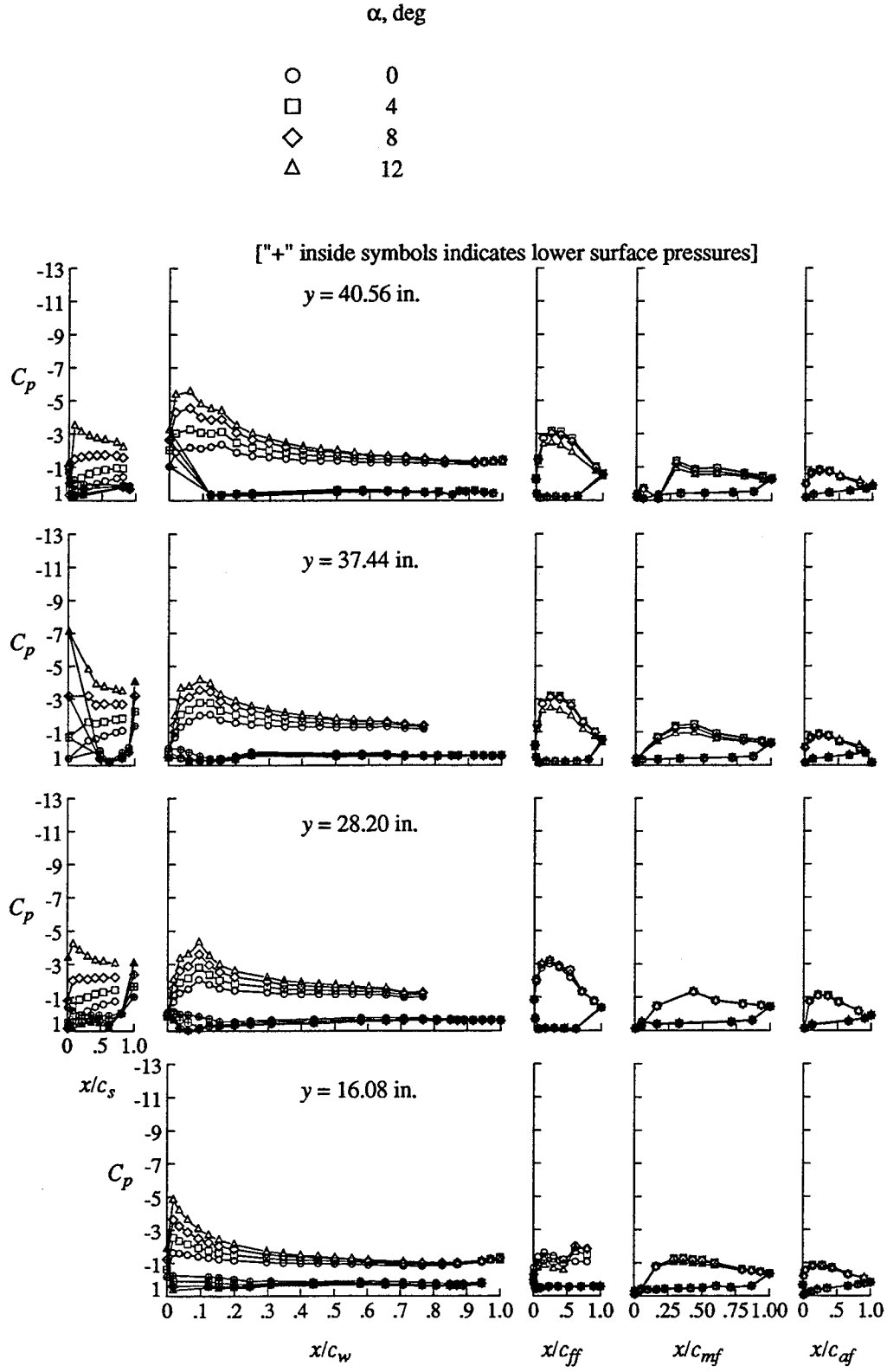

(c) Landing 1 configuration.

Figure 13. Continued.

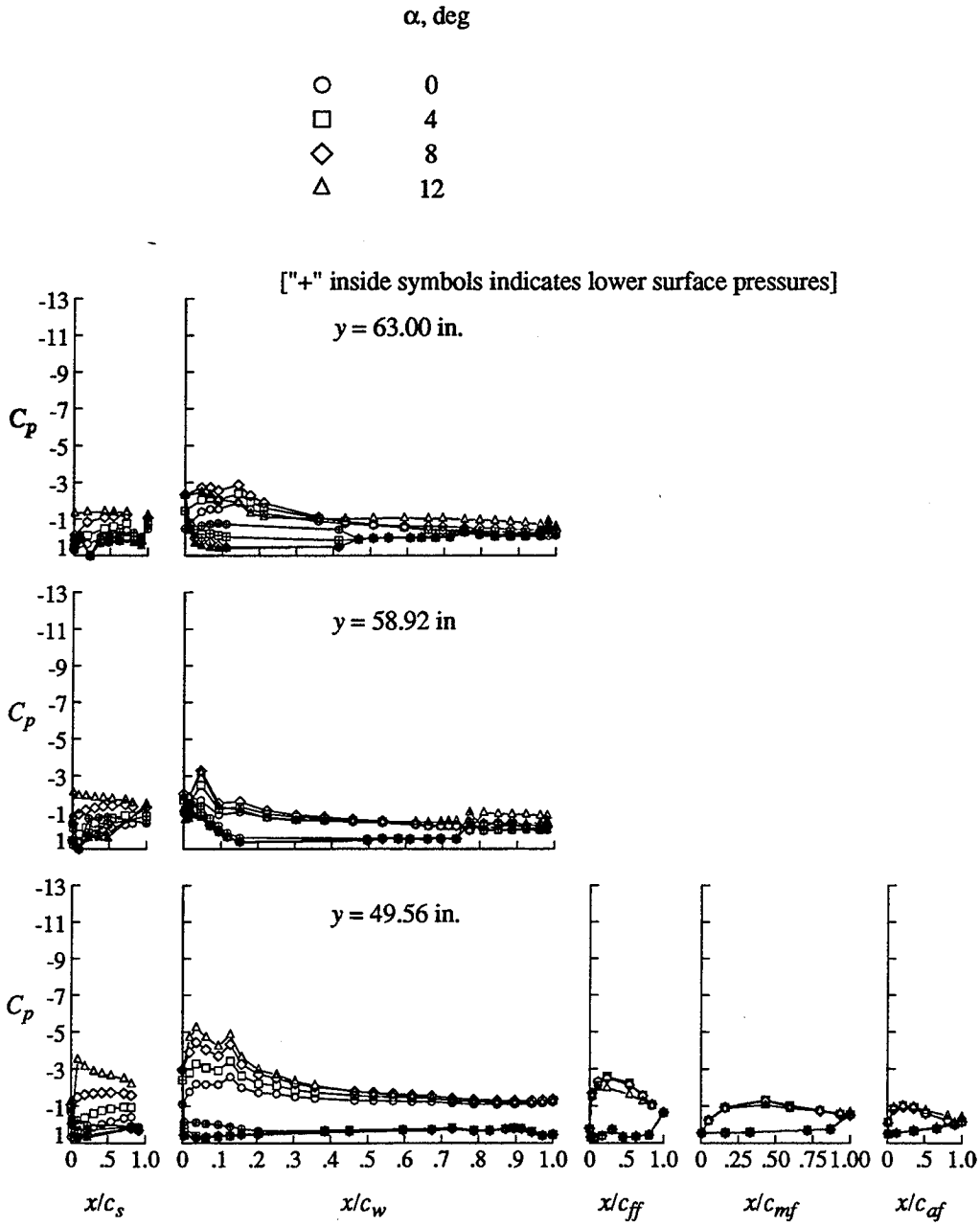

(c) Landing 1 configuration.

Figure 13. Continued.

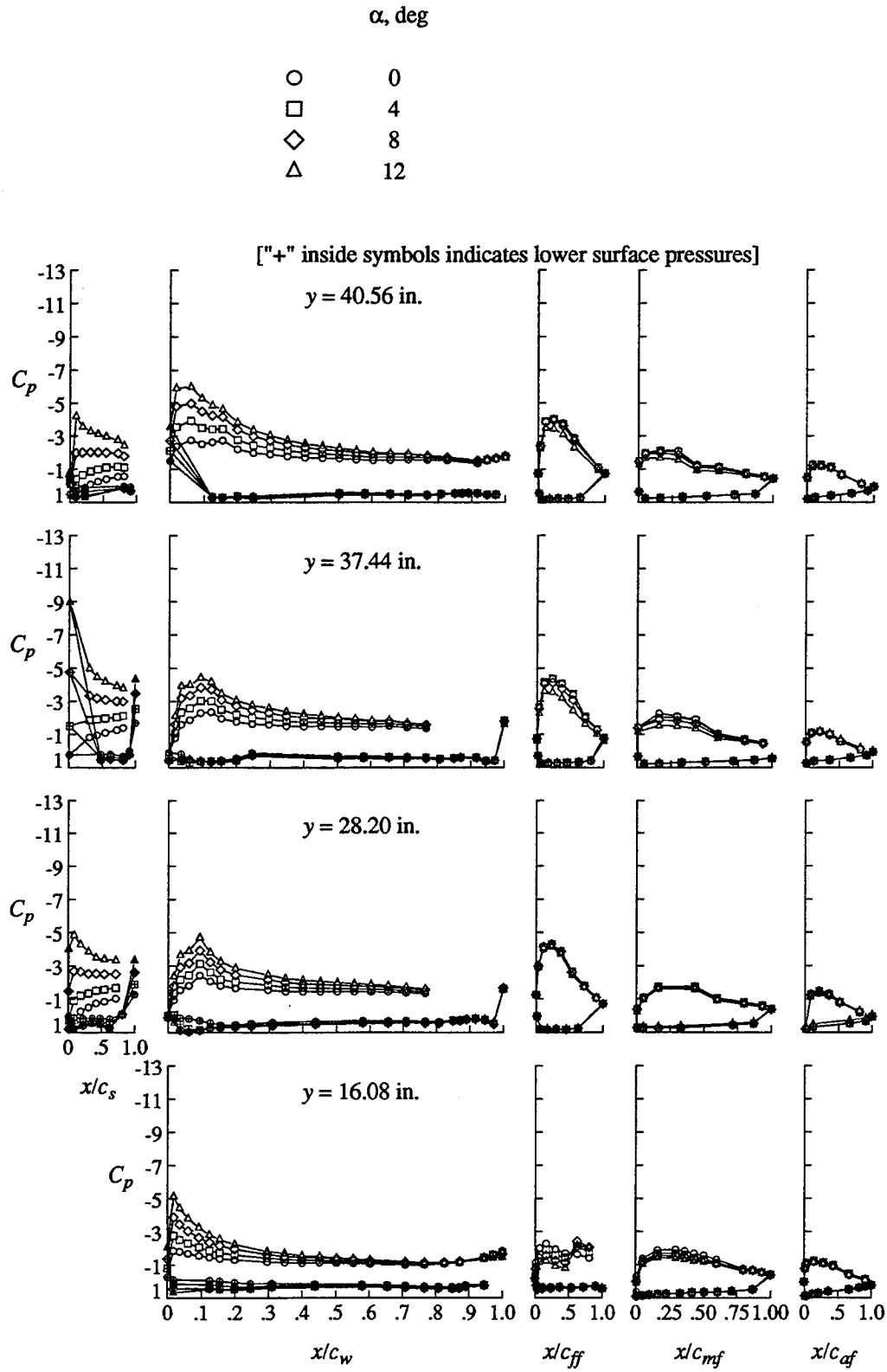

(d) Landing 2 configuration.

Figure 13. Continued.

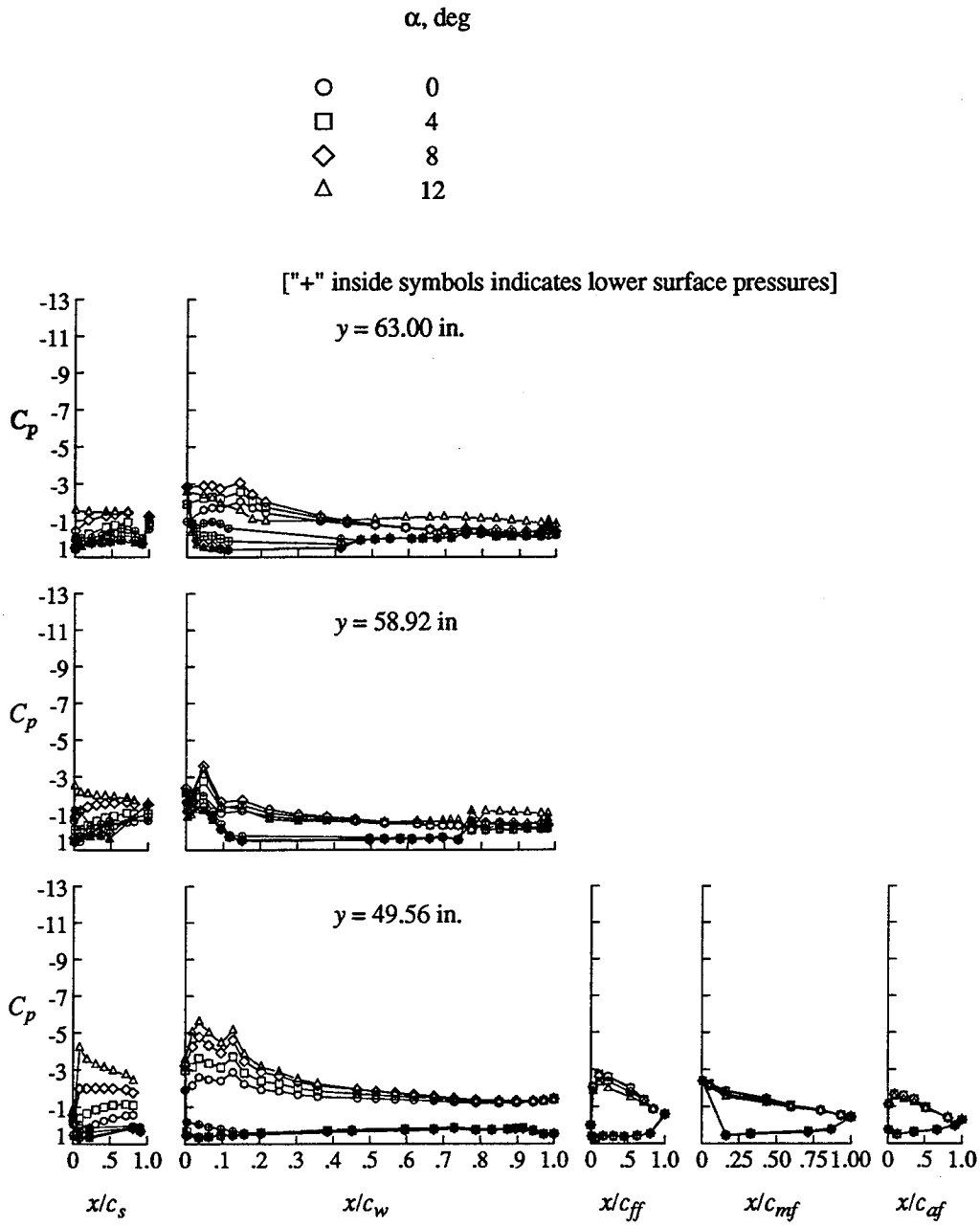

(d) Landing 2 configuration.

Figure 13. Concluded.

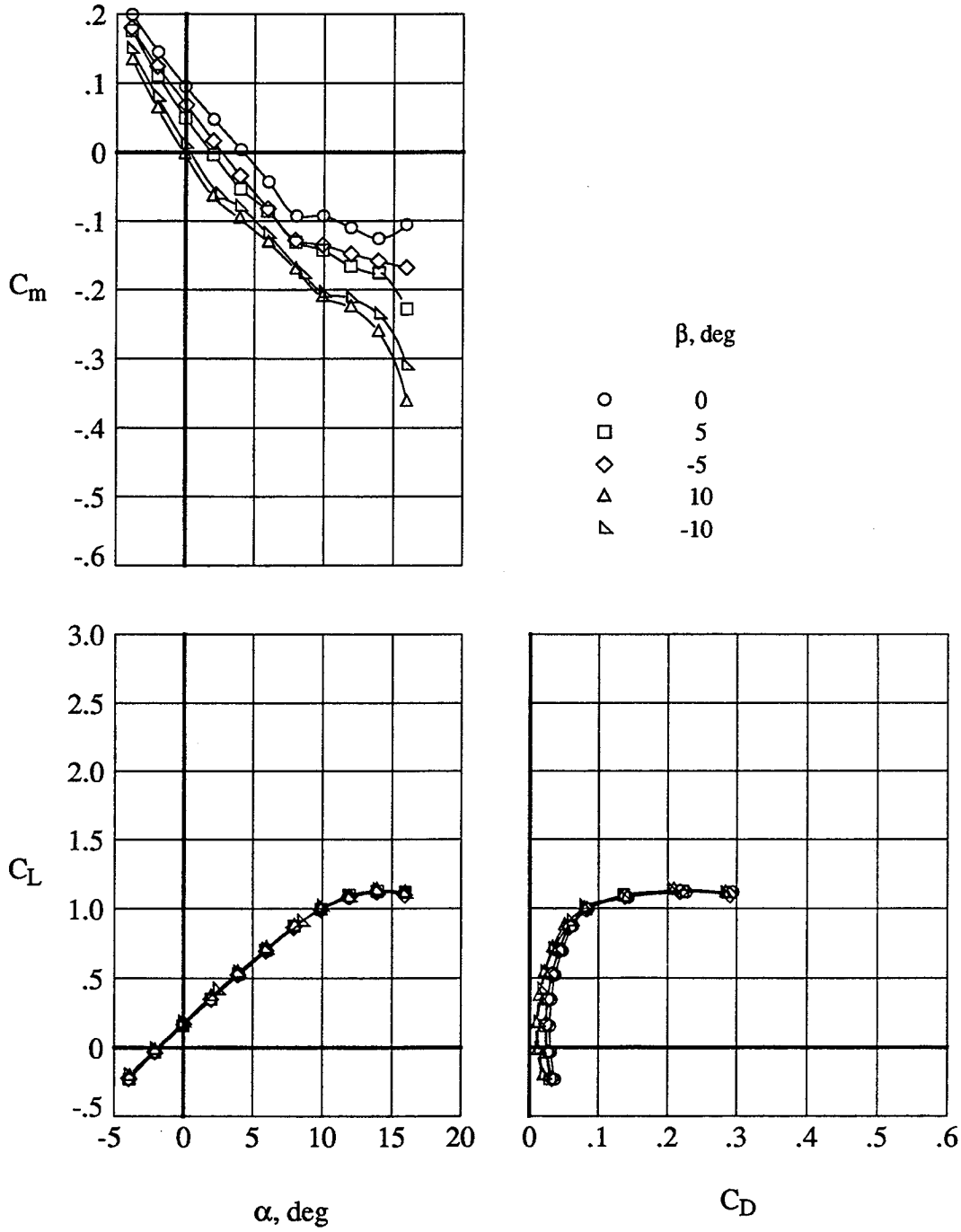

(a) Cruise configuration

Figure 14. Effect of sideslip on the longitudinal aerodynamic characteristics.
q_∞ = 40 psf.

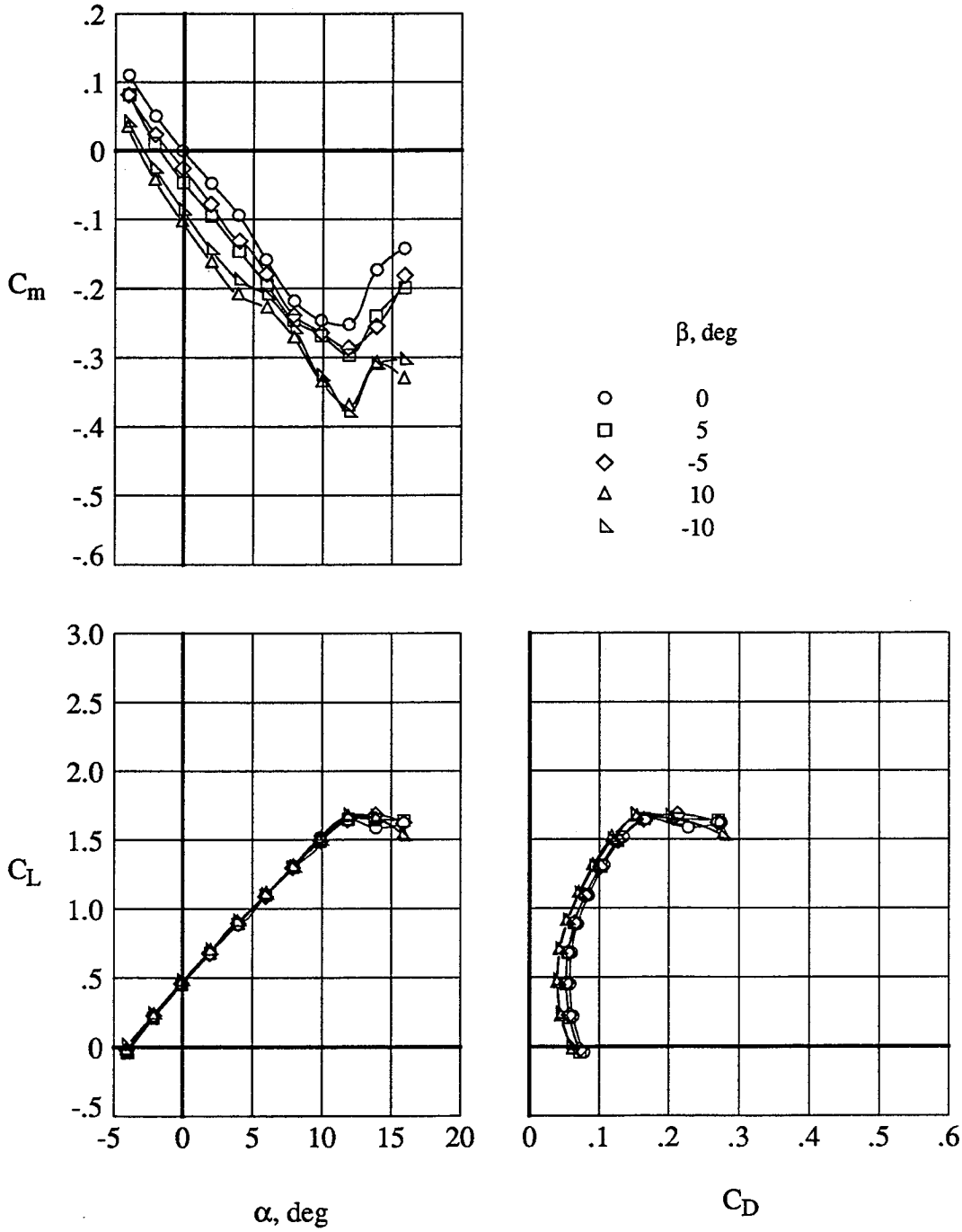

(b) Take-off configuration

Figure 14. Continued.

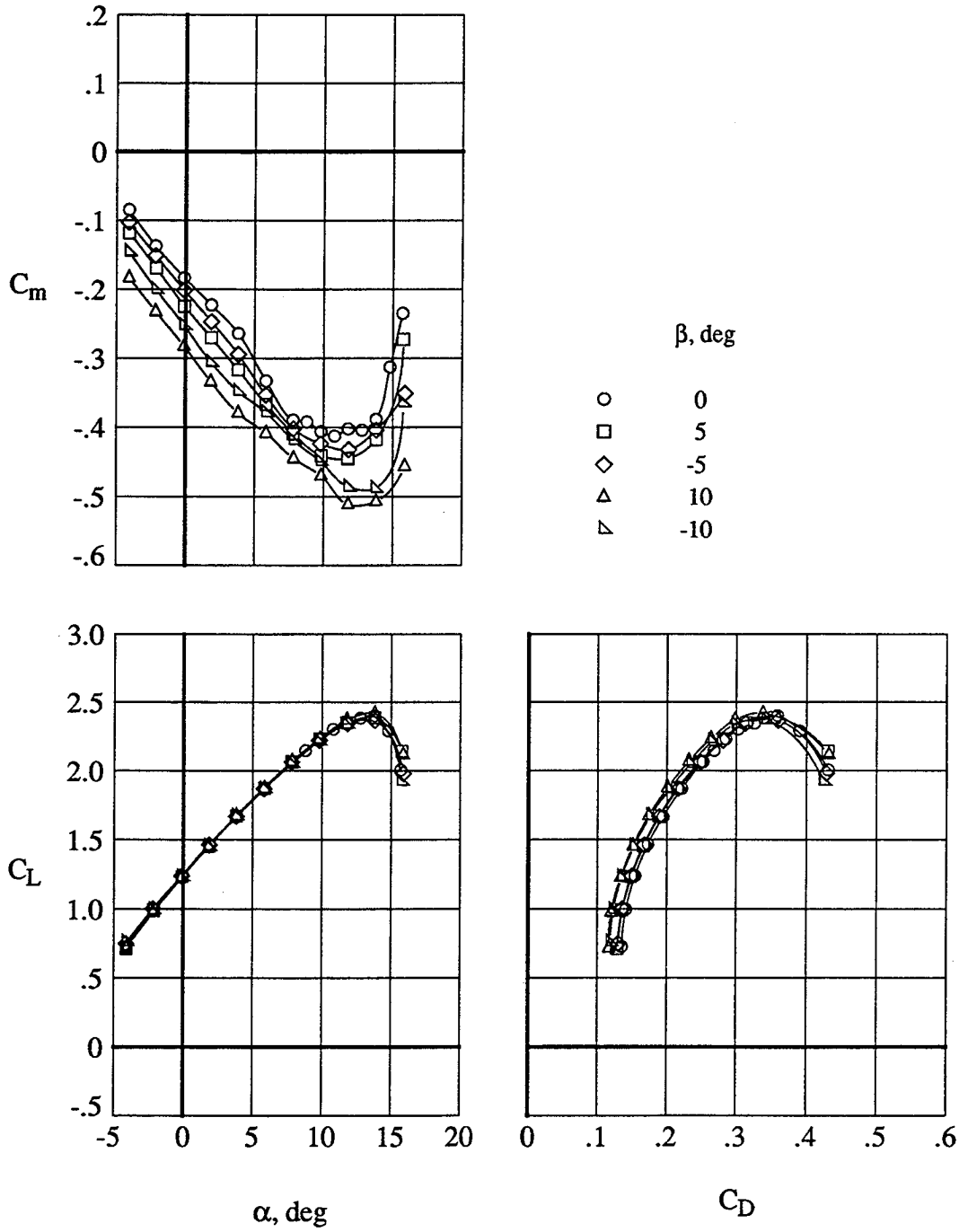

(c) Landing 1 configuration

Figure 14. Continued.

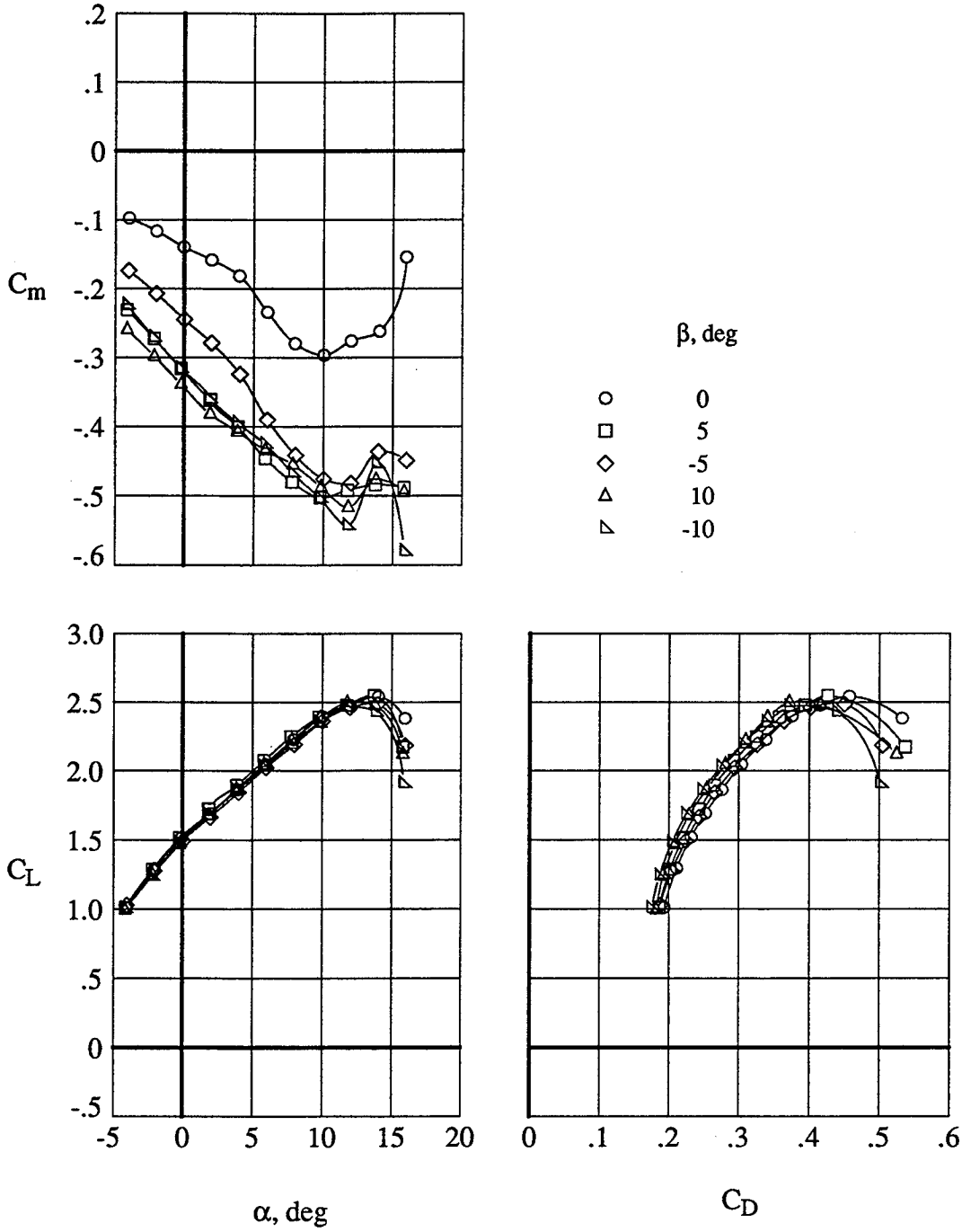

(d) Landing 2 configuration

Figure 14. Concluded.

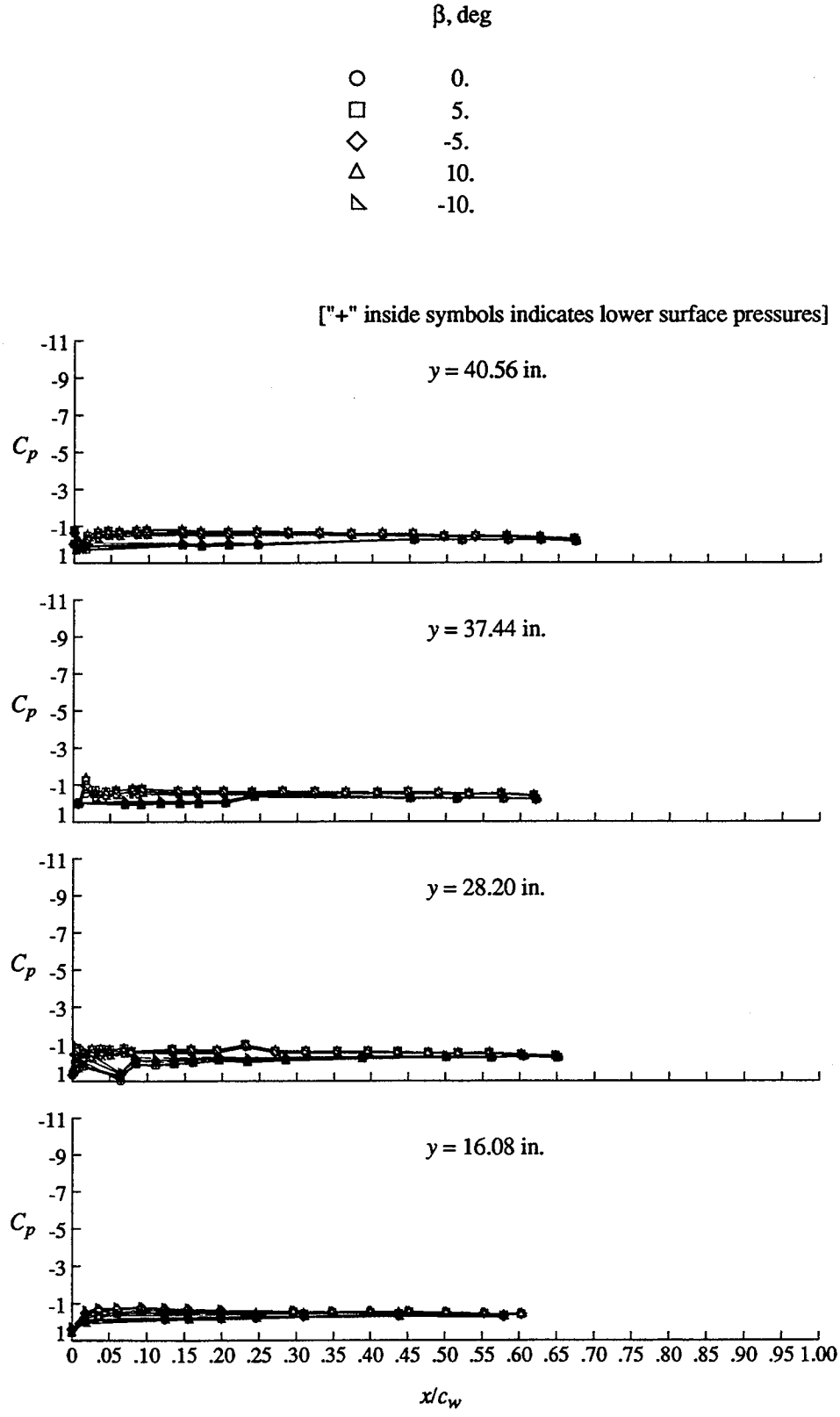

(a) $\alpha = 0°$.

Figure 15. Effect of sideslip on wing pressure distributions for Cruise configuration.

q_∞ = 40 psf.

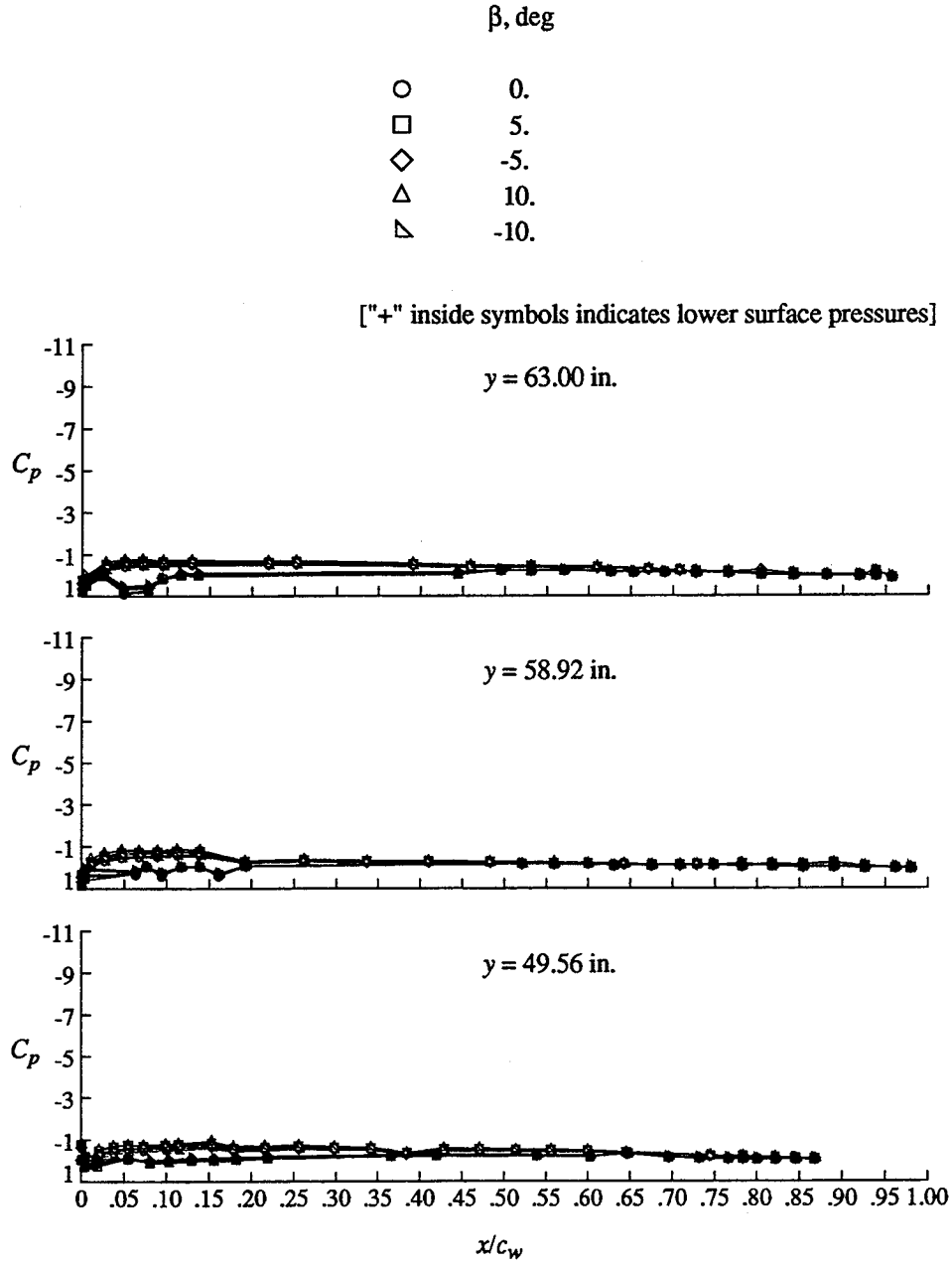

(a) $\alpha = 0°$.

Figure 15. Continued.

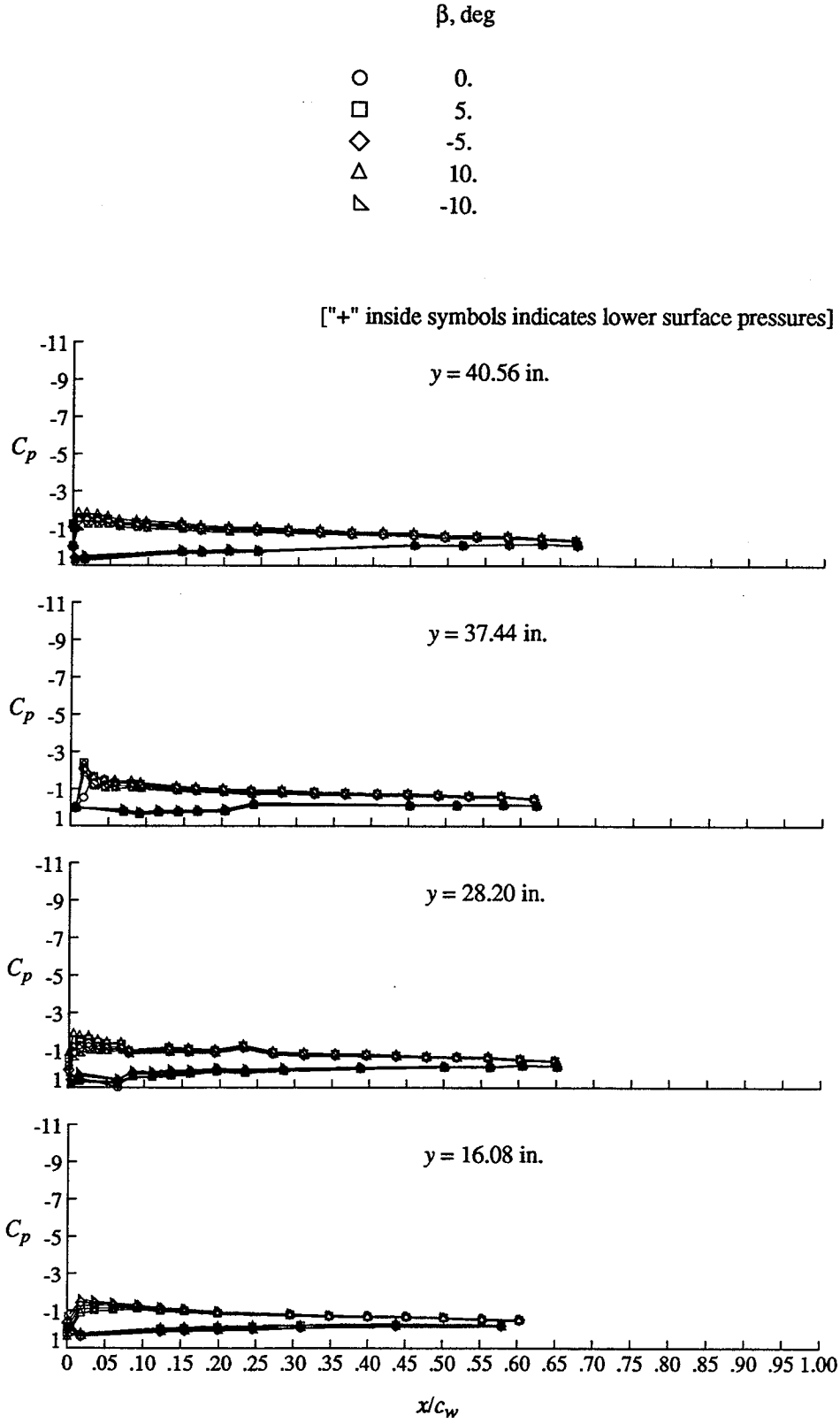

(b) $\alpha = 4°$.

Figure 15. Continued.

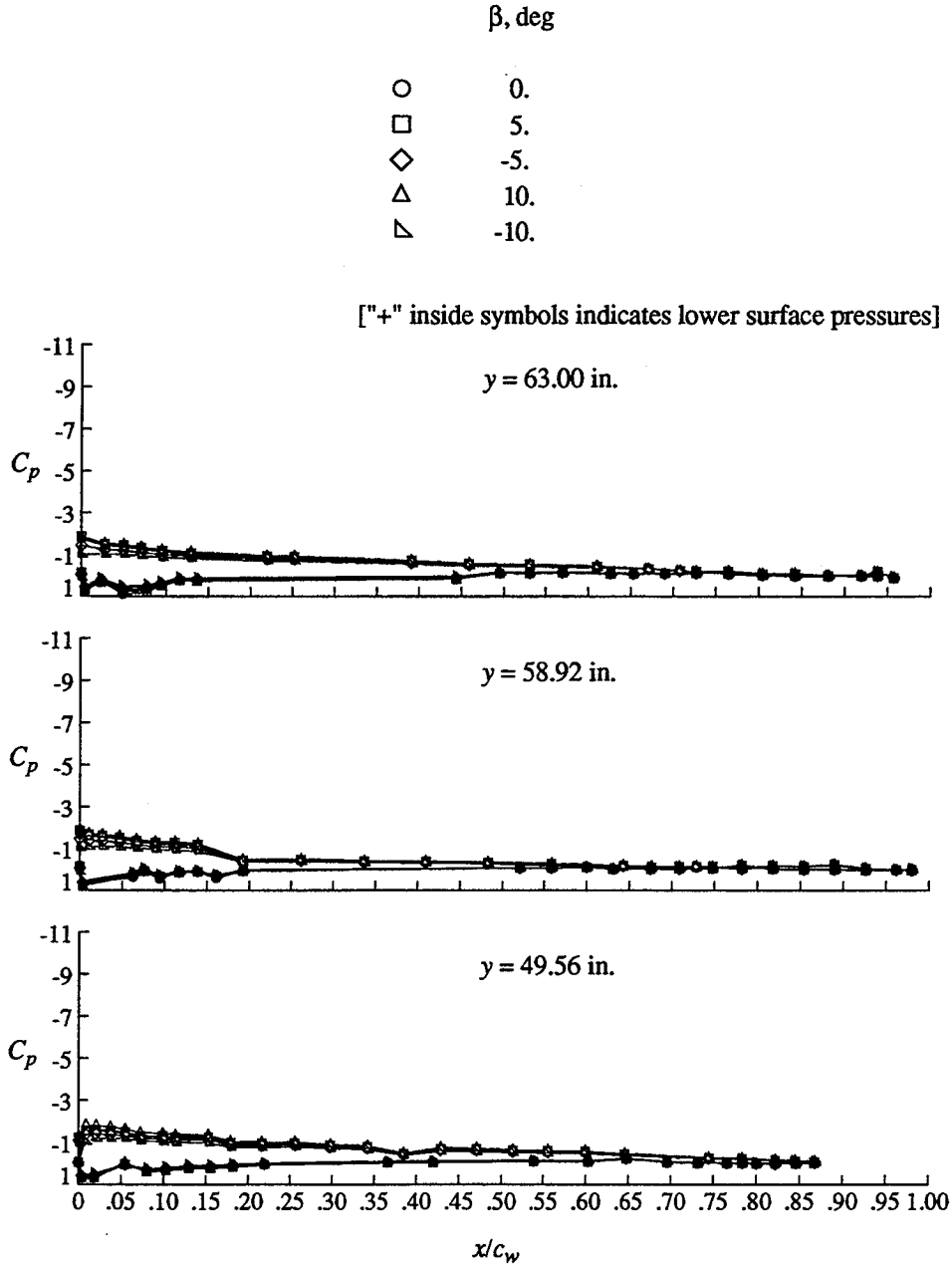

(b) $\alpha = 4°$.

Figure 15. Continued.

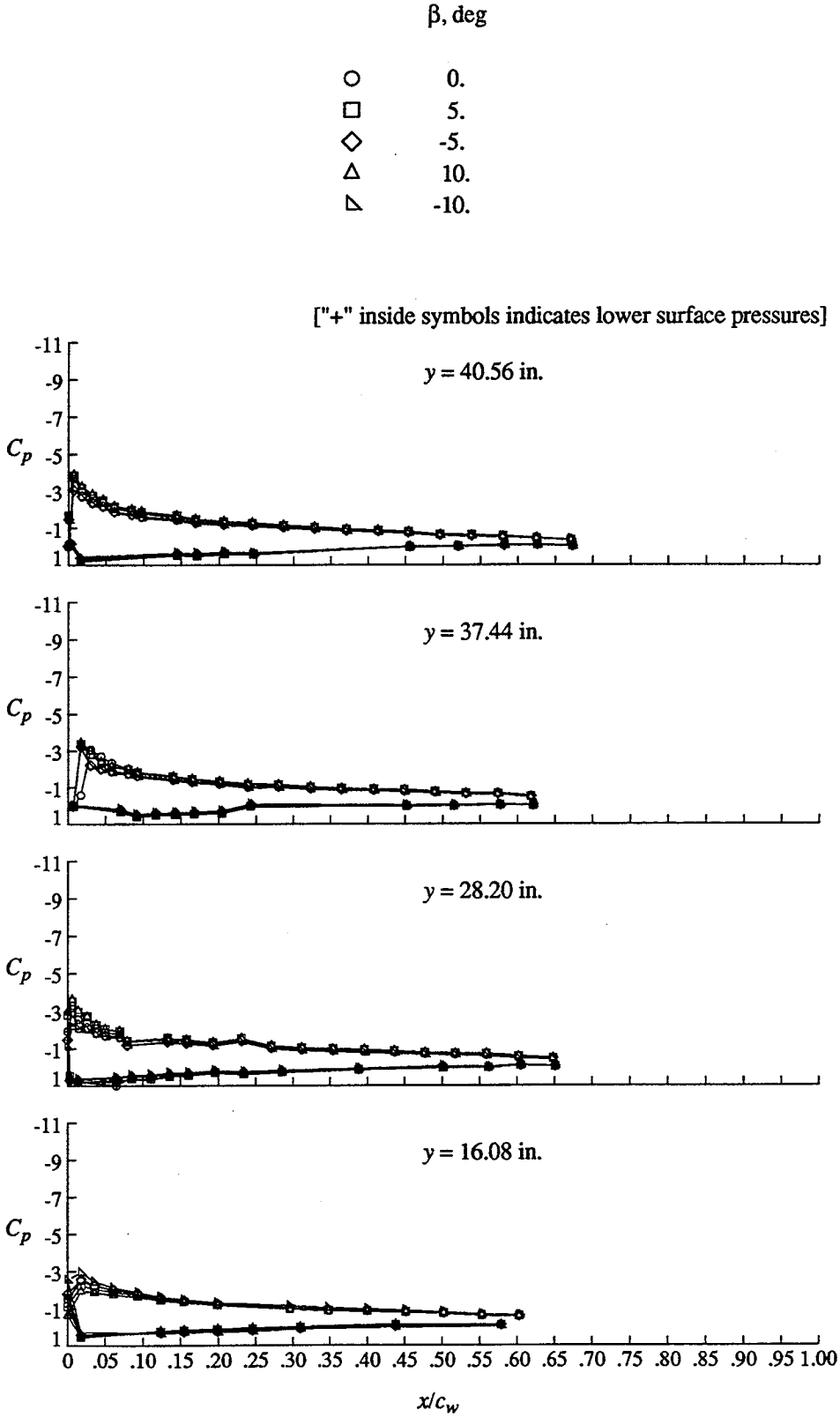

(c) $\alpha = 8°$.

Figure 15. Continued.

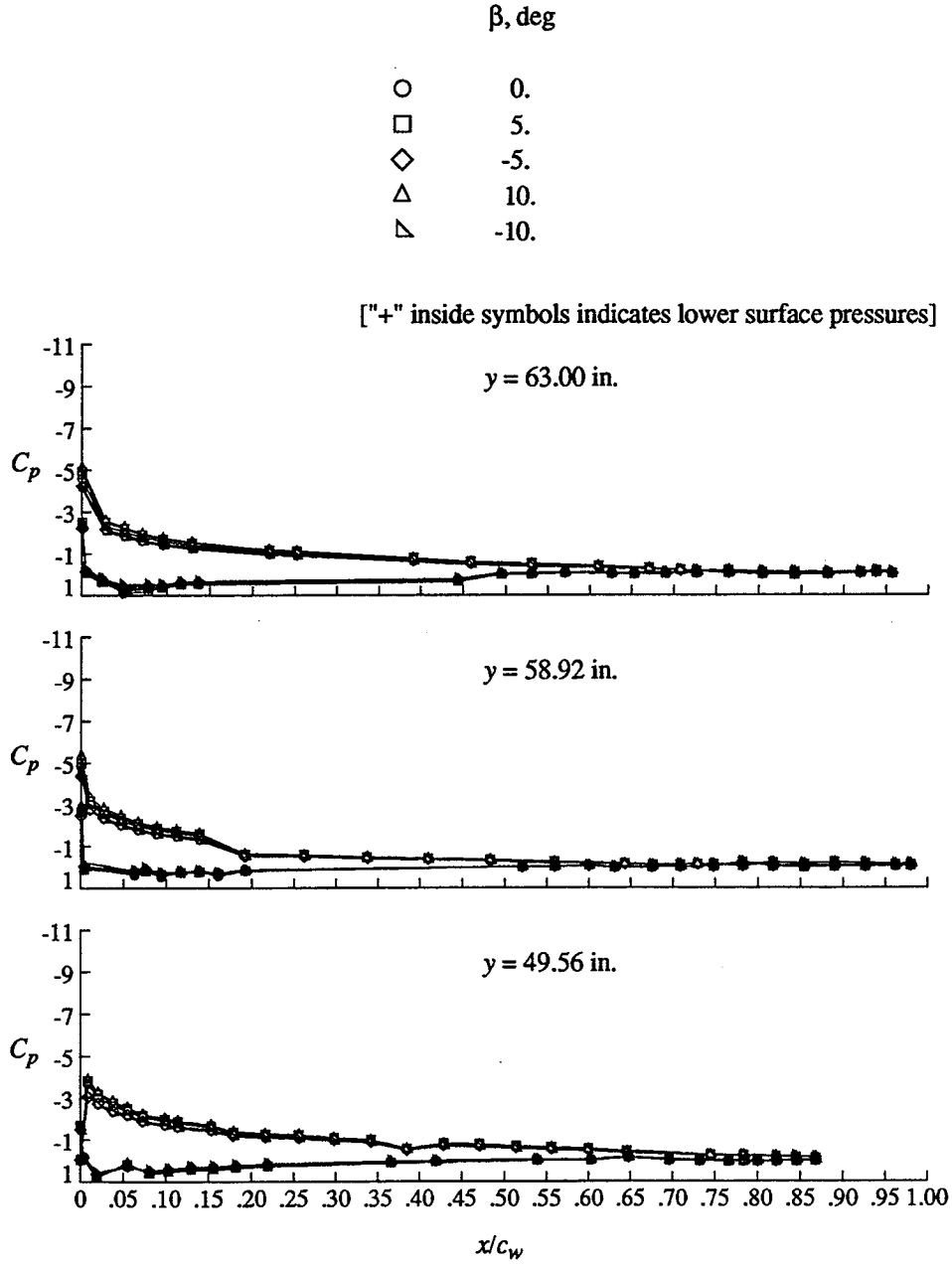

(c) $\alpha = 8°$.

Figure 15. Continued.

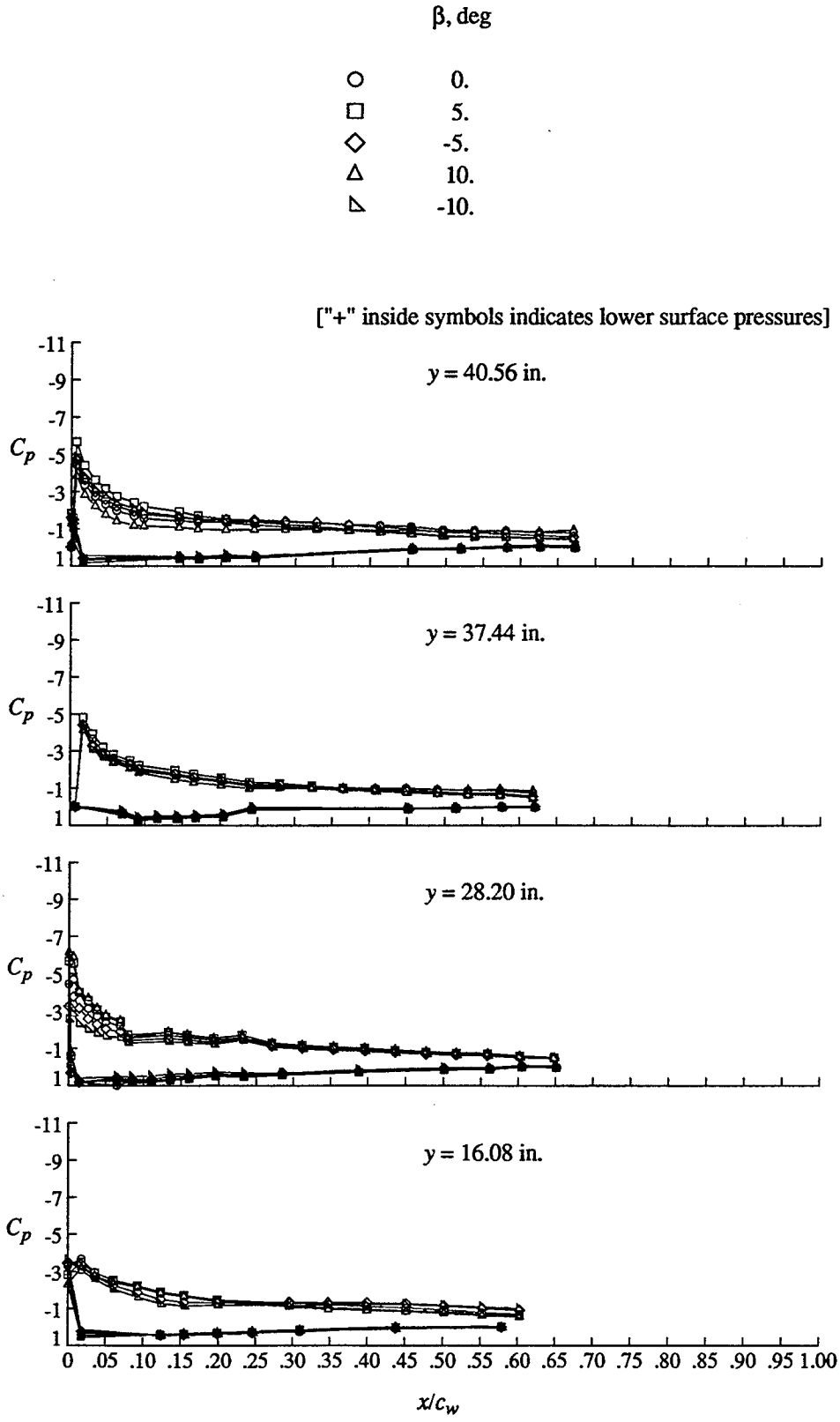

(d) $\alpha = 12°$.

Figure 15. Concluded.

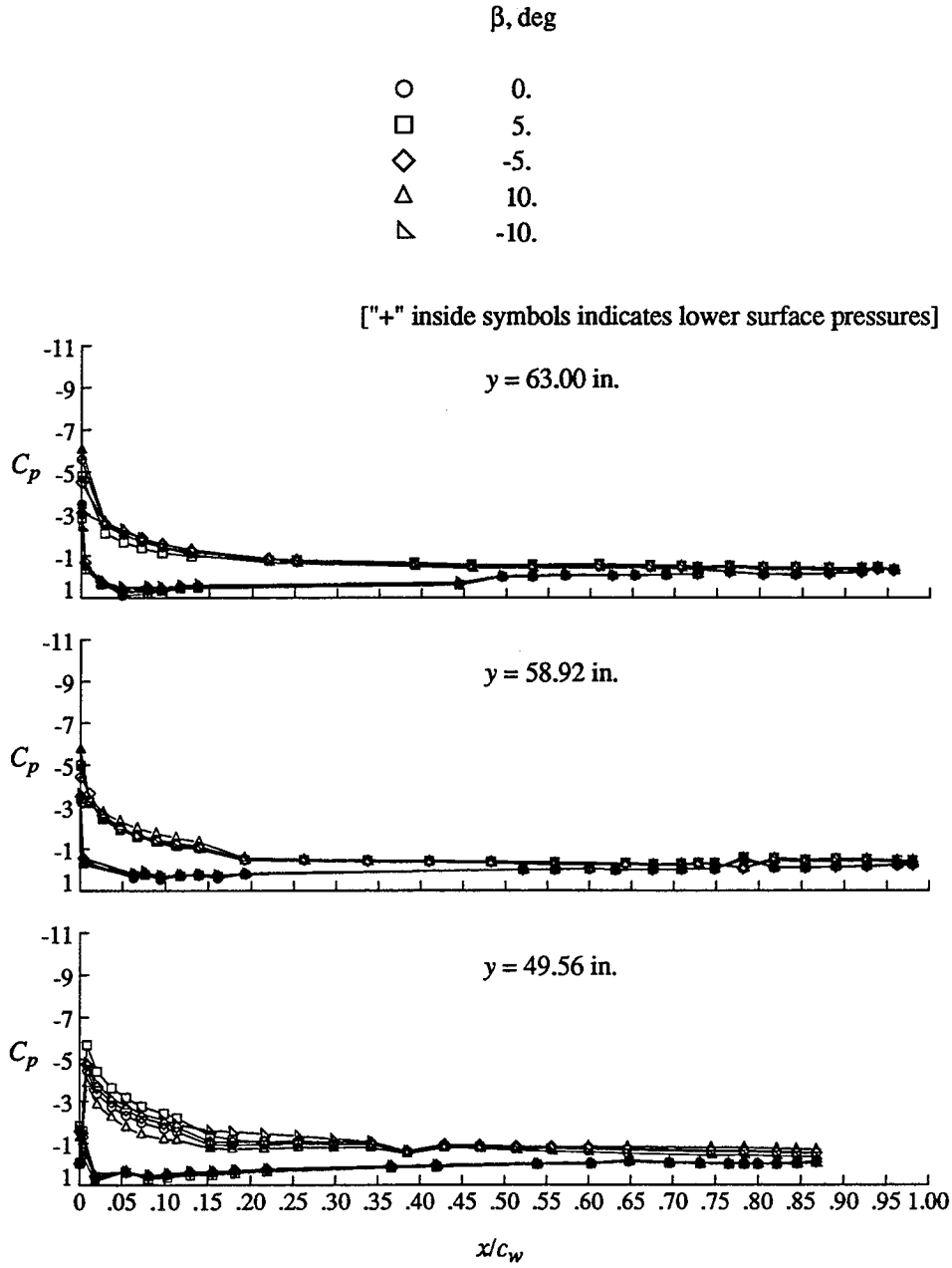

(d) $\alpha = 12°$.

Figure 15. Concluded.

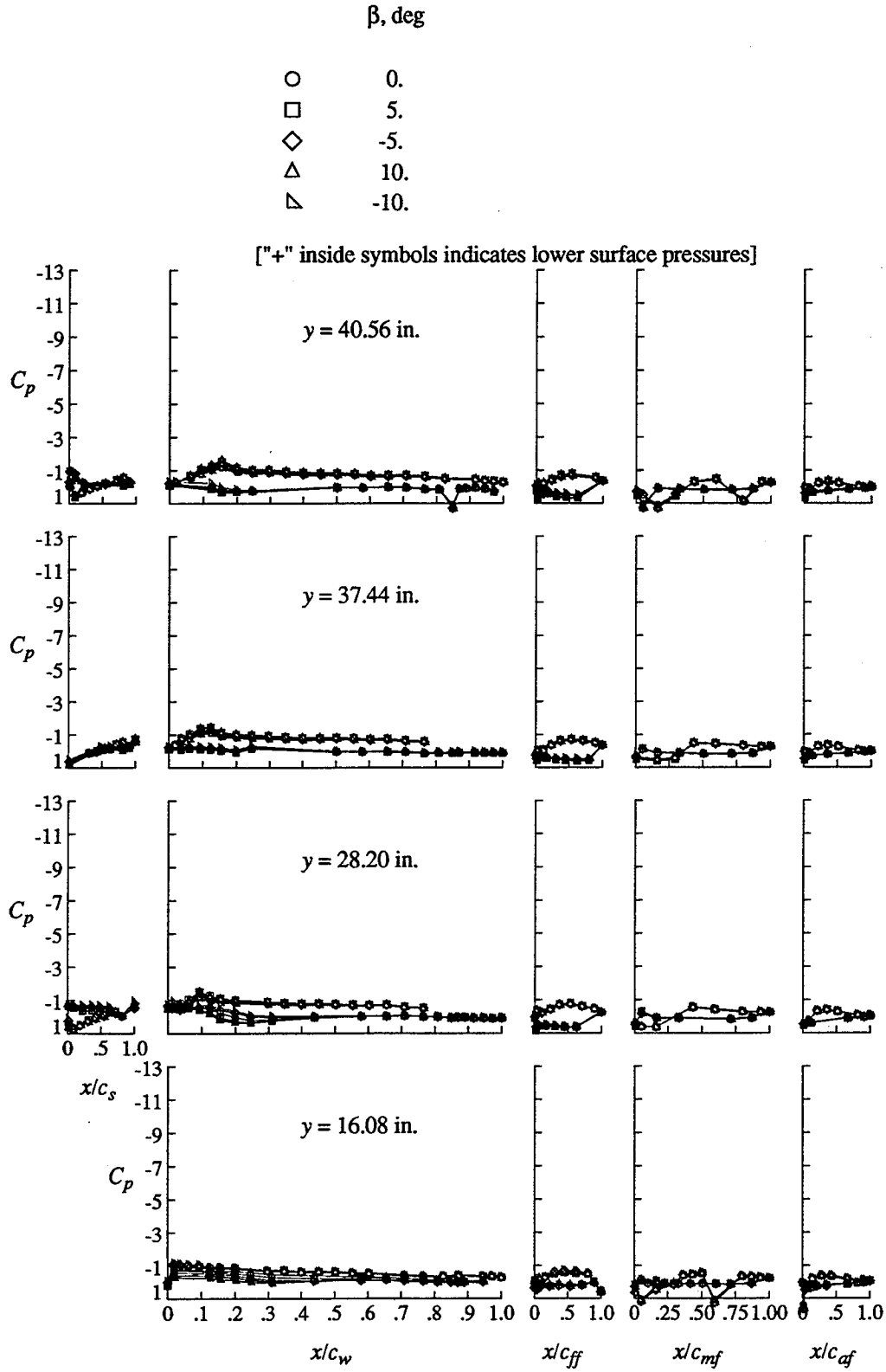

(a) $\alpha = 0°$.

Figure 16. Effect of sideslip on the wing pressure distributions of Take-off configuration.

q_∞ = 40 psf.

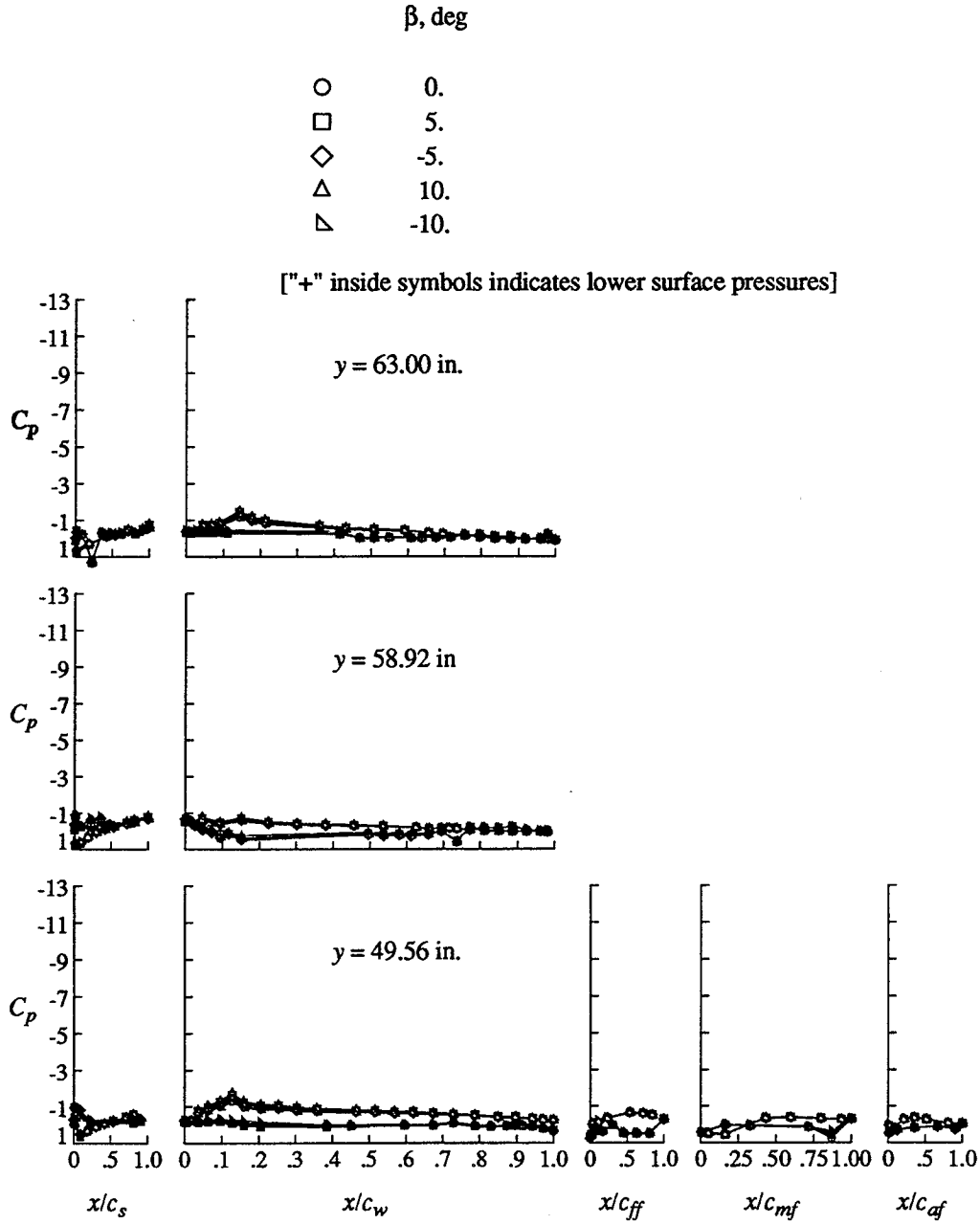

(a) $\alpha = 0°$.

Figure 16. Continued.

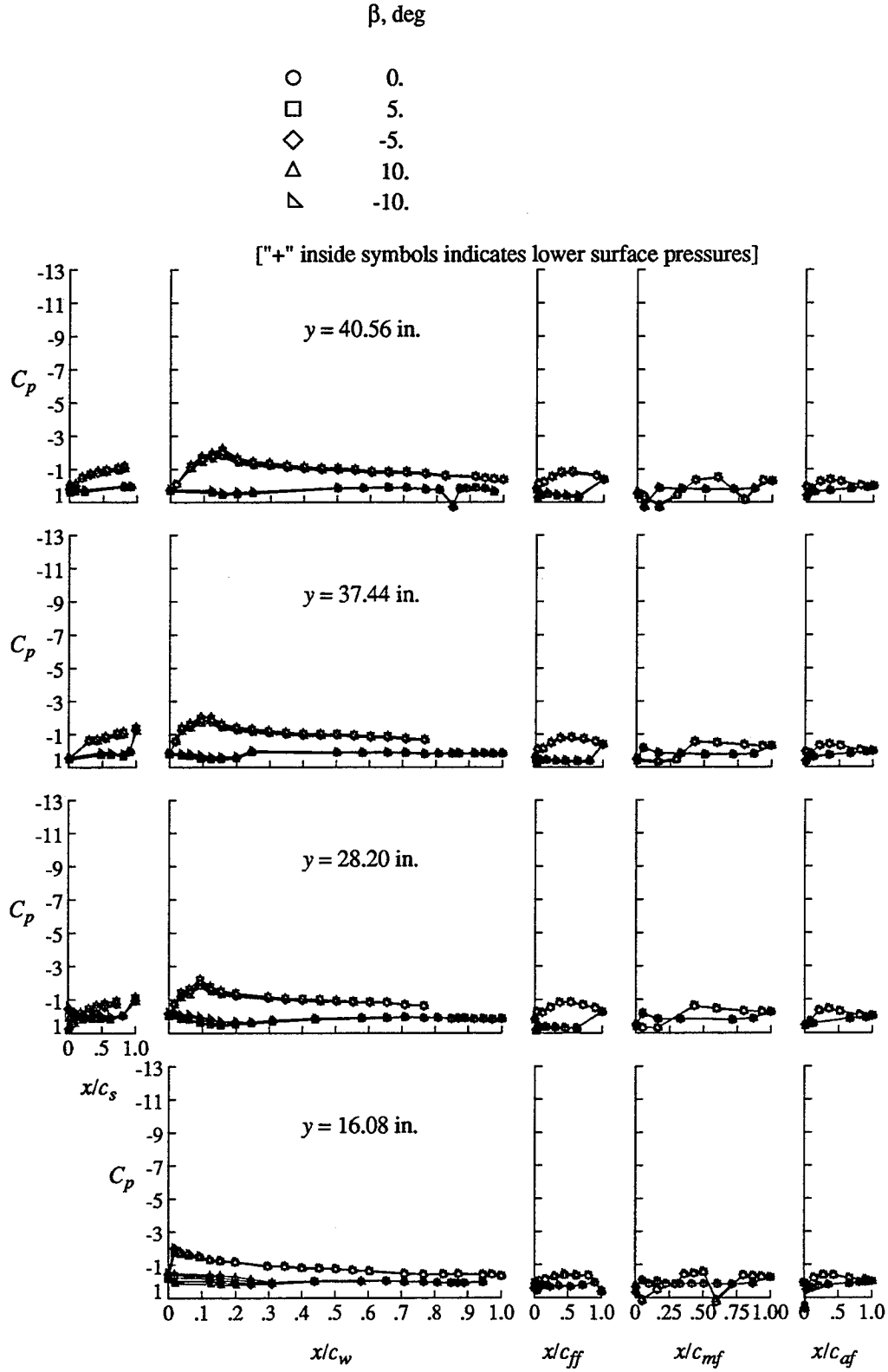

(b) $\alpha = 4°$.

Figure 16. Continued.

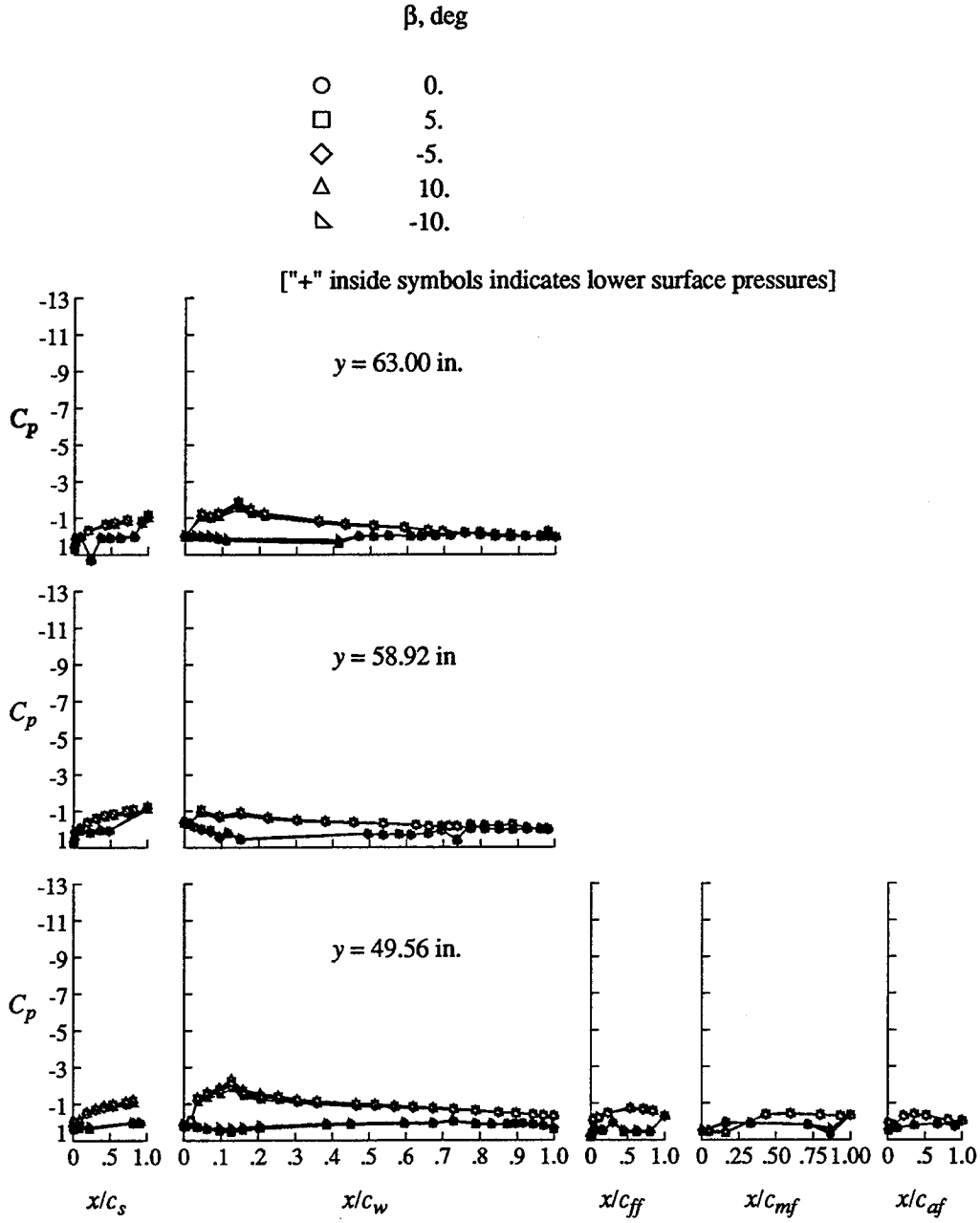

(b) $\alpha = 4°$.

Figure 16. Continued.

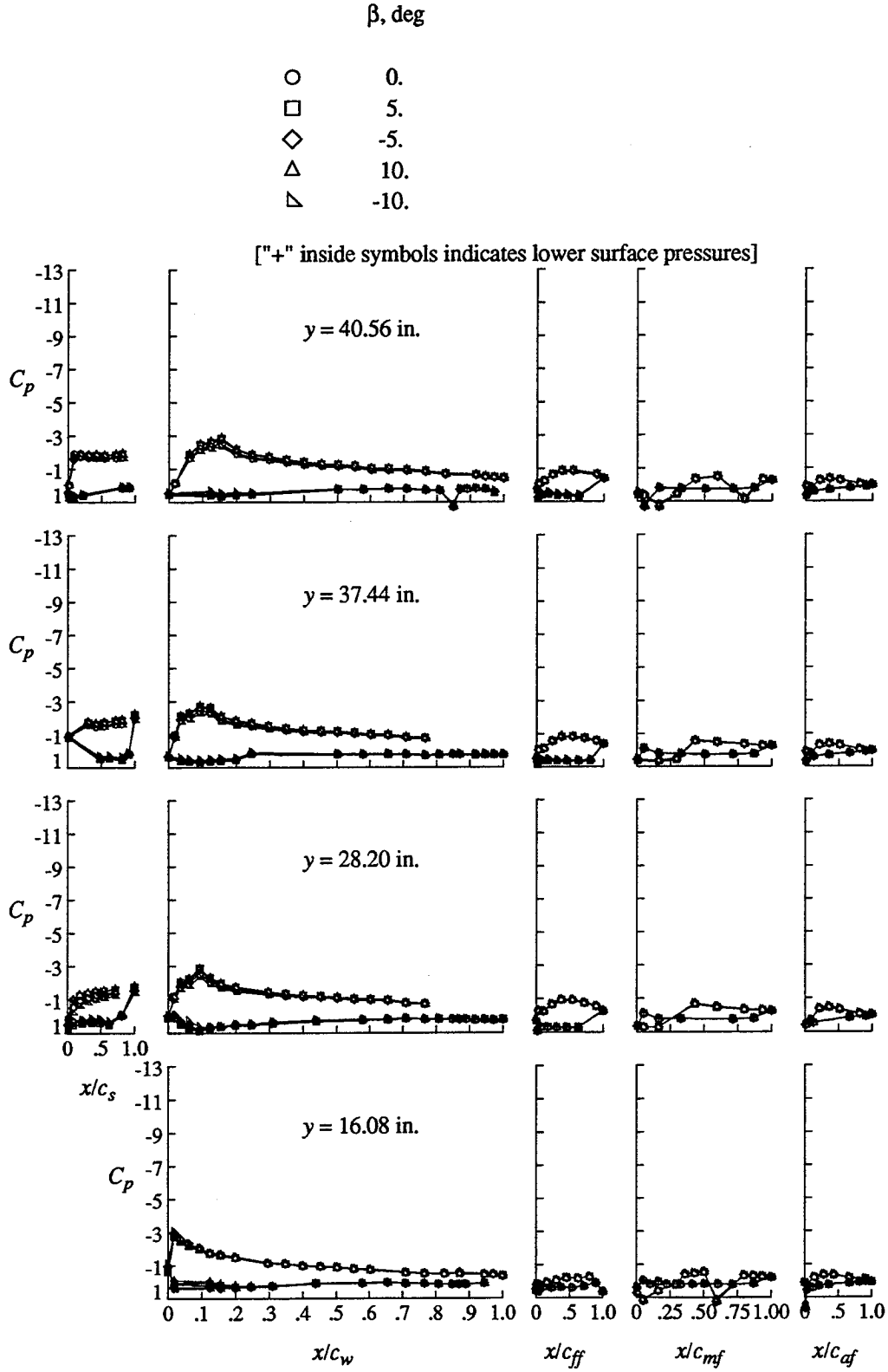

(c) $\alpha = 8°$.

Figure 16. Continued.

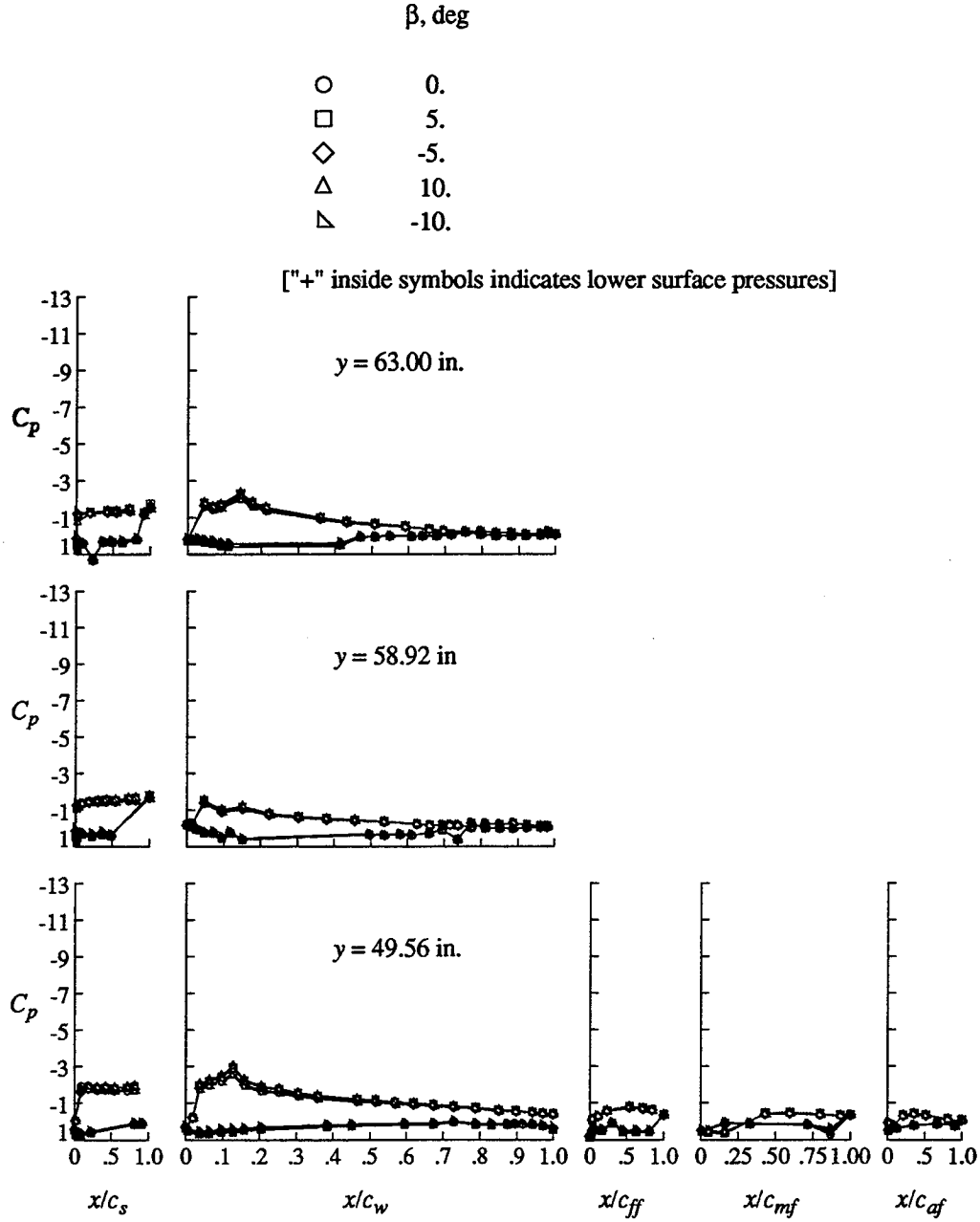

(c) $\alpha = 8°$.

Figure 16. Continued.

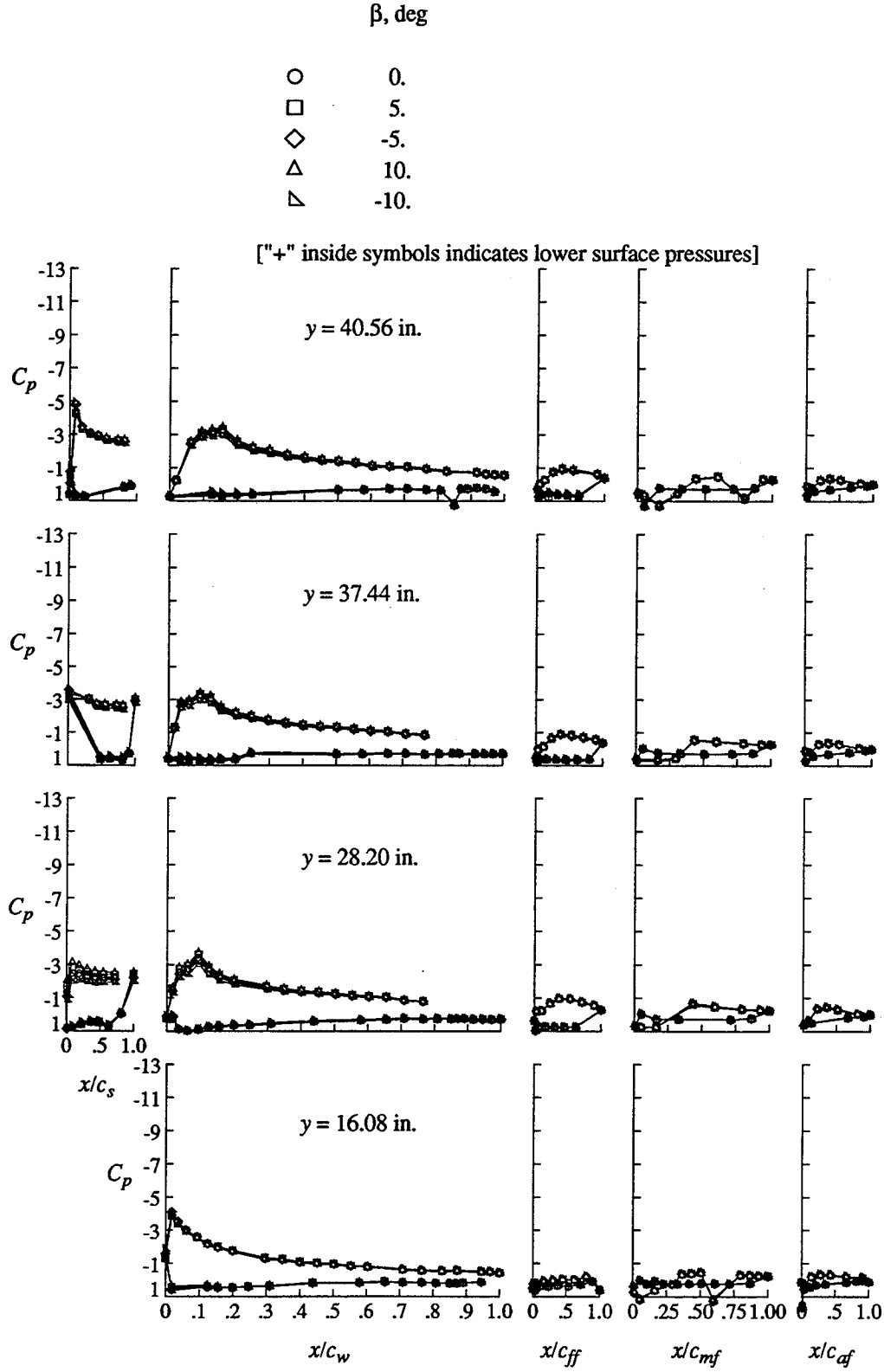

(d) $\alpha = 12°$.

Figure 16. Continued.

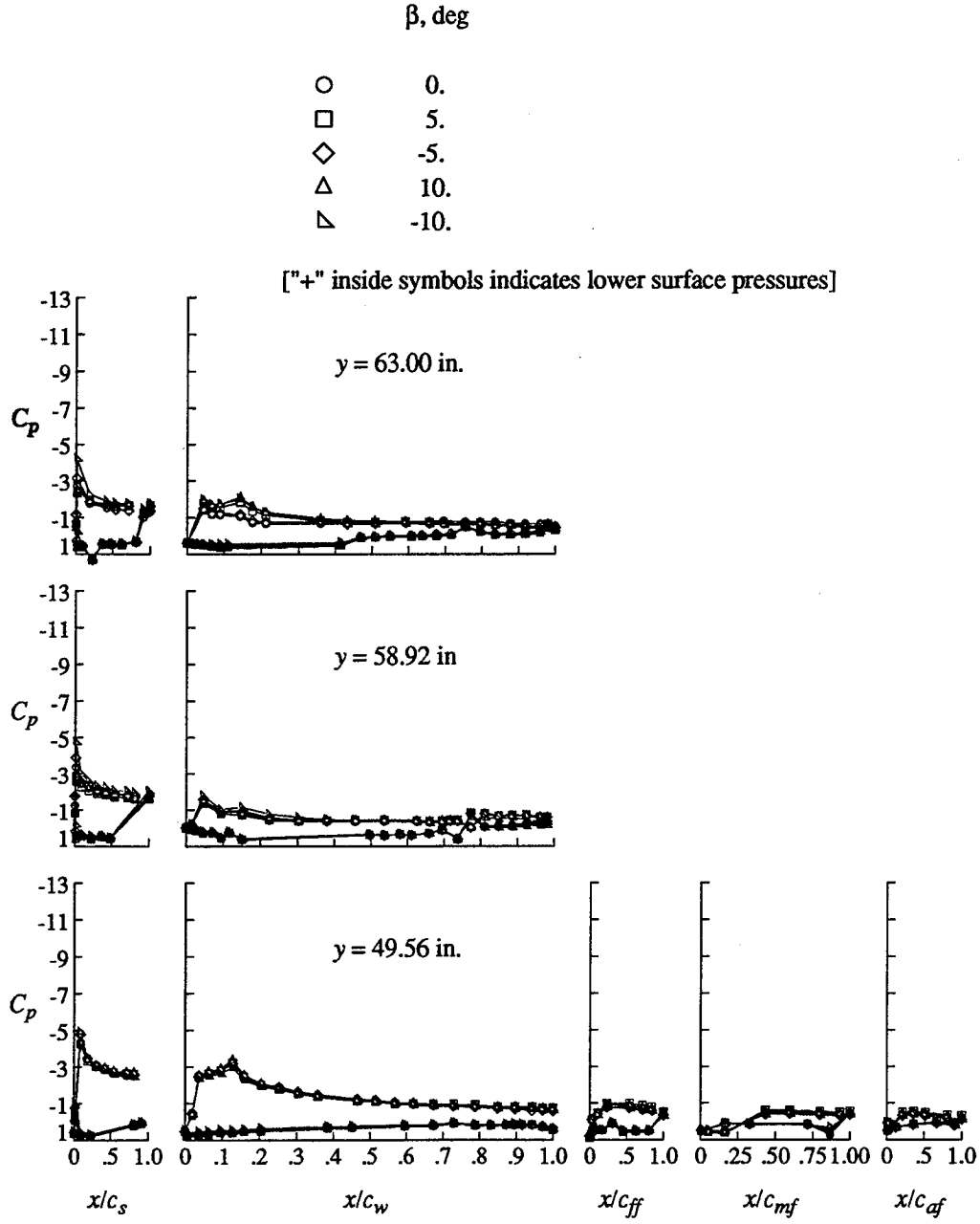

(d) $\alpha = 12°$.

Figure 16. Concluded.

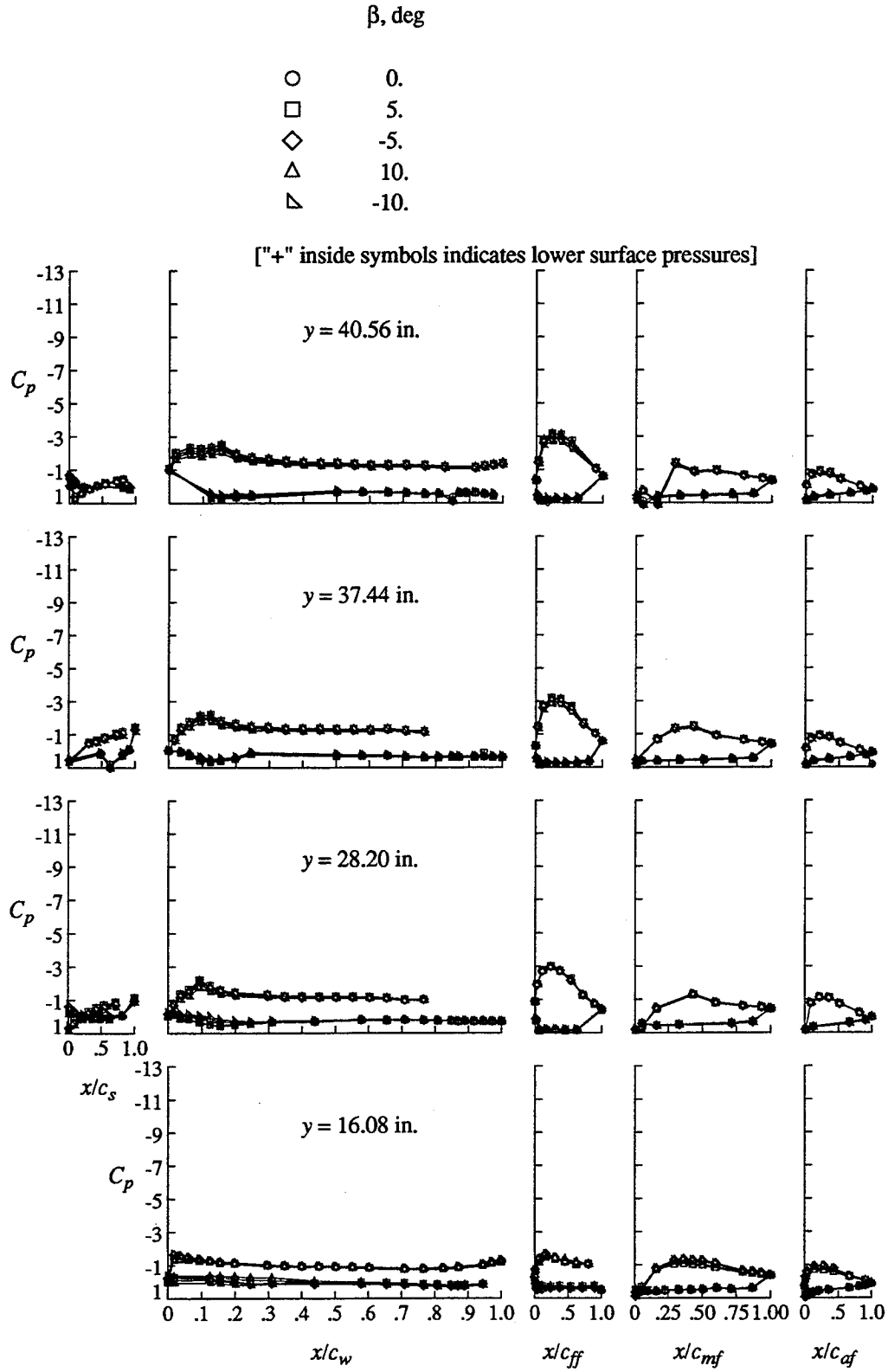

(a) $\alpha = 0°$.

Figure 17. Effect of sideslip on the wing pressure distributions of Landing 1 configuration.

$q_\infty = 40$ psf.

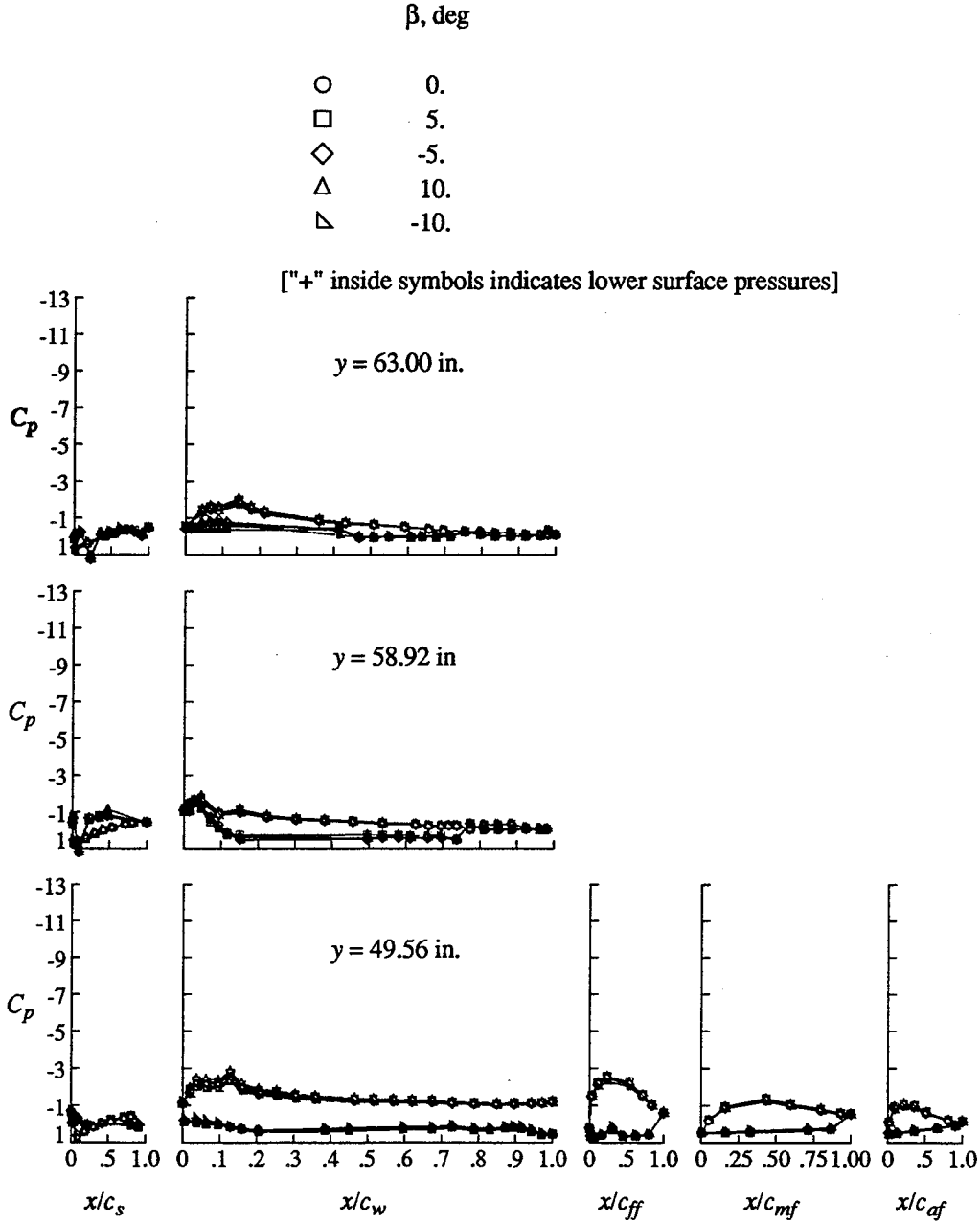

(a) $\alpha = 0°$.

Figure 17. Continued.

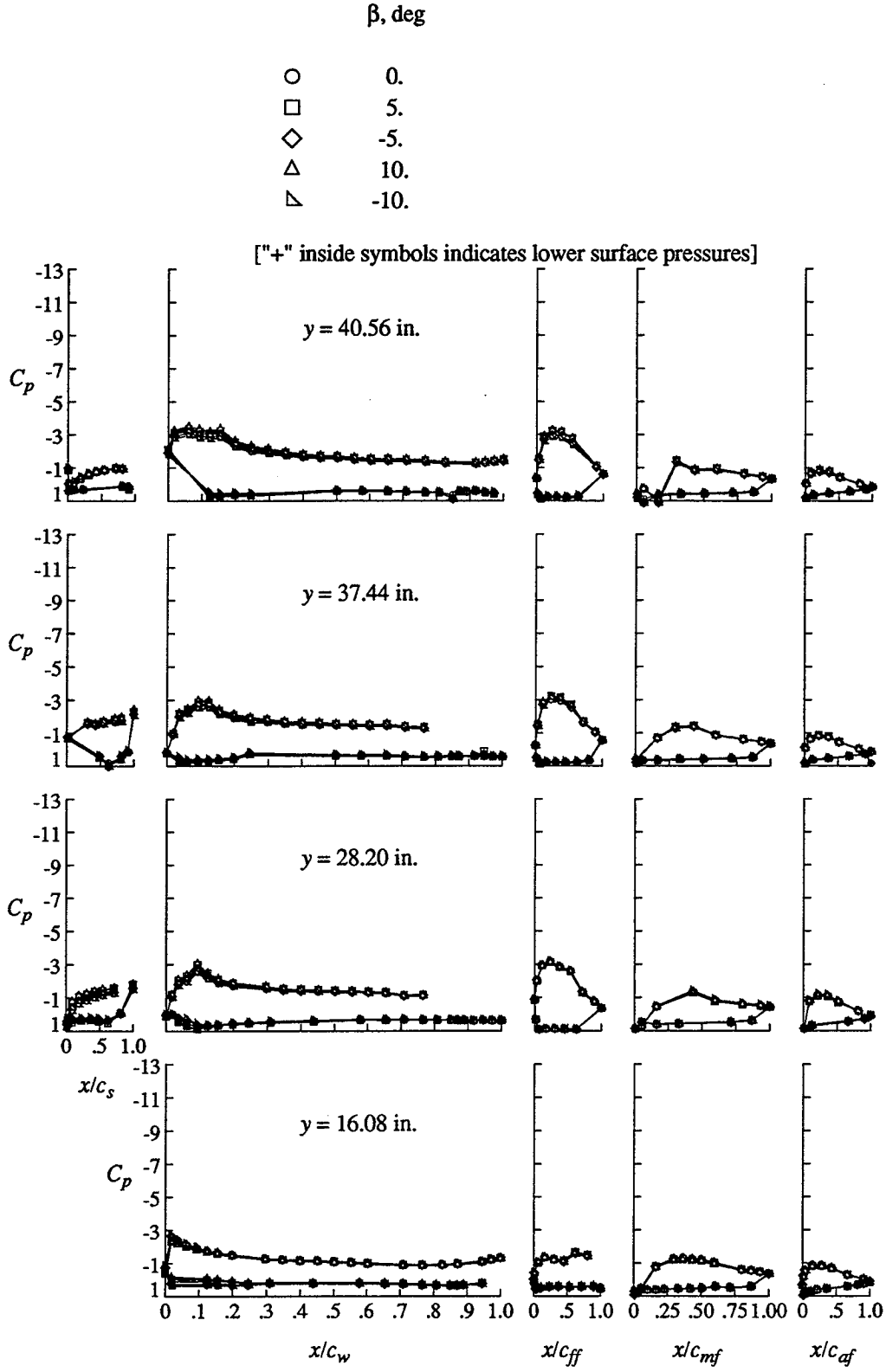

(b) $\alpha = 4°$.

Figure 17. Continued.

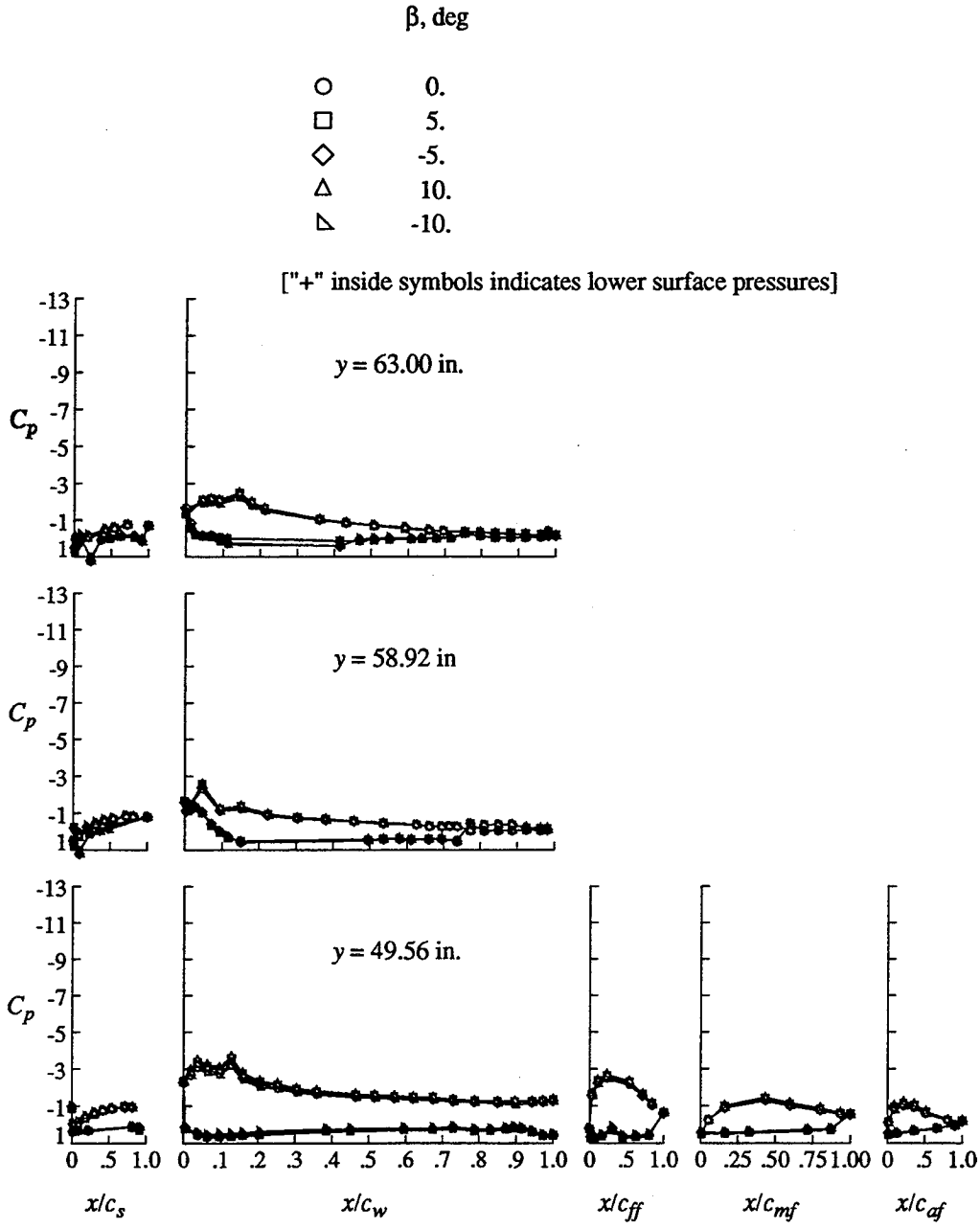

(b) $\alpha = 4°$.

Figure 17. Continued.

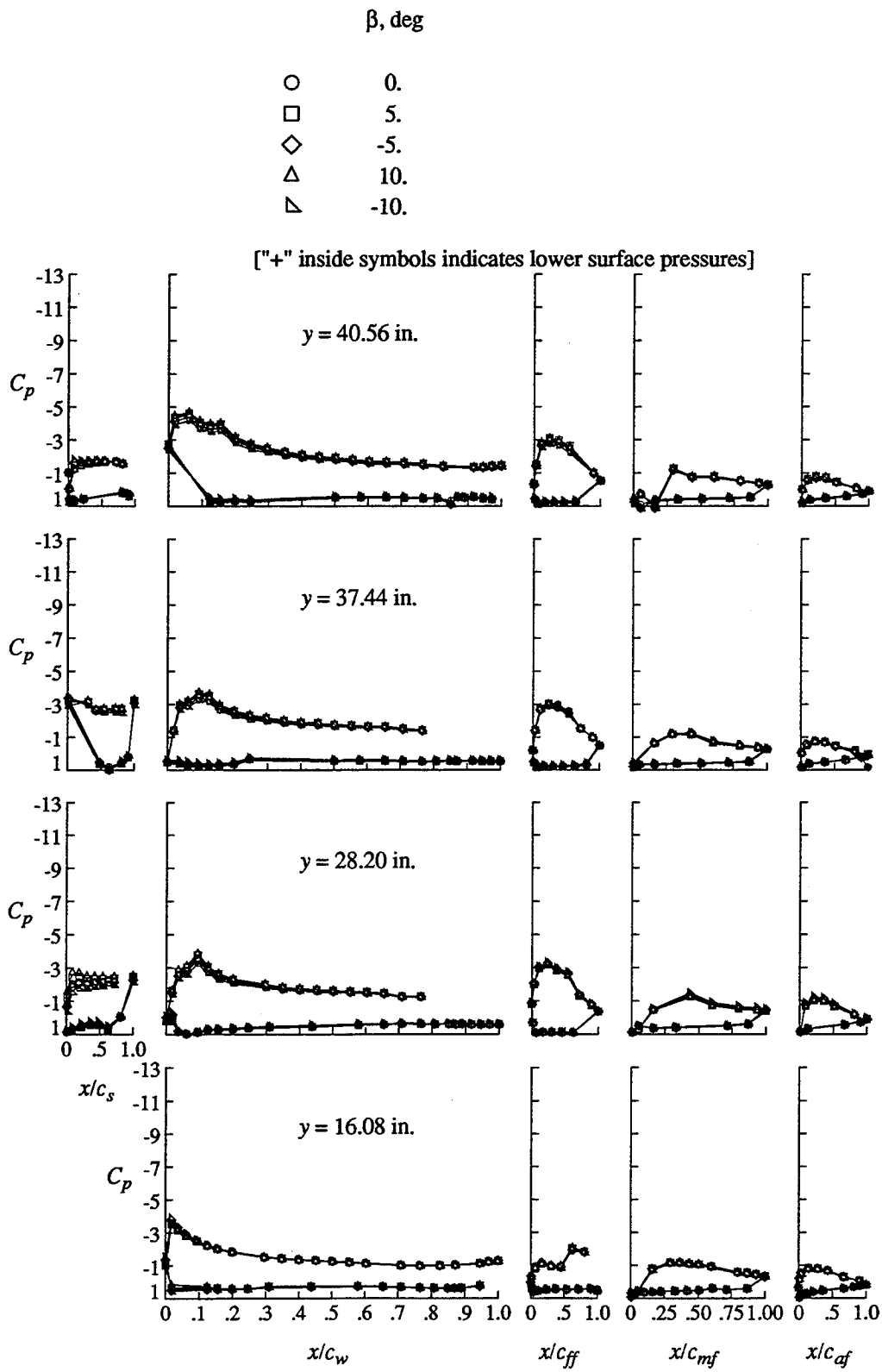

(c) $\alpha = 8°$.

Figure 17. Continued.

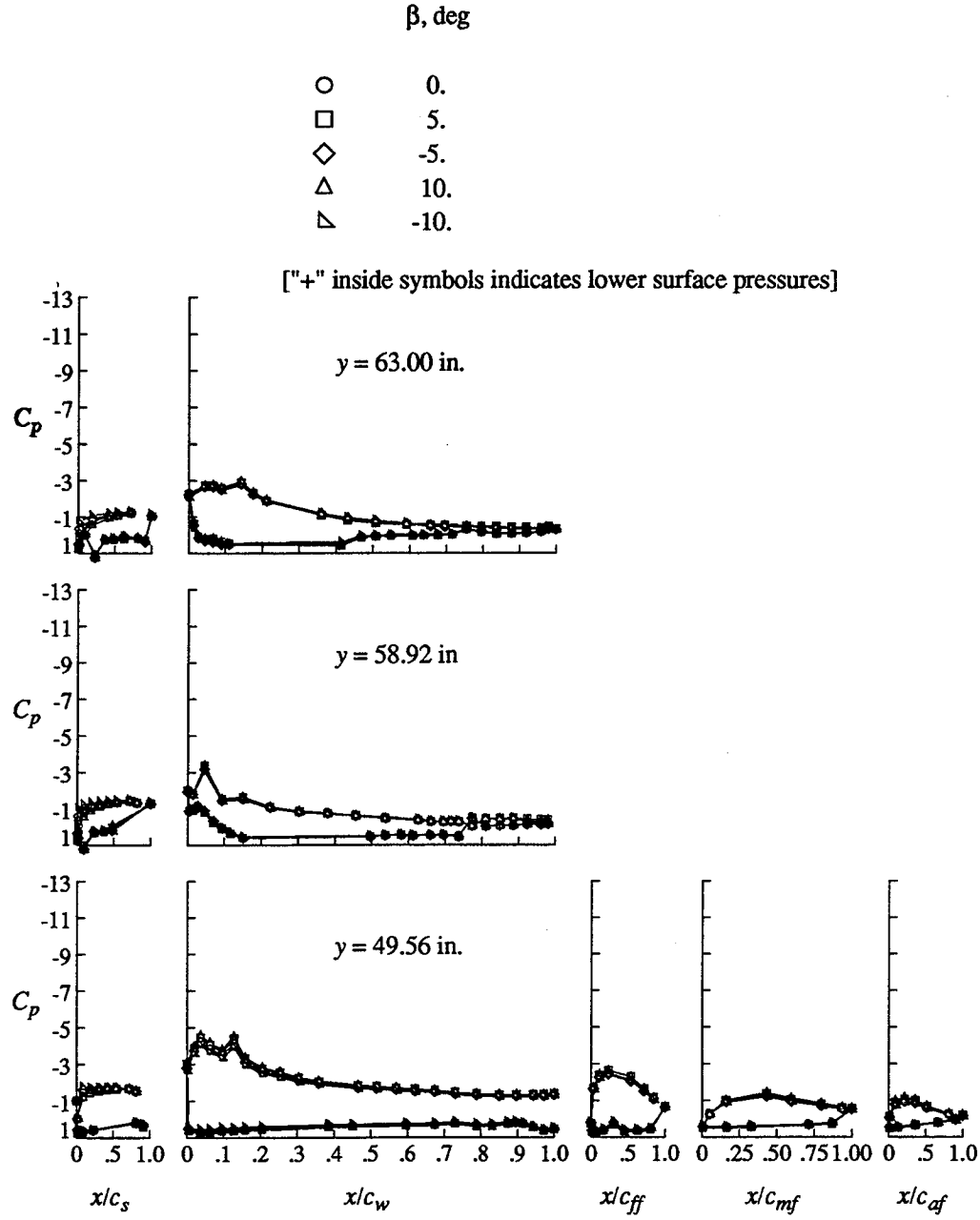

(c) $\alpha = 8°$.

Figure 17. Continued.

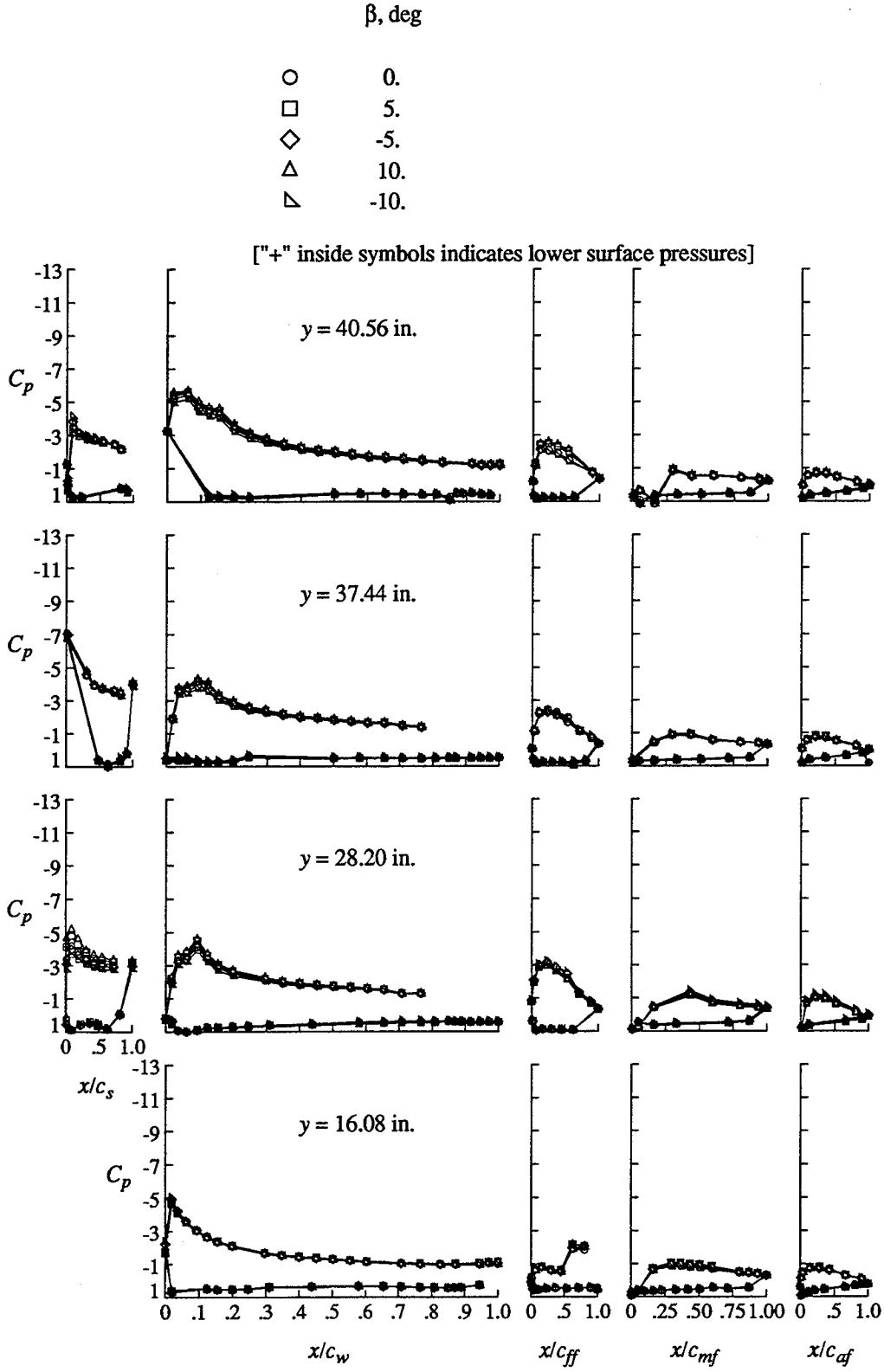

(d) $\alpha = 12°$.

Figure 17. Concluded.

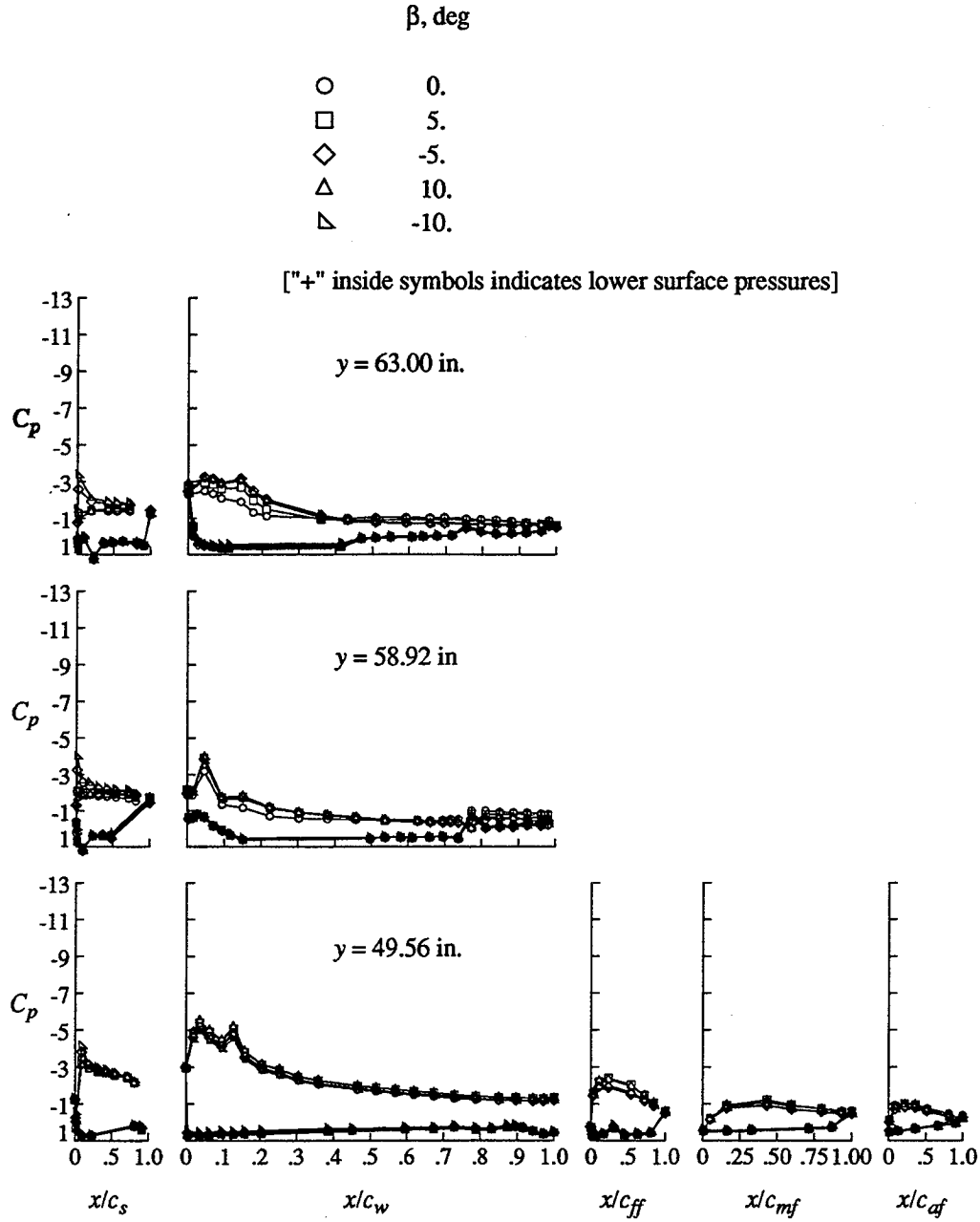

(d) $\alpha = 12°$.

Figure 17. Concluded.

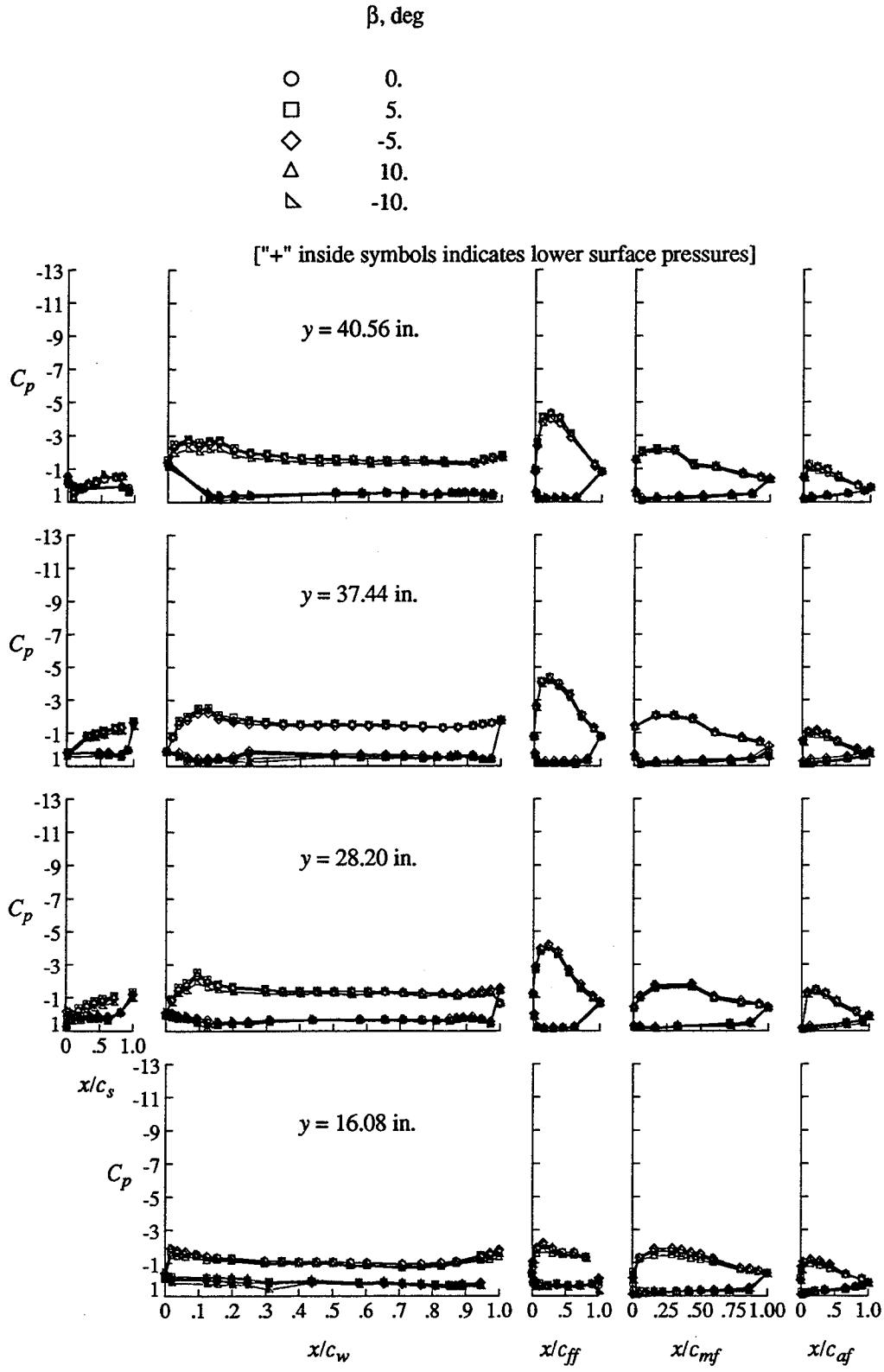

(a) $\alpha = 0°$.

Figure 18. Effect of sideslip on the wing pressure distributions of Landing 2 configuration.

q_∞ = 40 psf.

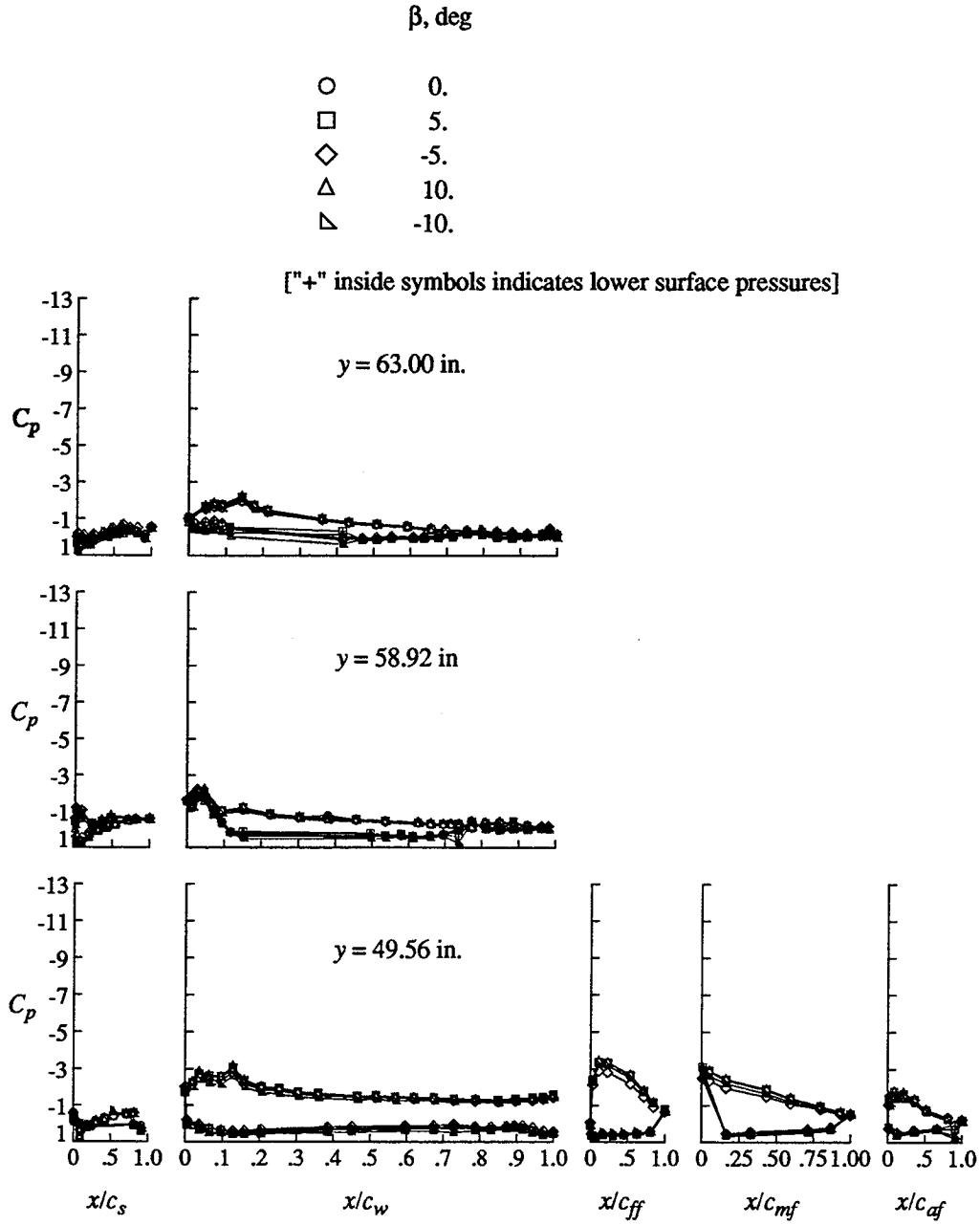

(a) $\alpha = 0°$.

Figure 18. Continued.

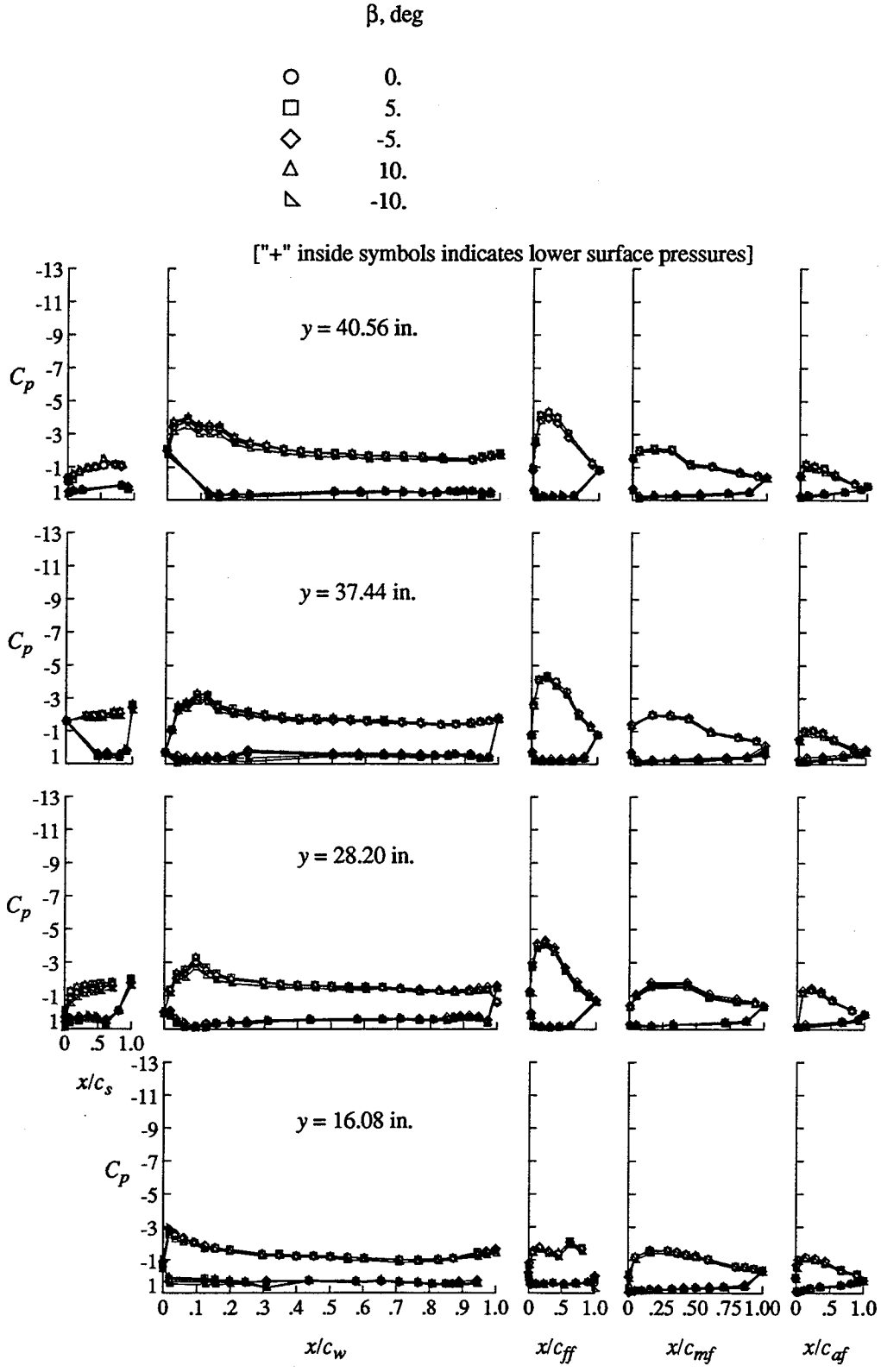

(b) $\alpha = 4°$.

Figure 18. Continued.

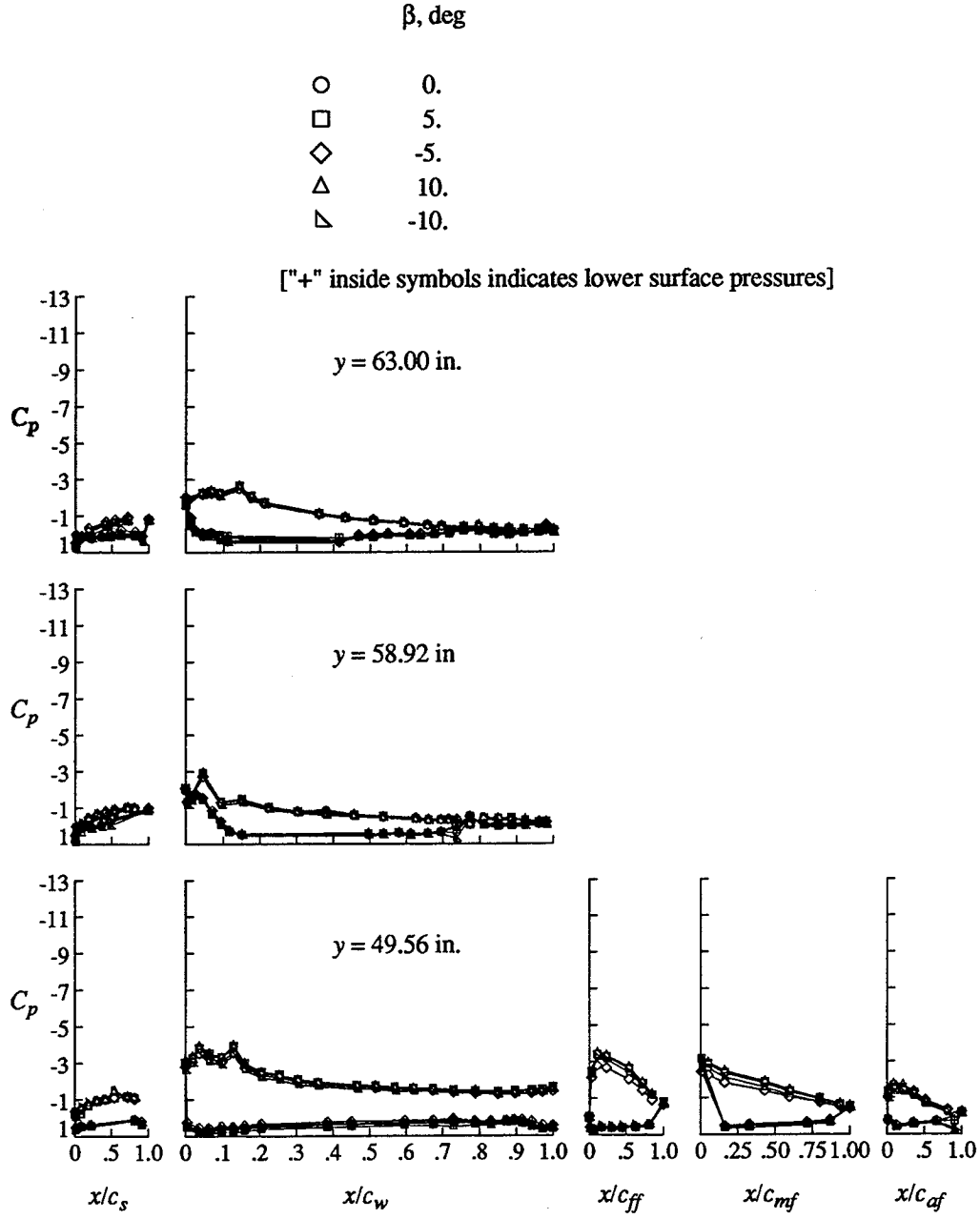

(b) $\alpha = 4°$.

Figure 18. Continued.

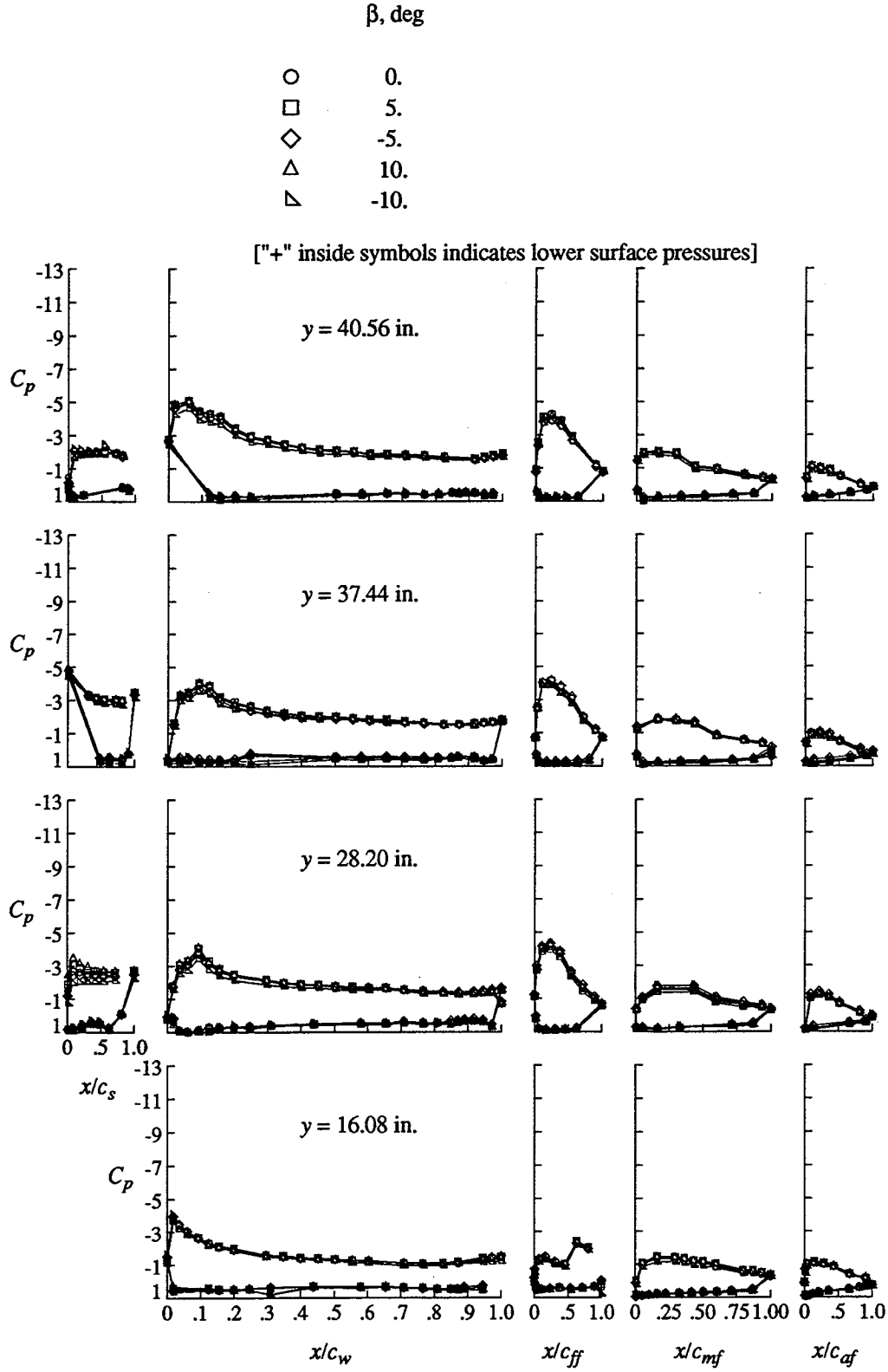

(c) $\alpha = 8°$.

Figure 18. Continued.

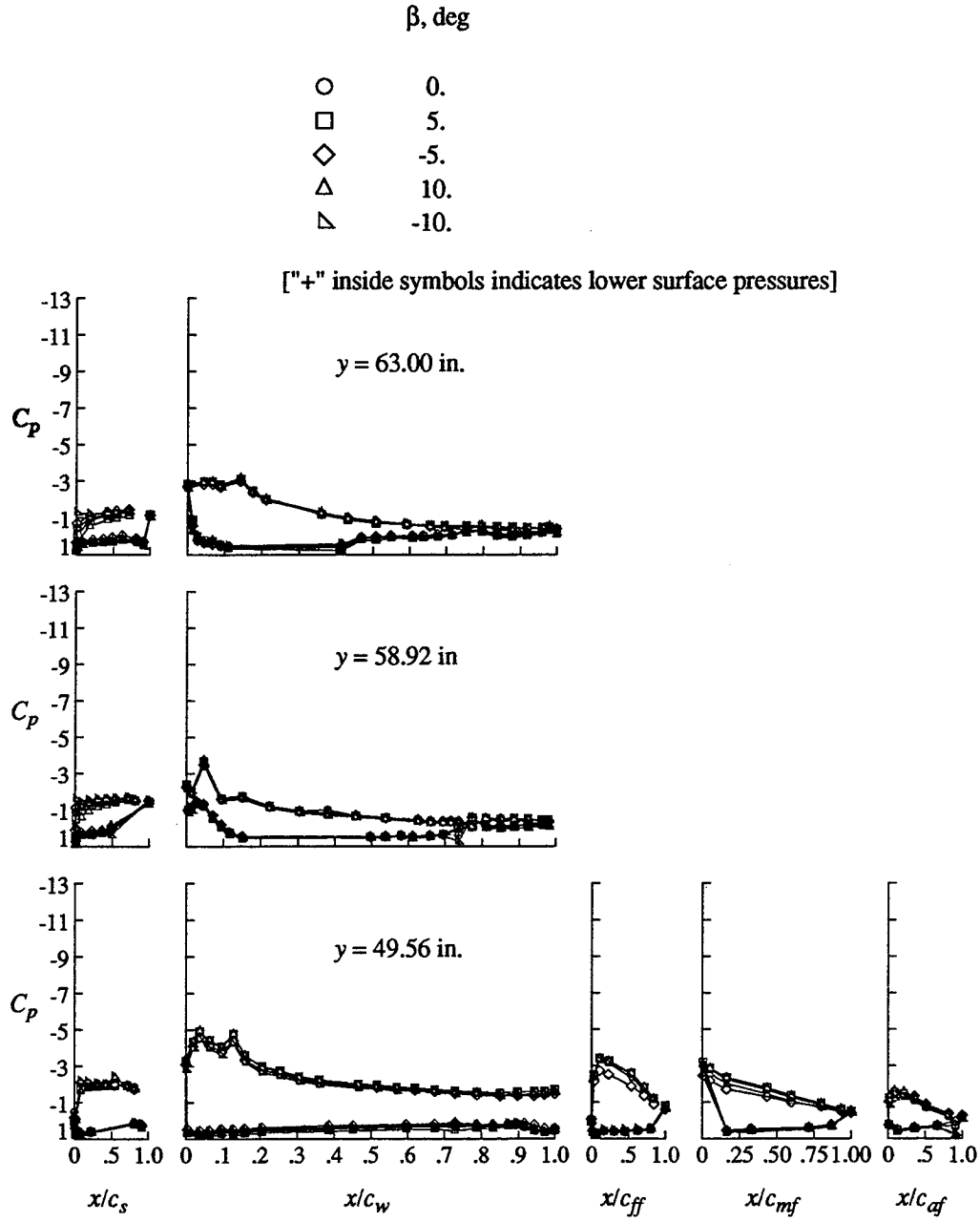

(c) $\alpha = 8°$.

Figure 18. Continued.

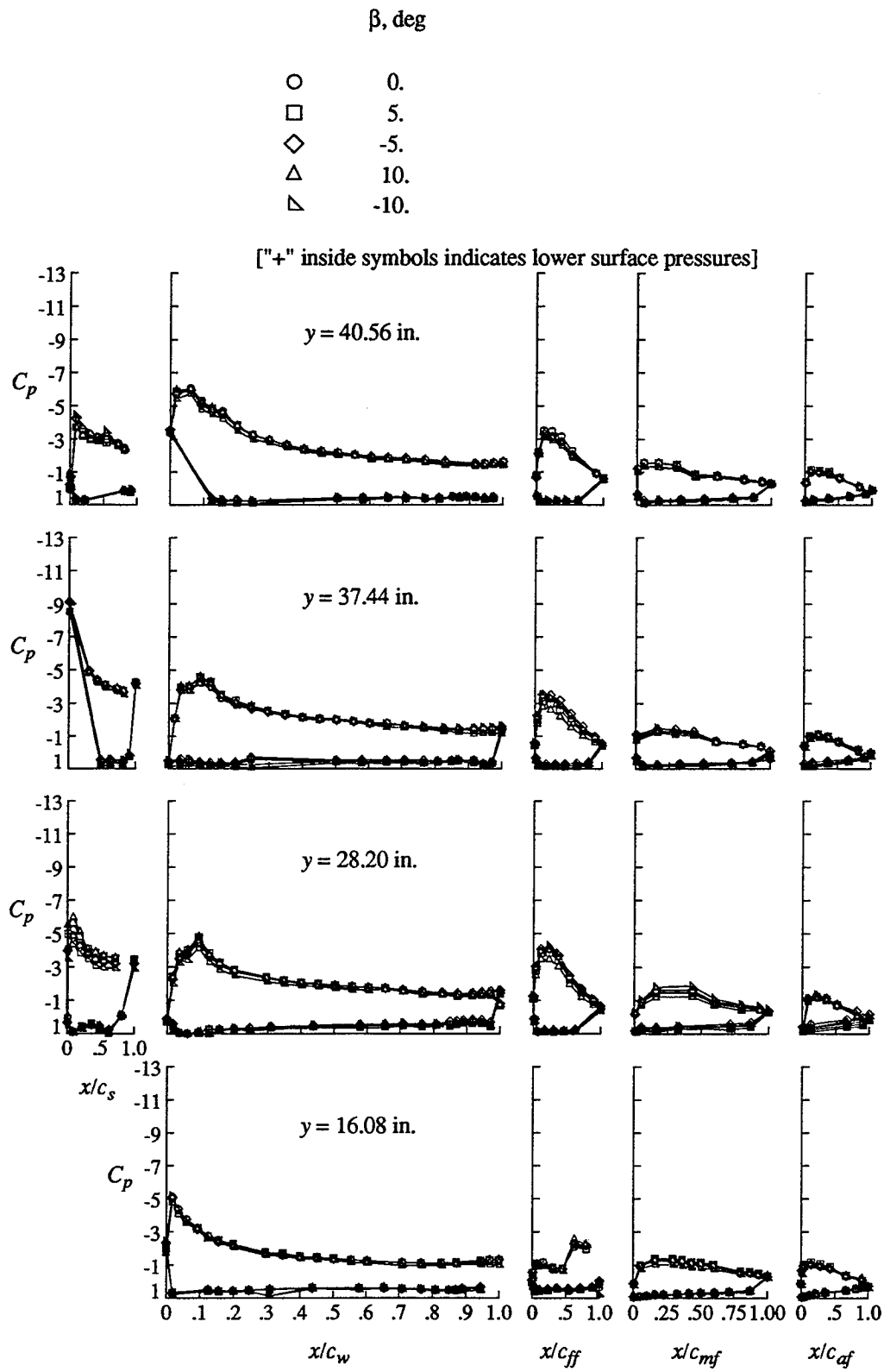

(d) $\alpha = 12°$.

Figure 18. Concluded.

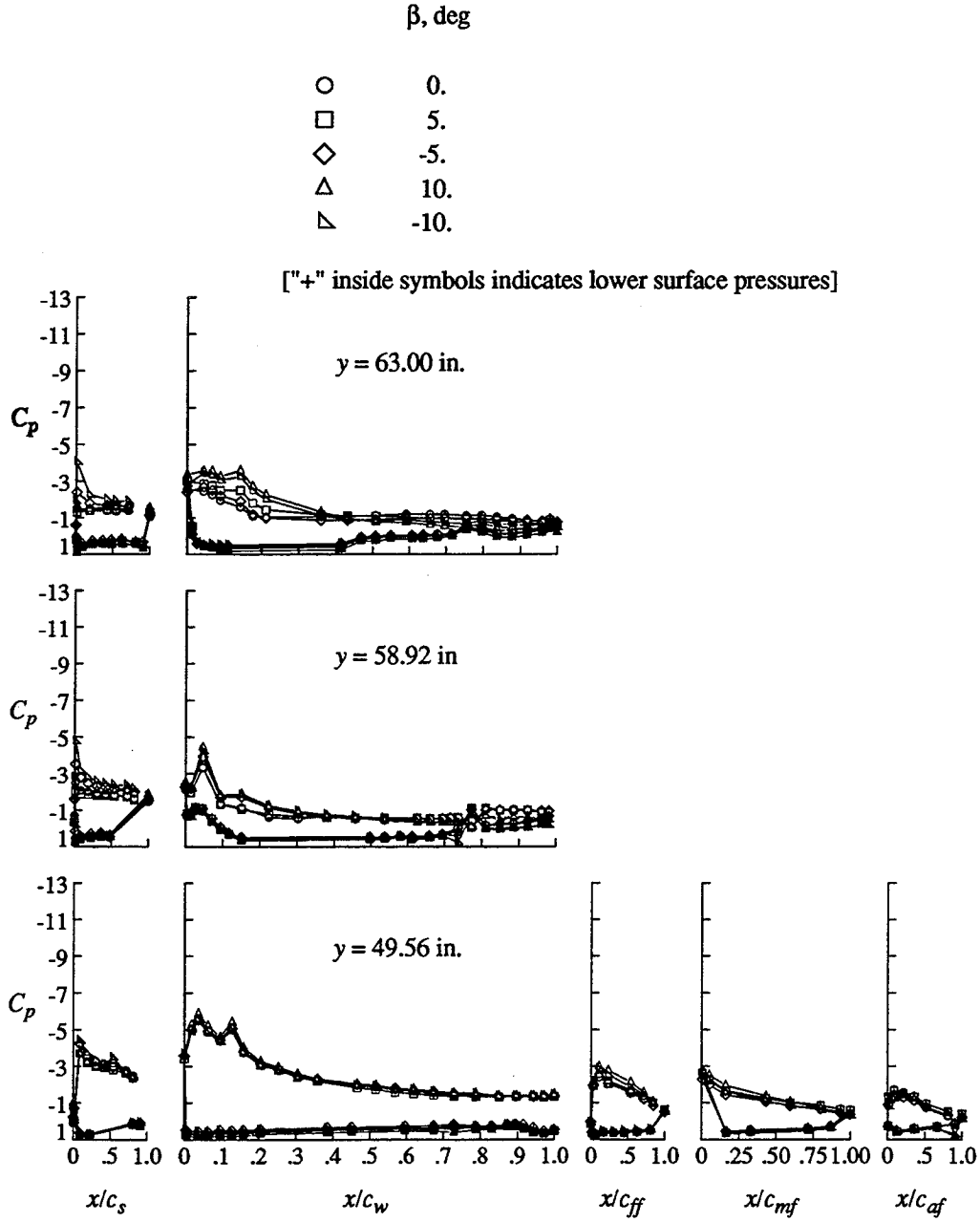

(d) $\alpha = 12°$.

Figure 18. Concluded.

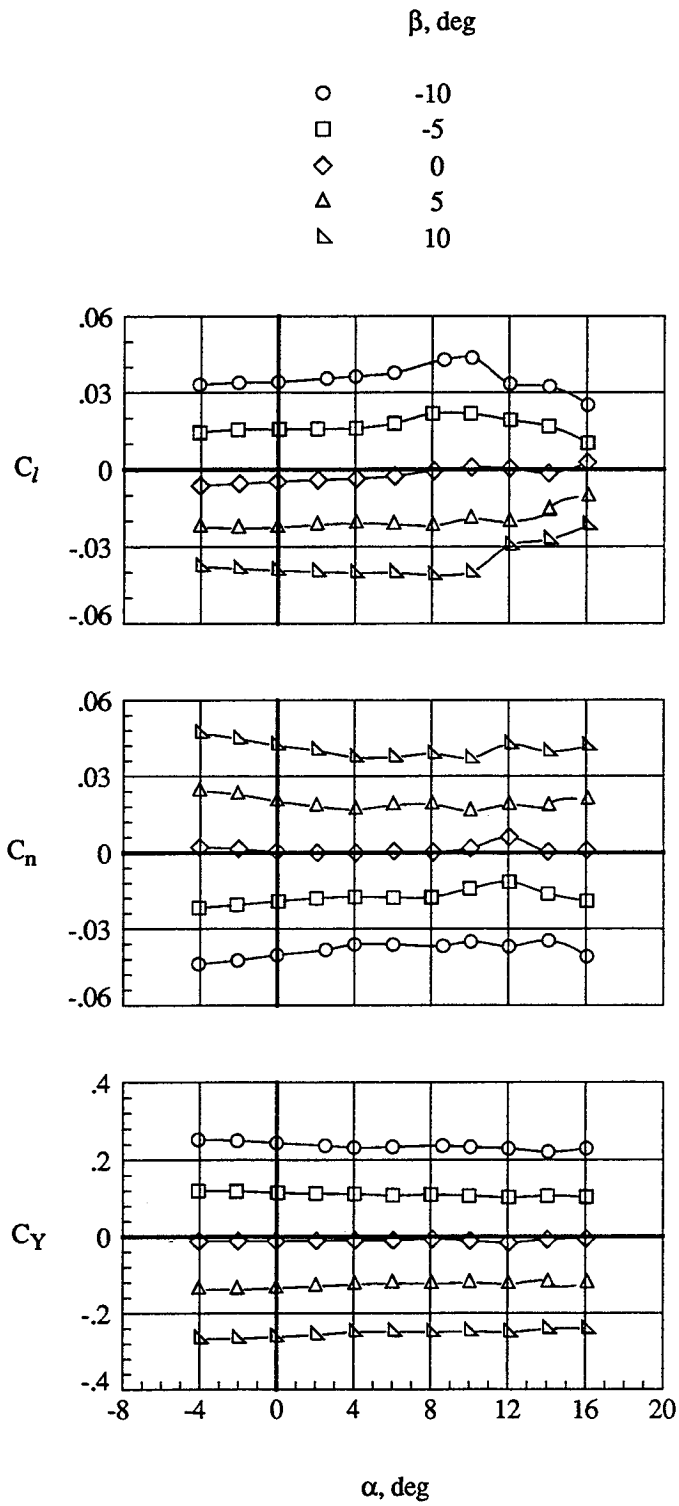

(a) Cruise configuration

Figure 19. Effect of sideslip on the lateral aerodynamic characteristics.

q_∞ = 40 psf.

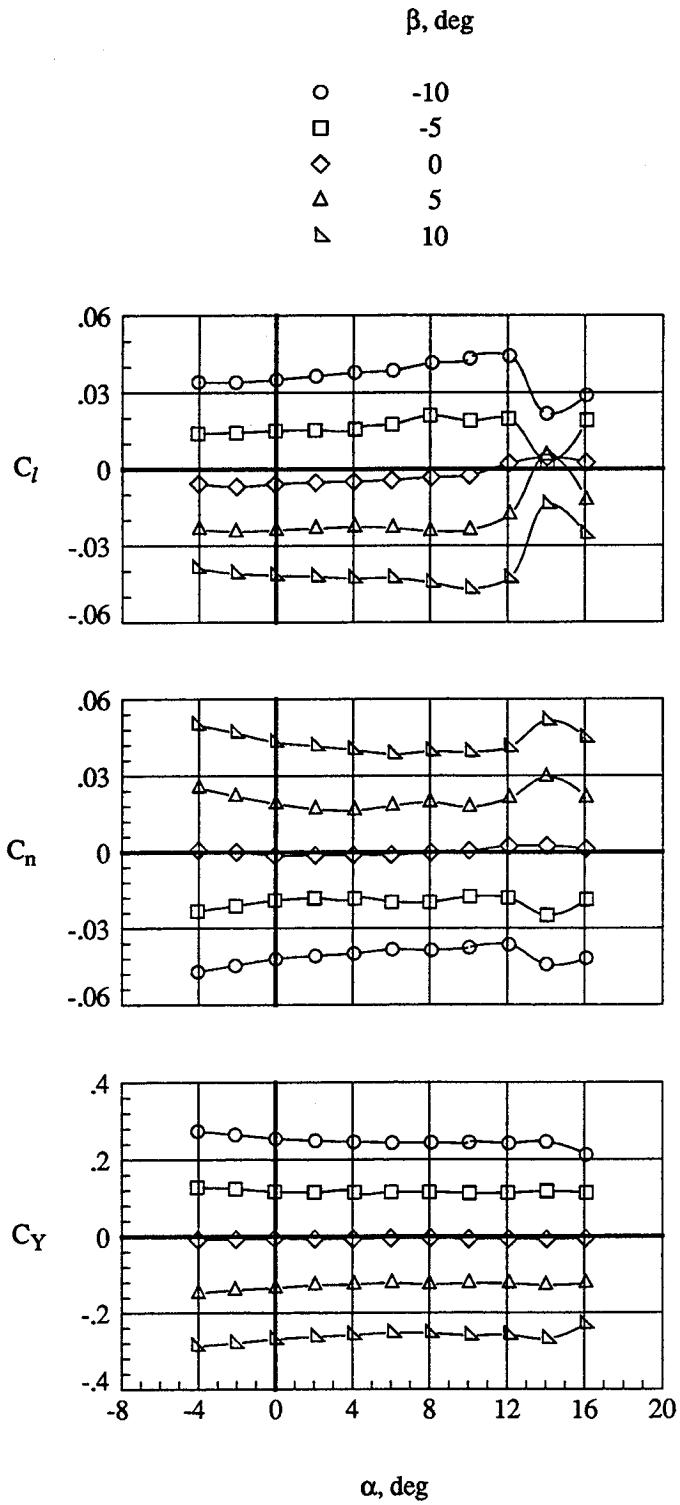

(b) Take-off configuration

Figure 19. Continued.

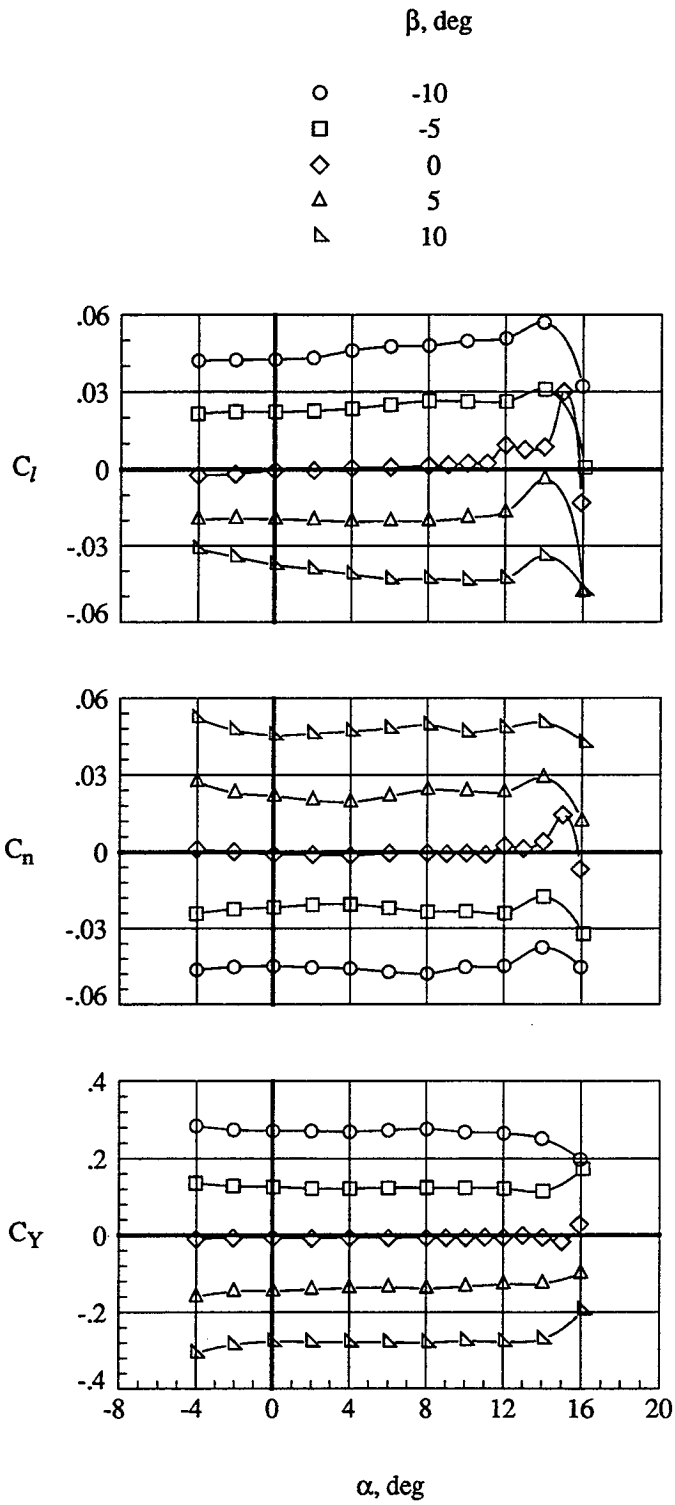

(c) Landing 1 configuration

Figure 19. Continued.

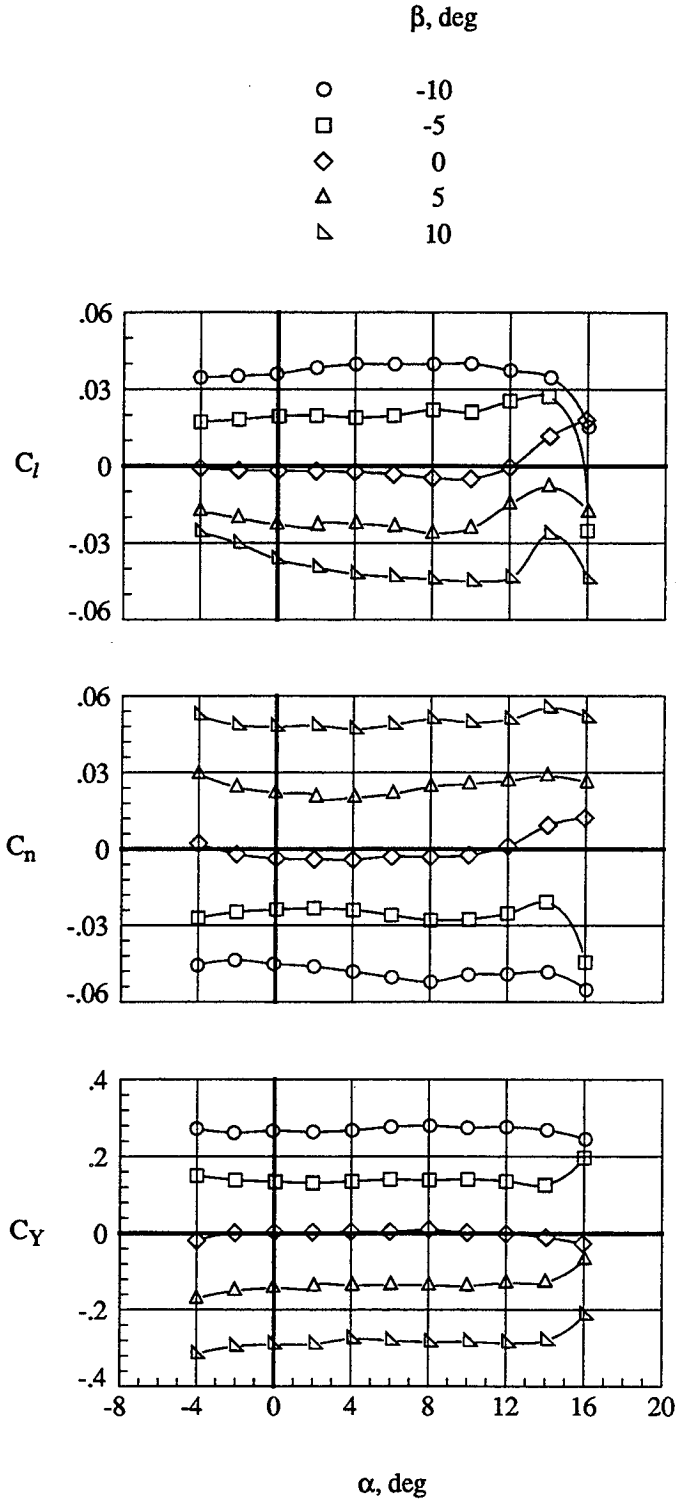

(d) Landing 2 configuration

Figure 19. Concluded.

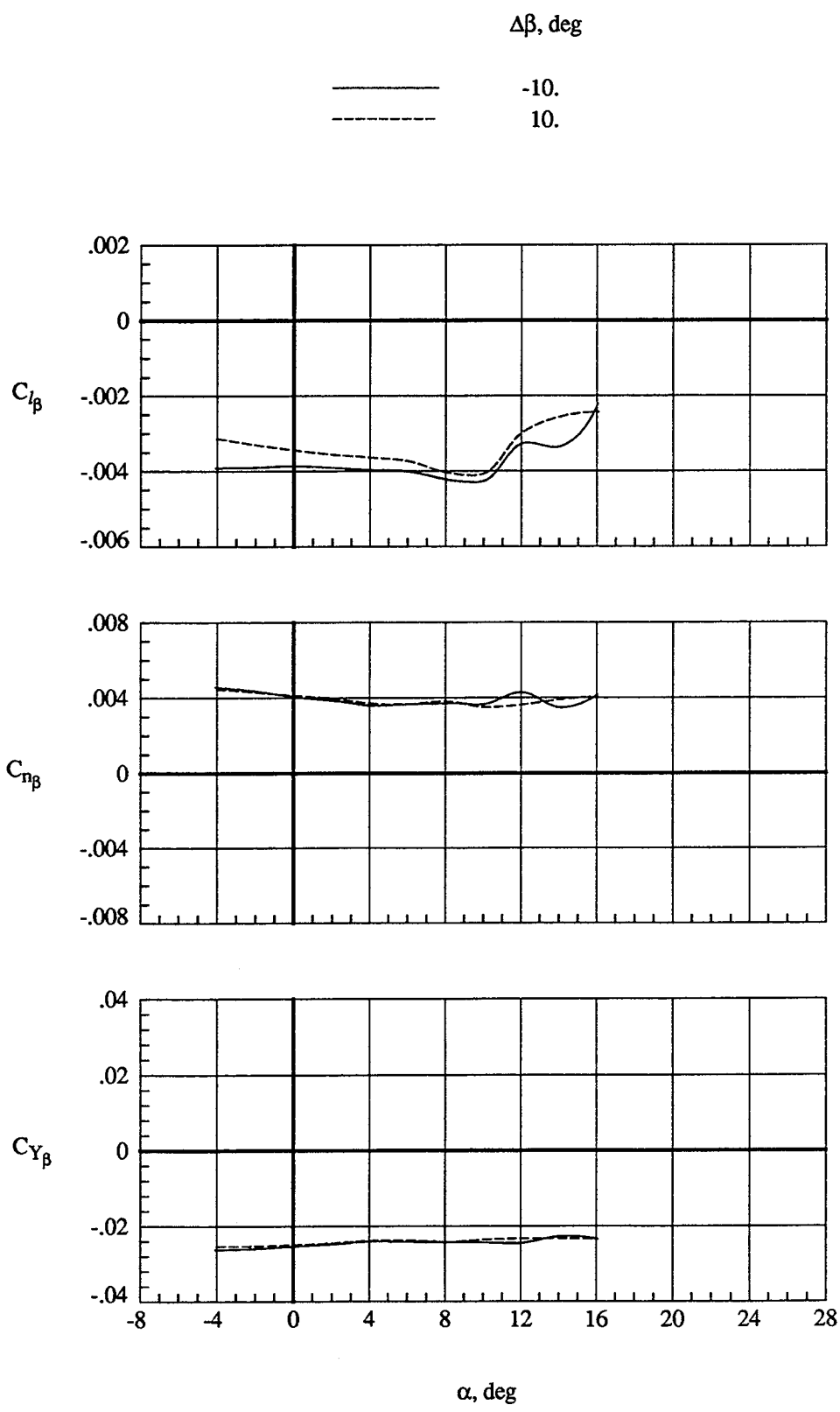

(a) Cruise configuration

Figure 20. Lateral directional stability derivatives.

q_∞ = 40 psf.

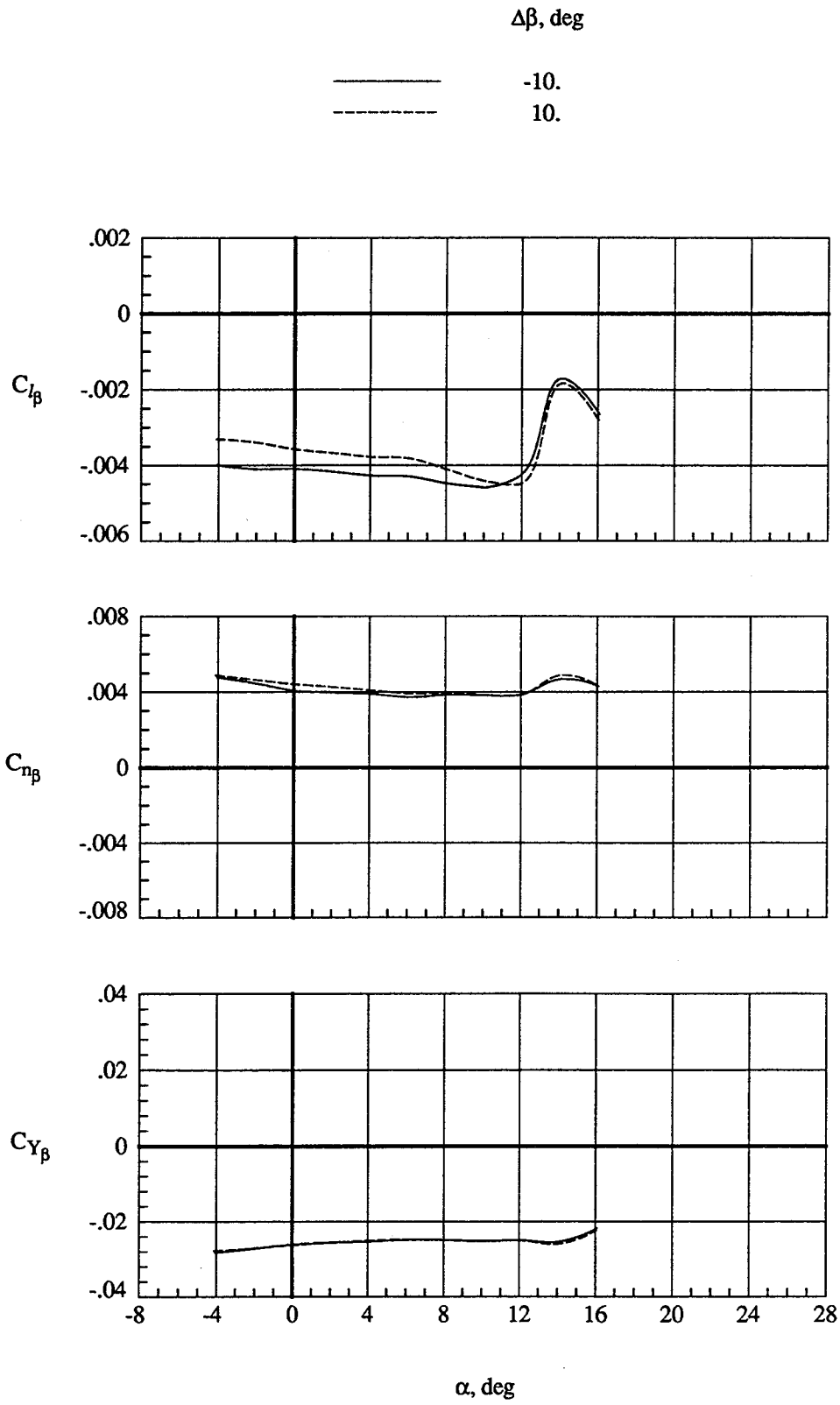

(b) Take-off configuration

Figure 20. Continued.

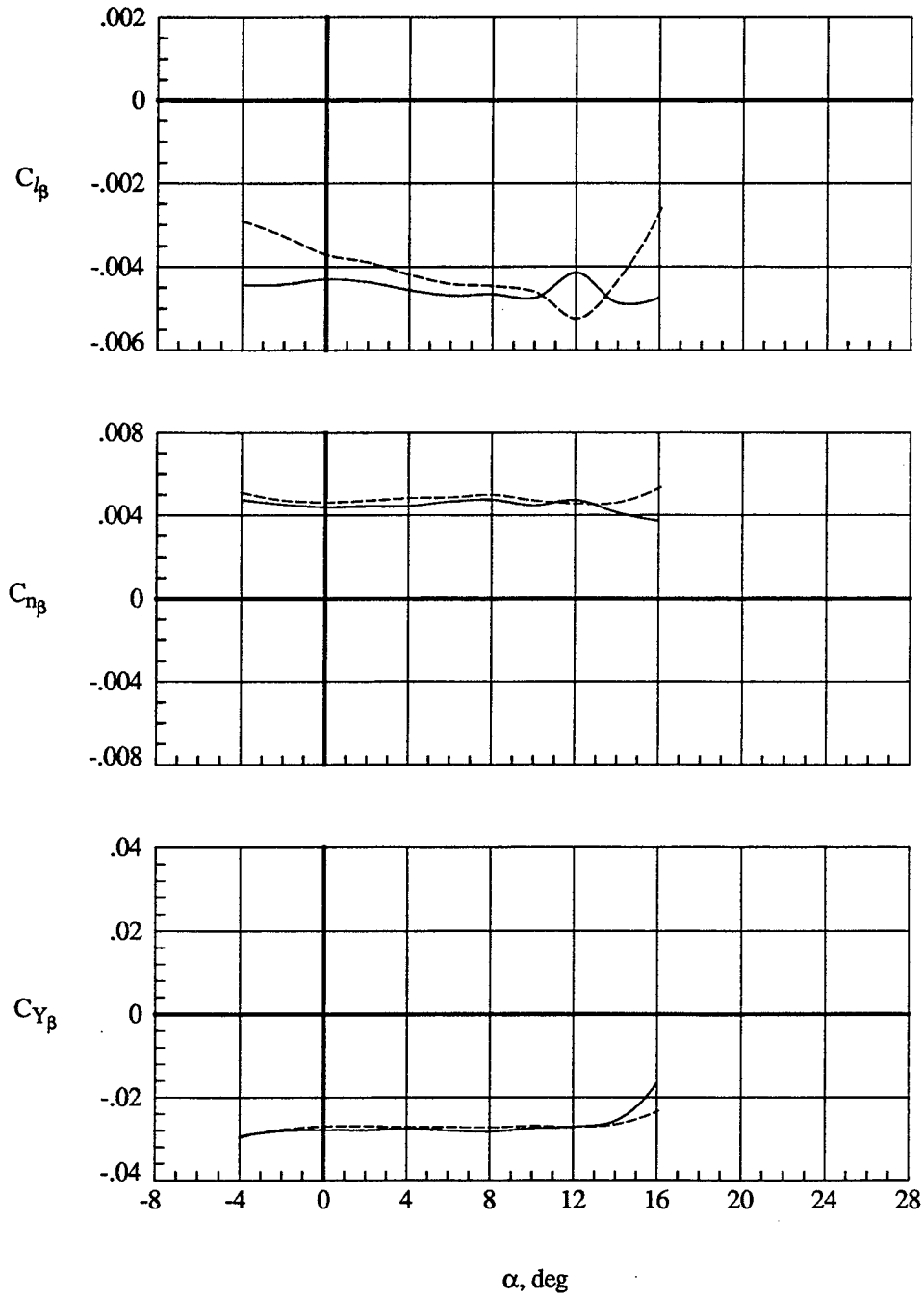

(c) Landing 1 configuration

Figure 20. Continued.

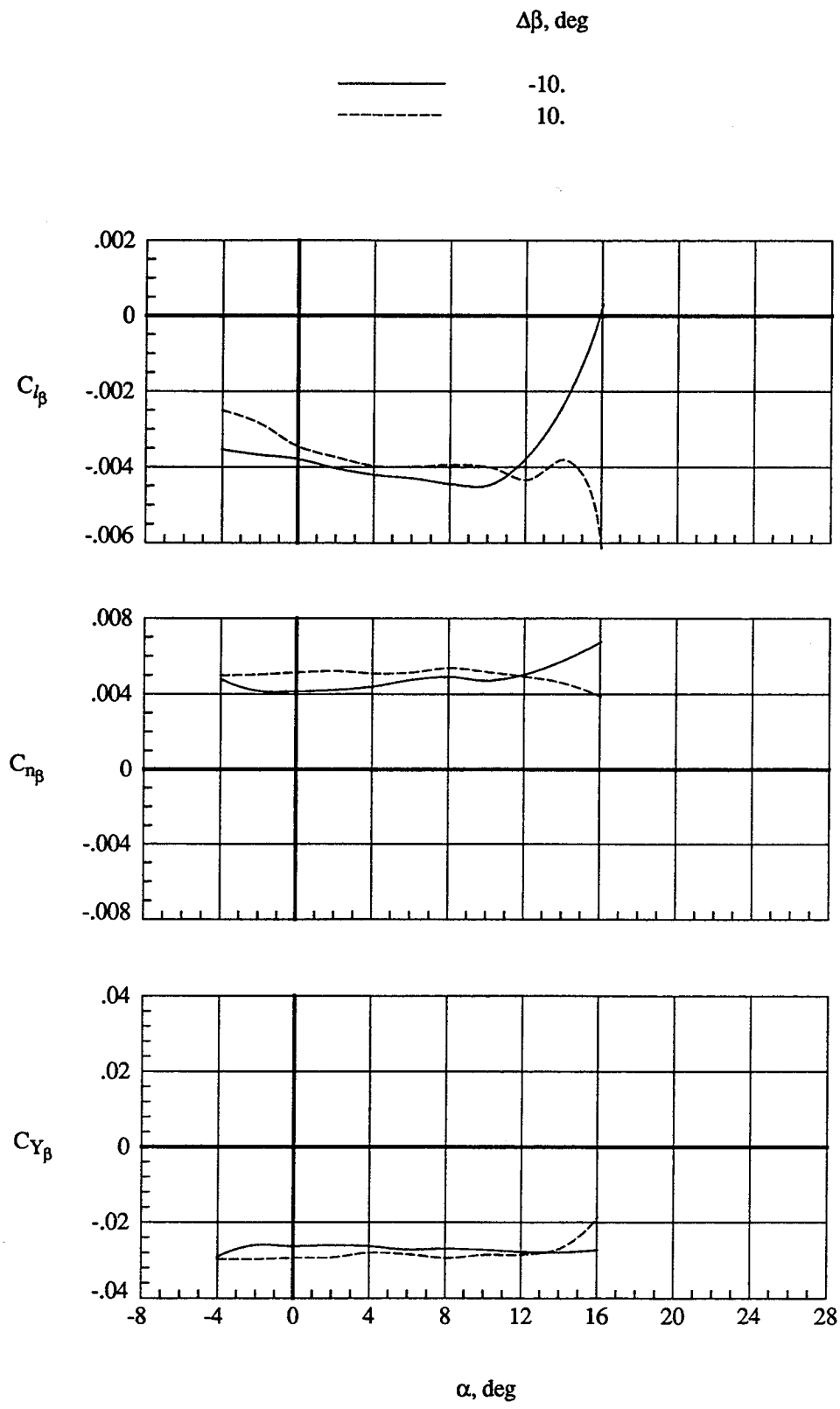

(d) Landing 2 configuration

Figure 20. Concluded.

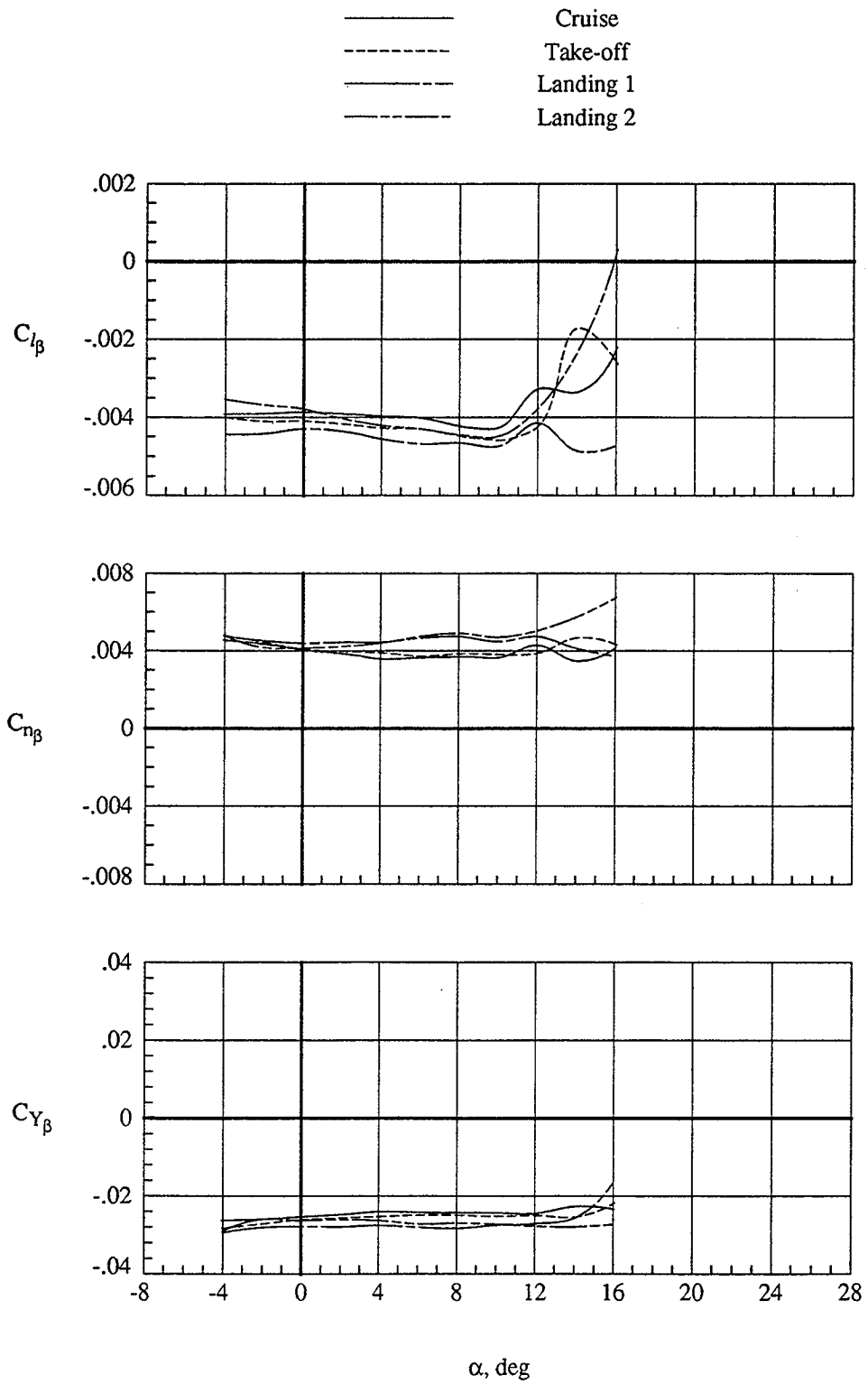

Figure 21. Effect of flap deflection on the lateral directional stability derivatives.
$q_\infty = 40$ psf.

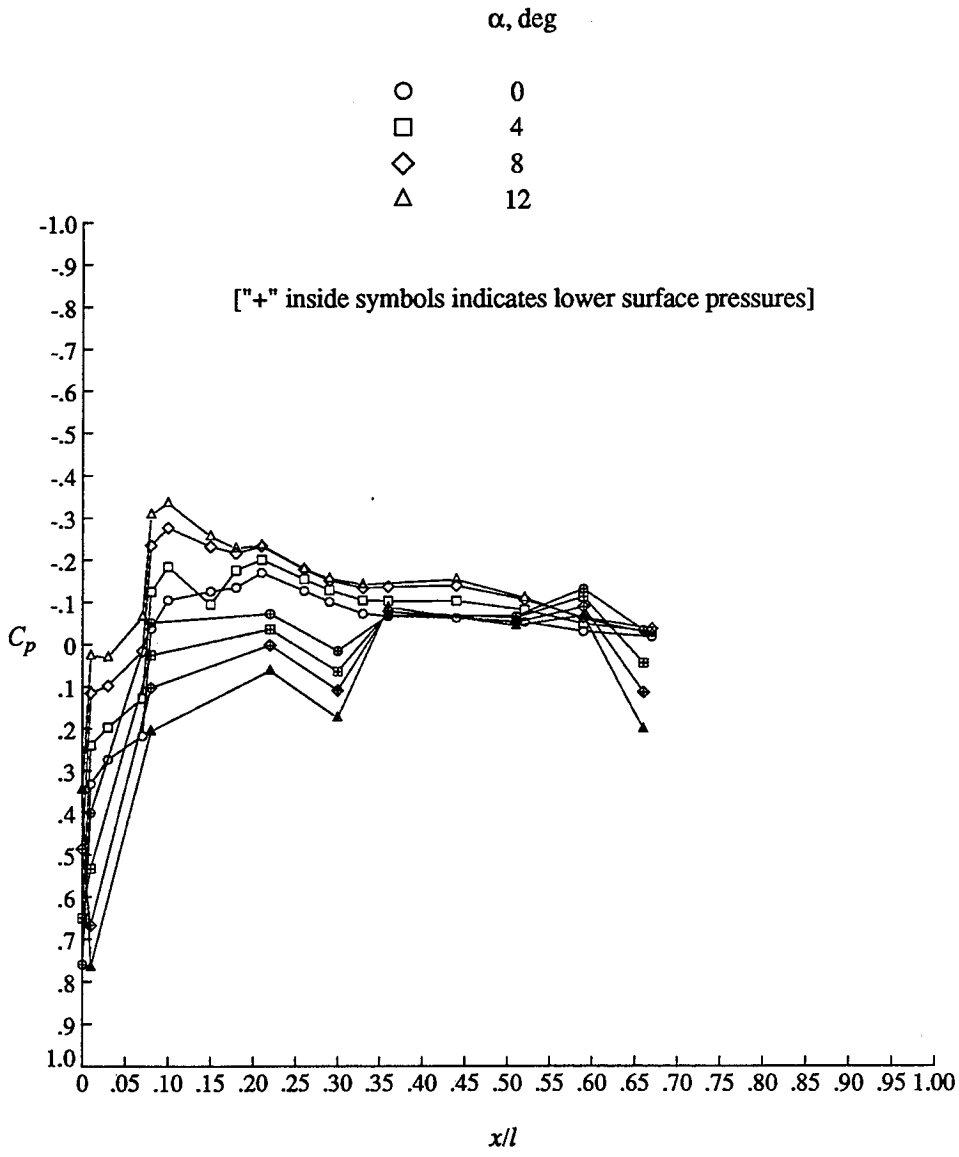

(a) Cruise configuration

Figure 22. Effect of alpha on the fuselage centerline pressure distributions.
q_∞ = 40 psf.

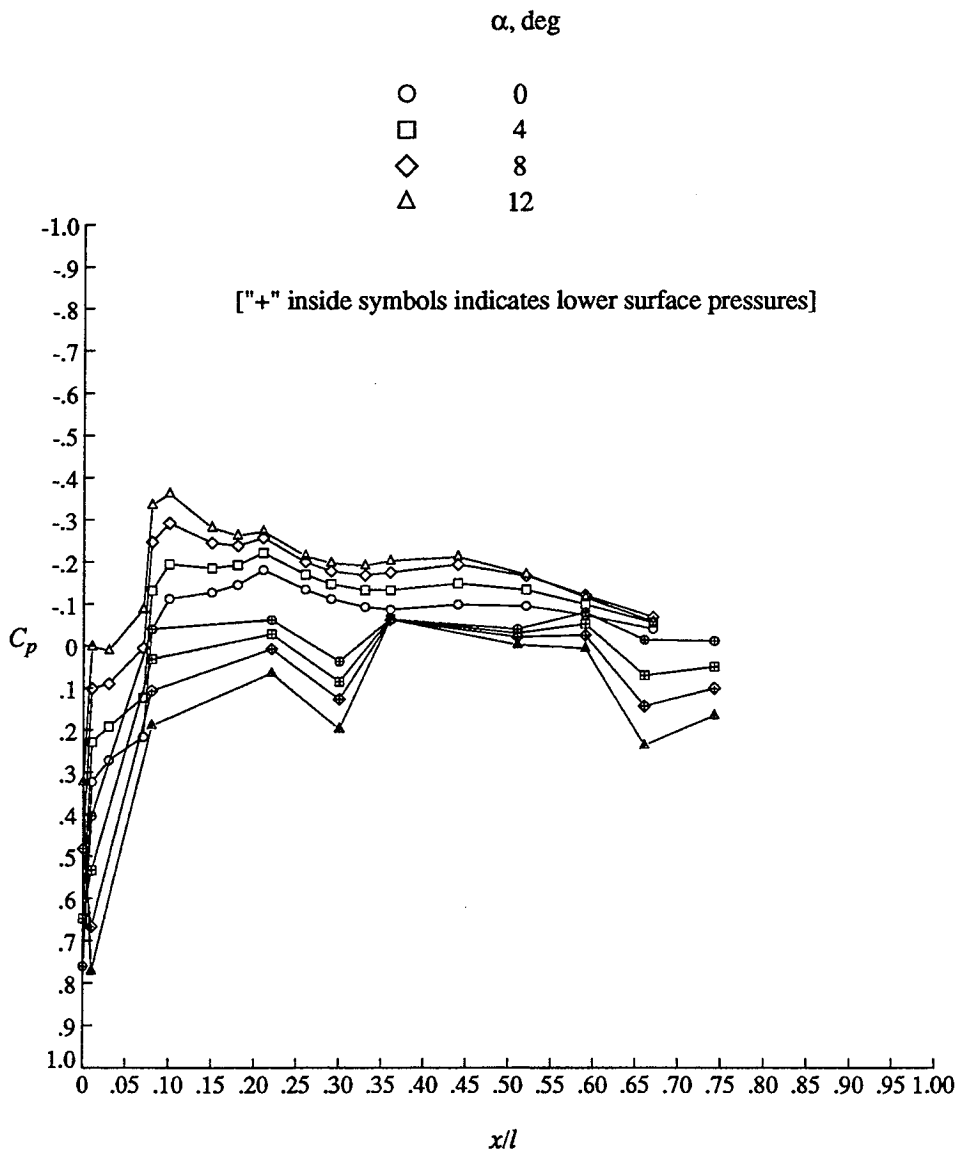

(b) Take-off configuration

Figure 22. Continued.

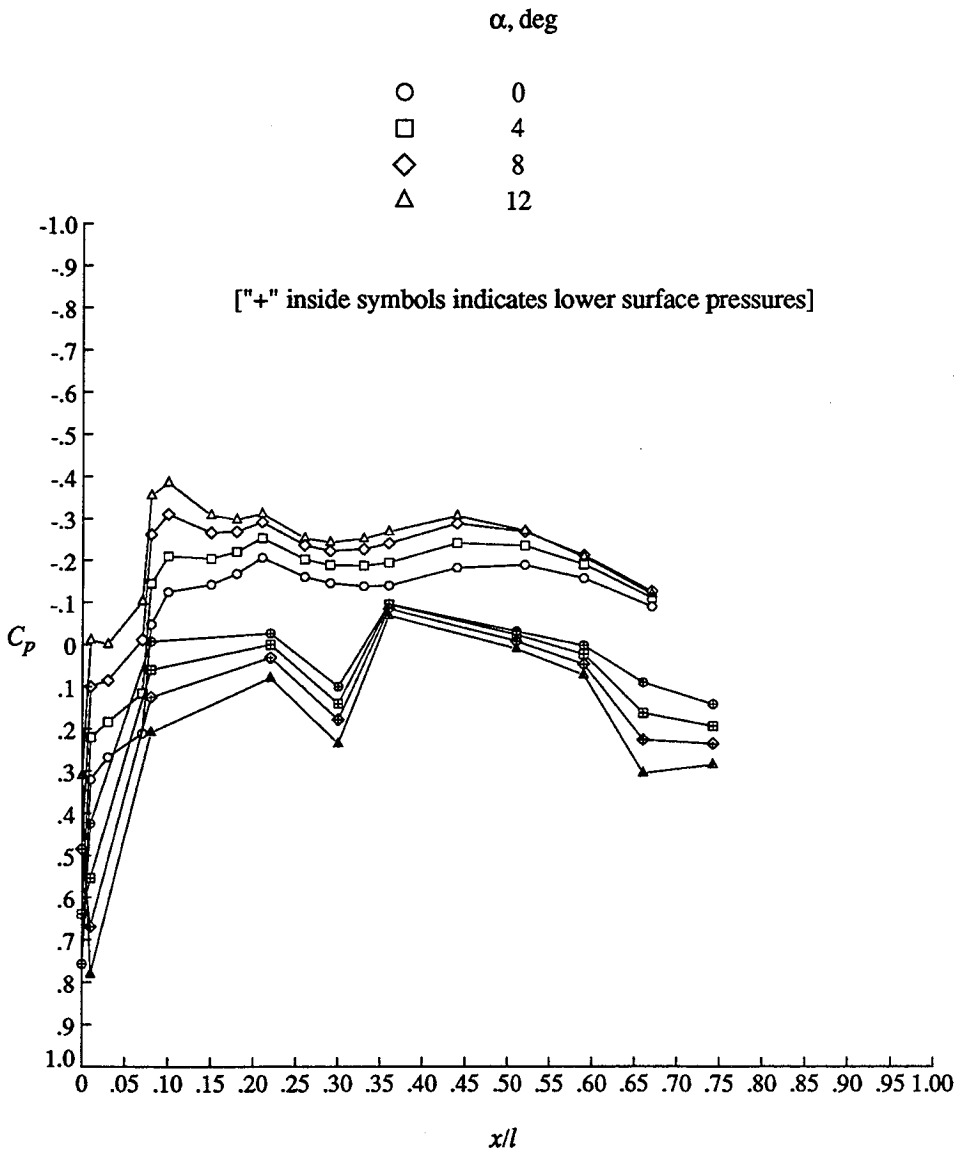

(c) Landing 1 configuration

Figure 22. Continued.

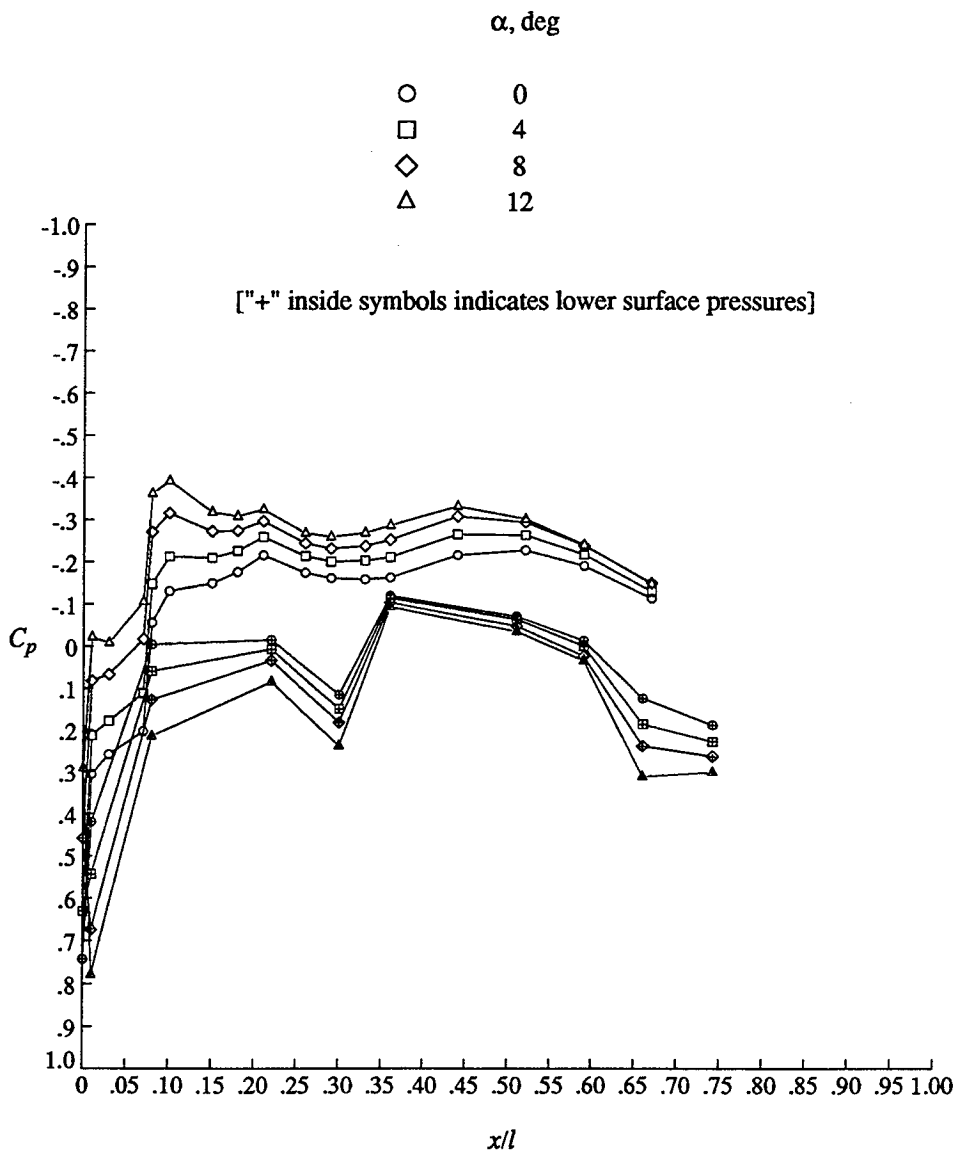

(d) Landing 2 configuration

Figure 22. Concluded.

REPORT DOCUMENTATION PAGE

Form Approved
OMB No. 0704-0188

1. AGENCY USE ONLY (*Leave blank*)	2. REPORT DATE	3. REPORT TYPE AND DATES COVERED
	March 1997	Technical Memorandum

4. TITLE AND SUBTITLE
Wind Tunnel results of the Aerodynamic Performance of a 1/8-Scale Model of a Twin-Engine Transport With Multi-Element Wing

5. FUNDING NUMBERS
538-05-14-01

6. AUTHOR(S)
Brenda E. Gile Laflin, Zachary T. Applin, and Kenneth M. Jones

7. PERFORMING ORGANIZATION NAME(S) AND ADDRESS(ES)
NASA Langley Research Center
Hampton, VA 23681-0001

8. PERFORMING ORGANIZATION REPORT NUMBER

9. SPONSORING / MONITORING AGENCY NAME(S) AND ADDRESS(ES)
National Aeronautics and Space Administration
Washington, DC 20546-0001

10. SPONSORING / MONITORING AGENCY REPORT NUMBER
NASA TM-110304

11. SUPPLEMENTARY NOTES

12a. DISTRIBUTION / AVAILABILITY STATEMENT
Unclassified - Unlimited
Subject Category 02

Availability: NASA CASI, (301)621-0390

12b. DISTRIBUTION CODE

13. ABSTRACT (*Maximum 200 words*)

A wind tunnel investigation was performed in the 14- by 22-Foot Subsonic Tunnel on a pressure instrumented 1/8-scale twin-engine subsonic transport to better understand the flow physics on a multi-element wing section. The wing consisted of a part-span, triple-slotted trailing edge flap, inboard leading-edge Krueger flap and an outboard leading-edge slat. The model was instrumented with flush pressure ports at the fuselage centerline and seven spanwise wing locations.

The model was tested in cruise, take-off and landing configurations at dynamic pressures and Mach numbers from 10 lbf/ft2 to 50 lbf/ft2 and 0.08 to 0. 17, respectively. This resulted in corresponding Reynolds numbers of 0.8 x 105 to 1.8 x 106. Pressure data were collected using electronically scanned pressure devices and force and moment data were collected with a six component strain gauge balance.

Results are presented for various control surface deflections over an angle-of-attack range from -4 degrees to 16 degrees and sideslip angle range from -IO degrees to IO degrees. Longitudinal and lateral directional aerodynamic data are presented as well as chordwise pressure distributions at the seven spanwise wing locations and the fuselage centerline.

14. SUBJECT TERMS	15. NUMBER OF PAGES
Aerodynamic Characteristics, Pressure Distribution, High-Lift, Subsonic Transport	128
	16. PRICE CODE A07

17. SECURITY CLASSIFICATION OF REPORT	18. SECURITY CLASSIFICATION OF THIS PAGE	19. SECURITY CLASSIFICATION OF ABSTRACT	20. LIMITATION OF ABSTRACT
UNCLASSIFIED	UNCLASSIFIED	UNCLASSIFIED	UNLIMITED